APPLICATION OF DUAL CYCLOCONVERTERS TO A DOUBLE FED MOTOR FOR TRACTION DRIVES

BY

© GERALD MURRAY BROWN, B.ENG., M.ENG.

A Thesis

Submitted to the School of Graduate Studies

in Partial Fulfillment of the Requirements

for the Degree

Doctor of Philosophy

McMaster University

April 1989

DUAL CYCLOCONVERTER TRACTION DRIVE

FOR DOUBLE FED MOTORS

DOCTOR OF PHILOSOPHY (1989)
(Electrical Engineering)

McMaster University
Hamilton, Ontario

TITLE: Application of Dual Cycloconverters to a Double Fed Motor for Traction Drives

AUTHOR: Gerald Murray Brown, M.Eng., (McMaster University)
B.Eng. (McMaster University)

SUPERVISOR: Dr. Barna Szabados, Department of Electrical and Computer Engineering

NUMBER OF PAGES: xii, 200

ABSTRACT

Variable speed AC drives have become the new standard for high performance drive systems. Very high power traction drives present a particular challenge for AC drive technology because of the simultaneous need for high-torque vibration-free operation at standstill, traction-limited dynamic braking, and high speed operation.

In this work, two independently controlled cycloconverters are used with a wound rotor machine to provide a double fed drive system that overcomes the frequency limitations of the cycloconverters and provides a stable high power drive, with potential for rapid torque response and power factor control.

A new 'Jitter' control method is derived for the firing angle control of the cycloconverter. This method effectively spreads the cycloconverter output harmonics over a broader spectrum and thus minimizes the filtering requirements.

The double fed motor (DFM) equations are applied to the DFM circle diagram and a simulation program has been written to plot the circle diagram and give a geometric interpretation of the developed torque. A new algorithm is proposed using δ_V, the pseudo torque angle, to give direct control of the torque using only position feed-back. A novel frequency hopping algorithm is also derived that allows the cyclo-

converters to be operated at high frequencies without generating harmonic torques.

A dual cycloconverter drive was built to verify the stability and torque-speed performance of such a system. Reliable operation was achieved by using bank switching sensors based on detecting the reverse bias across a series connected diode, and by short circuit detection circuits with automatic reset facilities. The control software displays system status information on the screen, with on-line parameter modification, and provides a complete range of manual and automatic modes of operation to facilitate system development and testing.

ACKNOWLEDGEMENTS

I am grateful for the many people who had a part in helping me complete this research. In particular, I would like to thank Dr. Barna Szabados for his encouragement and support throughout the project.

I would like to thank Mr. G. J. Hoolboom of Westinghouse for suggesting this work, and for his continued interest in its progress. Thanks also, to Dr. M. Poloujadoff for his helpful input into the double fed motor theory contained in Chapter 3.

Special thanks are due to Mr. Laurent Magnard for his diligent work writing the computer plotting program of Chapter 2, and to Mr. Steve Spencer for his programming assistance in Chapters 2 and 3.

I would like to thank Mr. Ray Gillan, Mr. Walter Wolkow and Mr. Adam Marianski for their technical support and advice. Thanks also to Dr. Dan McCrackin, who often times had the right suggestion at just the right time when I seemed to be at an impasse.

This work has been made possible by the support NSERC.

And of course, I am very thankful for Deb, my wife, who has been very patient and supportive since I began this work. She also typed the entire thesis for me, in addition to her many other responsibilities.

May the Lord be praised for his guidance and provision. "I sought the Lord, and he answered me; He delivered me from all my fears. Those who look to him are radiant; their faces are never covered with shame." (Psalm 34:4-5)

TABLE OF CONTENTS

LIST OF FIGURES

CHAPTER 1

INTRODUCTION

Solid state variable speed AC motor drives are used in an increasingly wide range of applications that were previously the domain of DC drive systems. The rugged squirrel cage induction motor is less expensive to build and maintain than its DC counterpart, and is more compact, making it very attractive as a prime mover. The drawback, however, is to be able to provide a similarly rugged and economical static power supply which can supply AC power over the required range of frequency and voltage so that the AC drive system can perform as well or better than a DC system.

Traction drives present a particularly challenging set of performance criteria for AC drive technology. They require a relatively long period of start-up, during which time they must produce a smooth vibration-free torque. Start-up and low speed operation is also usually under full load, with a reduced tractive effort required at higher than base speed [1]. In addition, with increased vehicle speeds, or high acceleration and deceleration requirements, it is desirable to have dynamic braking that is only limited by track adhesion, and not by the motor drive system [2]. A torque-speed curve for a typical traction drive is shown in Figure 1.1.

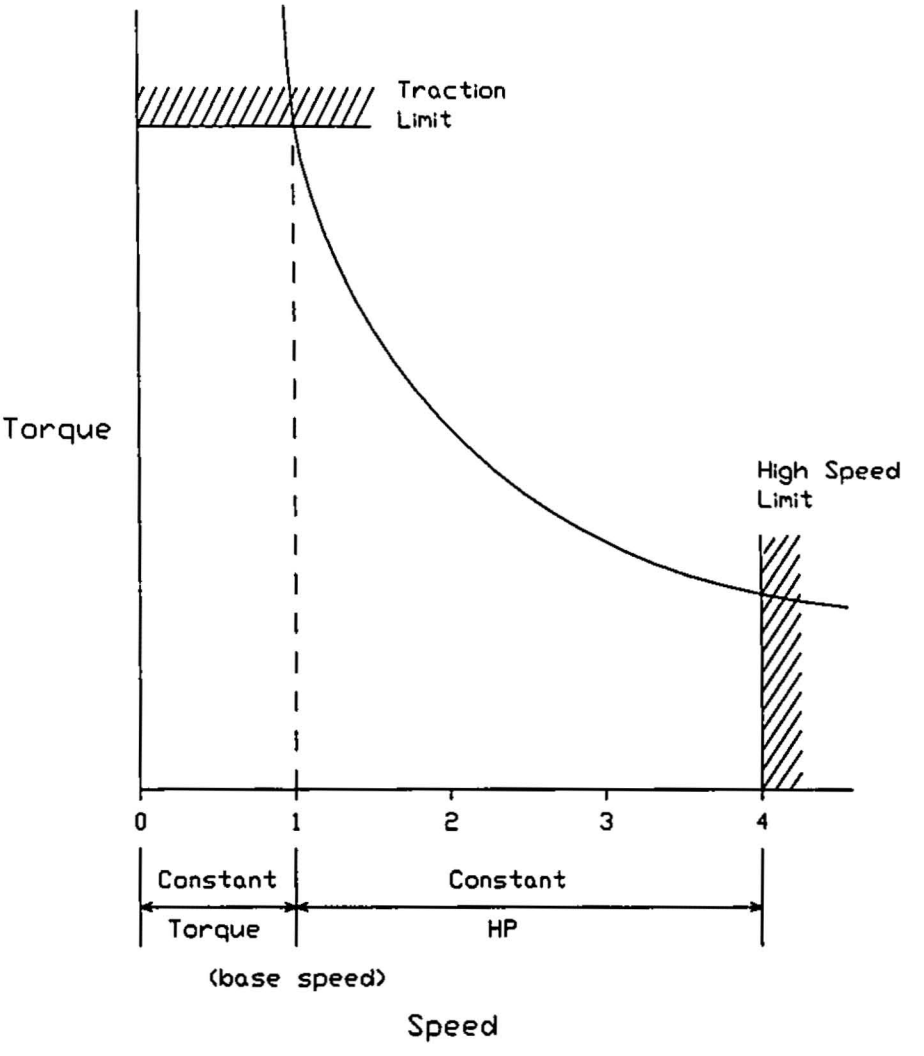

Figure 1.1 - TORQUE SPEED CURVE FOR TRACTION APPLICATIONS
Smooth, traction-limited torque is required at standstill, with a reduced tractive effort required above the base speed.

In a Master's thesis [3], entitled, "Hybrid Control of a Cycloconverter for Double Fed Motors in Traction Drives", it was proposed to use two 3-phase cycloconverters to independently supply the stator and rotor windings of a wound rotor induction machine, as in Figure 1.2. This configuration makes use of the cycloconverter's strengths; natural commutation, very high power, and smooth torque at standstill and at low speed. It also overcomes the frequency limitation of cycloconverters in that such a double fed system behaves as a synchronous motor with AC excitation on the rotor [4]. That is, the rotor speed will be proportional to the sum (or difference) of the individual cycloconverter's output frequencies, and full speed (ie. 60 Hz) operation is obtainable.

A second advantage of this arrangement is that low speed operation no longer requires a low stator voltage to keep the volts/Hz ratio constant and prevent saturation. Instead, the stator and rotor voltages and frequencies can both be kept high, even at standstill, since it is their difference frequency that determines the rotor speed.

This dual cycloconverter configuration also introduces several other new degrees of freedom in controlling the cycloconverters, including the elimination of harmonic producing torques at higher output frequencies, and power factor control. In addition, since this configuration is inherently double fed, with power being supplied directly to or from both the stator and rotor windings simultaneously, the system is able to provide adhesion-limited braking and torque-speed characteristics similar to those obtained with DC motors.

A brief review of previous work with double fed motor (DFM)

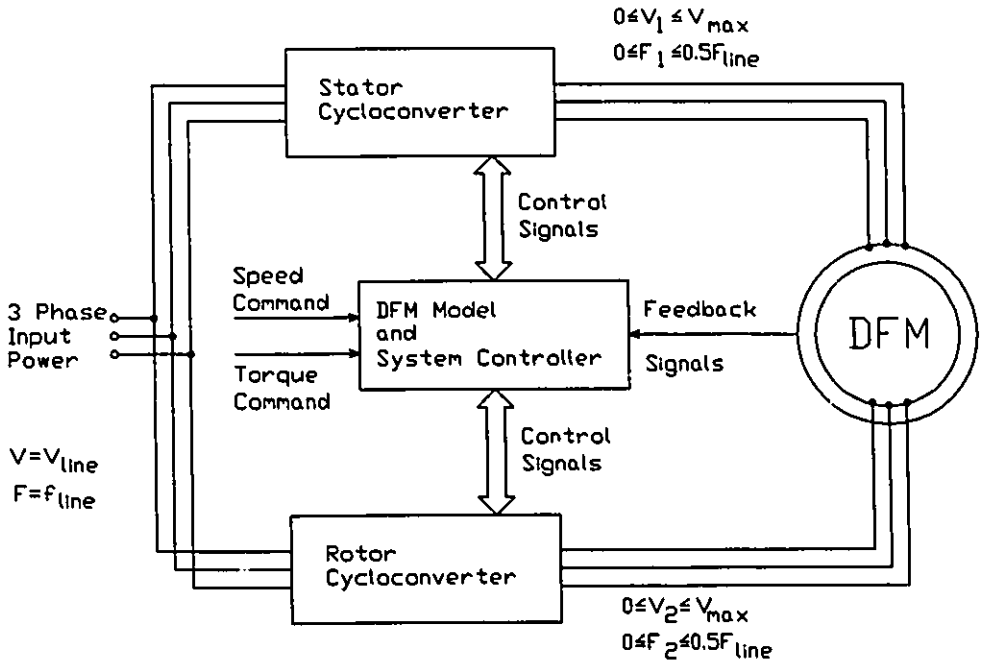

Figure 1.2 - DOUBLE FED MOTOR (DFM) WITH DUAL CYCLOCONVERTERS

where: V_{line} = Line Voltage (constant)
f_{line} = Line Frequency (constant)
$V_{max} \leq V_{line}$, Set by the System Controller
1,2 = Stator,Rotor subscripts, respectively

systems will serve to put this present research in perspective.

Historically, 3-phase variable frequency power from static converters, suitable for driving polyphase AC machines over a wide range of speed, was not available. As such, the focus on double fed machines was to connect the stator and rotor to the same fixed frequency mains supply and operate in the double speed mode. Analysis and performance tests have shown that this configuration produces no starting torque and is dynamically unstable, since the coefficient of viscous damping is negative [5][6][7]. Although such a configuration would be limited to fixed speed applications (using mains frequency power), the high peak power capability and double speed potential of this system make it very appealing, if these limitations could be overcome [8].

The availability of static variable frequency AC converters later facilitated the development of variable speed, static slip energy recovery drives [1]. In these, the stator is connected to the constant frequency mains supply and a thyristor converter is connected to the rotor windings via the slip rings.

For small power drives, the converter can be a simple rectifier-chopper combination that controls the effective resistance of the rotor circuit, and thus the rotor speed. For medium and large power applications, the relatively low frequency output of the rotor is fed through a rectifier and inverter combination back to the mains to provide slip energy recovery (over a limited speed range) [9]. If the converter is capable of bidirectional power flow, then the system can be doubly fed, or simply 'double fed', and supersynchronous operation can be obtained when power is supplied to both the stator and rotor windings

simultaneously.

The double fed machine can also be used as a generator to provide constant frequency output from a variable speed shaft (VSCF). Saleh et.al. [10] applied this principle to a wind energy conversion system. Their work shows the flexibility of the DFM as a power conversion device when the magnitude and phase of the injected rotor voltage can be controlled.

When configured as a double fed drive, the rotor converter may use force-commutated, line-commutated, or load-commutated inverter configurations, or a cycloconverter. Each of these present different possibilities regarding speed range, power capacity, presence or absence of torque pulsations and starting torque capabilities. Yet none is suitable for traction drives in that either the high power and smooth torque are not possible at standstill, or the speed range is restricted to only ±30% of the mains frequency synchronous speed.

Long and Schmitz [11] used a cycloconverter to supply the series connected stator and rotor windings of a wound rotor machine in an effort to develop a traction drive with a wide range of speed. Theirs was essentially a double speed system, but with a variable frequency supply. They successfully overcame the system's inherent instability by using the rotor position to control the phase of the rotor and stator mmf waves, but they had difficulty with bank shorts in the cyclo-converter and could only operate the system over a limited range of frequencies. They also used a 400 Hz supply, which, although it increases greatly the useful output frequency of the cycloconverter, requires a special power source instead of the standard mains power.

Pacas [12] later applied the principles of field oriented control to the series connected double fed induction motor, with favorable results. The use of the series connection, allows double speed operation, yet minimizes the complexity of the control laws as well as the hardware requirements.

The approach in this research, using two separate cycloconverters, with torque angle control of the stator and rotor mmf waves, is an extension of these previous investigations. The use of independent cycloconverters introduces two extra degrees of freedom to the drive system; any number of frequency combinations can be used to obtain a given rotor speed, and separate stator and rotor voltages can be supplied. This opens up new possibilities to maximize the output torque, minimize the cycloconverter harmonics, and to improve the input power factor at every operating point, according to some specified control law or performance criteria.

The first half of this thesis (Chapters 2, 3 and 4) is largely analytical in nature and introduces several new approaches to DFM drive theory and control. The second half (Chapters 5, 6, and 7) deals with the practical implementation of some of these concepts in a working double fed motor drive system. Several novel techniques to facilitate testing and to provide reliable performance of the cycloconverters are included.

Chapter 2 reviews the standard derivation of the cycloconverter output harmonics and includes a 3-dimensional graphical depiction of the results. Discussion of the implications follows, and a novel 'Jitter' control method is derived to effectively spread the output harmonics of

the cycloconverter over a broader frequency spectrum and thereby improve its performance.

Chapter 3 presents the double fed motor (DFM) system equations and the corresponding circle diagram. An interactive plotting program was developed to simulate the double fed motor performance and to draw the DFM circle diagram. From this, control principles are derived for the double fed motor drive.

Chapter 4 applies these ideas to a double fed motor supplied by two independent cycloconverters. Control of the rotating flux, in magnitude and phase, via the torque angle δ_V, ensures dynamic stability of the DFM drive. The new degree of freedom available in choosing the stator frequency (quite independently of the rotor speed) is explored, and a 'frequency hopping' control method is proposed which can eliminate specific torque producing harmonics from the cycloconverter outputs.

Chapter 5 contains a description of the control and power circuits. To provide reliable operation of the cycloconverters, short circuit detection and bank switching circuits were developed, as well as a very useful automatic short circuit reset capability (ASCR). Complete circuit schematics are given in a separate document [13].

Chapter 6 summarizes the features of the DFM software. Since this is a development system, there is provision for on-line parameter modification. A complete range of manual and automatic operating modes are available, as well, to facilitate system development and diagnostics.

Chapter 7 reviews the performance of the present DFM system, contains a discussion of the work, and proposes several avenues for

further development of the hardware and software. These include theoretical issues, as well as practical items to improve performance and simplify construction.

CHAPTER 2

CYCLOCONVERTER OUTPUT HARMONICS

2.1 Definition of Terms

α = thyristor firing angle

α_p, α_n = firing angle of positive,negative converter

δ = Jitter angle (not the motor torque angle)

f_i, f_o = input (supply) frequency,output frequency

r = $\hat{v}_o/\hat{v}_{o_{max}}$ = desired output voltage ratio

ϕ_o = load current angle

$r\text{Sin}\theta_o$ = desired output voltage (without scaling factor)

θ_i, θ_o = input,output angular frequency

v_a, v_b = output voltage of 3-pulse bridge a,b

v_p, v_n = output voltage of positive,negative converter

v_o = output voltage of one phase of cycloconverter

$\hat{v}_i$, $\hat{v}_o$ = peak input,output voltage

2.2 Introduction

Practical high power cycloconverters (using natural commutation)

allow direct conversion of electrical energy from one frequency to another. In addition to the output power at the desired fundamental frequency, they also produce a highly complex pattern of undesirable harmonic components, which vary in frequency and amplitude according to operating conditions of the load such as f_o, r and ϕ_o. Minimizing, or otherwise controlling, these harmonic terms is an important problem.

In general, the relationship between the controlled output frequency f_o, and the output voltage v_o, is determined by the load (typically a large AC motor) and by operating conditions of the load, such as the torque and speed, which in turn determine the current phase angle ϕ_o. For a given converter topology, therefore, the output voltage harmonics of a cycloconverter (and by duality, its input current harmonics) are dictated by the requirements of the load. In this sense, they are said to be uncontrollable. This presents a difficult filtering problem due to the wide range of harmonic frequencies present, and to the variation of their amplitude and frequency as f_o varies.

PWM type inverters, using high switching frequencies and judicious control methods, can minimize harmonics in both the output voltage and the input current waveforms. Unfortunately, since they require forced commutations, they cannot be used in very high power applications [14].

In response to this problem, a novel addition is made to the typical firing pattern of the cycloconverter thyristors. This new method is coined the 'Jitter' control method and allows the harmonic energy in the cycloconverter output to be more evenly distributed, and thus to reduce the amplitude of the dominant harmonics [15].

This chapter will first review the standard derivation of the output harmonics of a 6-pulse cycloconverter, and then present the derivation for the harmonics present using Jitter control. 3-D graphs are included to aid in the interpretation of the results.

2.3 Cycloconverter Harmonics with the Standard Control Method

2.3.1 Derivation of the Standard Cycloconverter Output Harmonics

The method of Gyugyi and Pelly [16][17] is used here to derive the cycloconverter output harmonics. In the analysis, it is assumed that the filtering action of the load results in only a pure sinusoidal load current at the desired output frequency f_o . Also, the source inductance and the finite time for commutation to occur between thyristors are not considered.

Standard cycloconverters are composed of series and parallel combinations of the basic 3-pulse converter circuit. Analysis can be carried out on this general basis, and then the results are modified according to the pulse number and configuration of the actual converter. The output spectrum for a 3-pulse cycloconverter is shown in Figure 2.1. Omitting the harmonic families $3(2n-1)f_i$ (i.e. the 3^{rd}, 9^{th}, 15^{th},... harmonics) gives the spectrum for a 6-pulse converter (as in Fig. 2.5), and omitting the families $6(2n-1)f_i$ (i.e. the 6^{th}, 18^{th}, 30^{th},... harmonics) gives the spectrum for a 12-pulse converter. When 3-pulse converters are configured into higher pulse number converters, certain

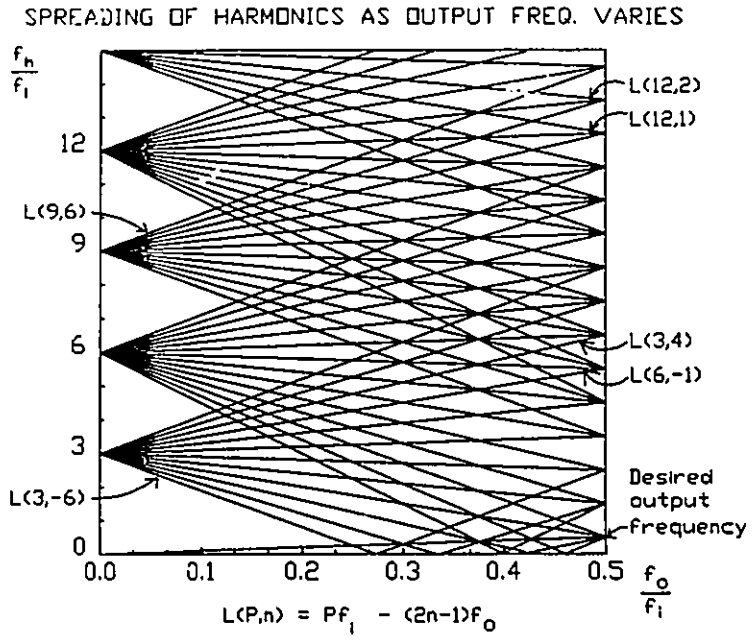

Figure 2.1 - OUTPUT HARMONICS OF A 3-PULSE CYCLOCONVERTER
As the output frequency increases, the harmonics diverge from those of a 3-pulse rectifier.

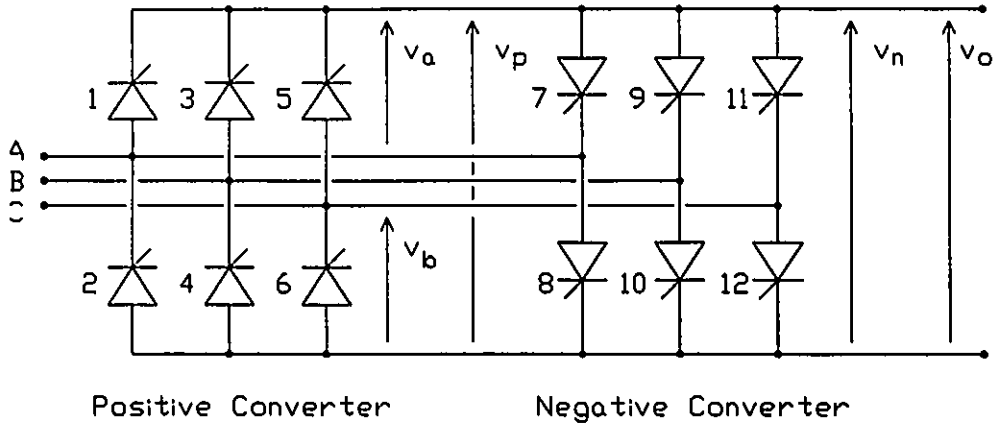

Figure 2.2 - NATURALLY COMMUTATED CYCLOCONVERTER - Composed of two 6-pulse phase controlled rectifiers.

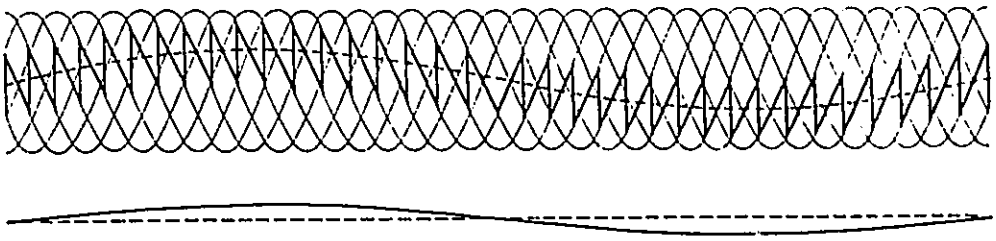

Figure 2.3 - CYCLOCONVERTER OUTPUT WAVEFORM (Single Phase) With $\tau = 0.5$, $\phi_o = 0^o$, and $f_o/f_i = 1/3$.

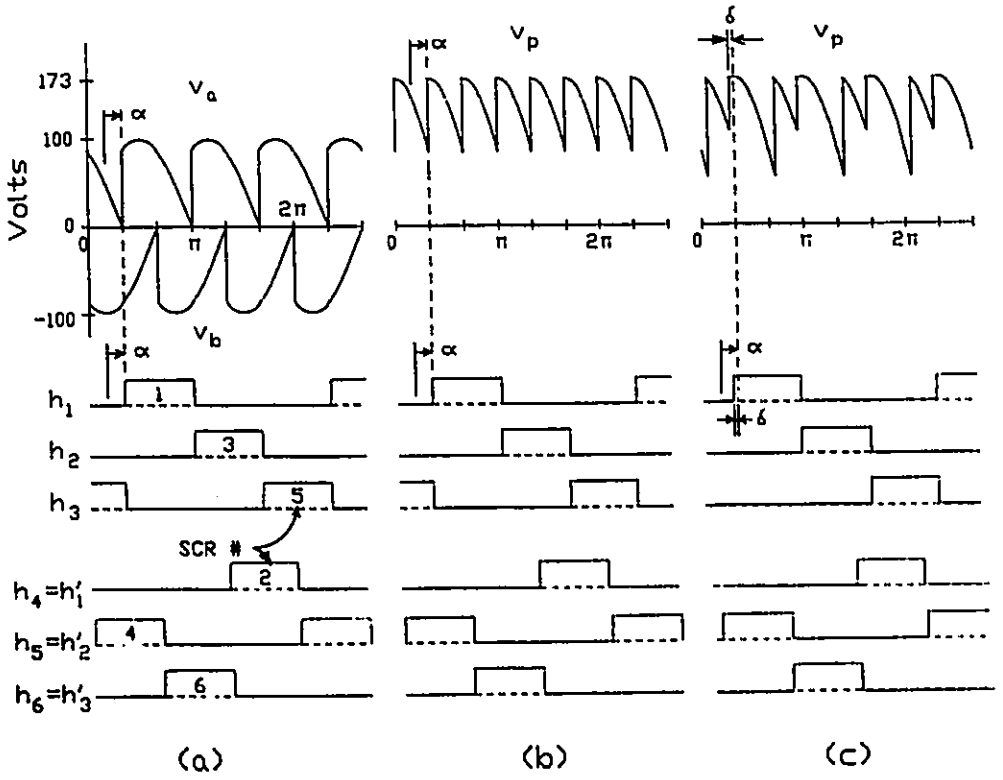

Figure 2.4 - WAVEFORM FABRICATION FROM TWO 3-PULSE CONVERTERS
(a) The output voltage v_p is the algebraic sum of the two 3-pulse outputs, v_a and v_b.
(b) Standard Control (c) Jitter Control.

families of harmonics exactly cancel. This has the very significant consequence that, as each harmonic family is removed (or cancelled out), the remaining harmonic families do not change in amplitude, and the total harmonic energy decreases.

The naturally commutated cycloconverter of Figure 2.2 is composed of two 6-pulse phase-controlled rectifiers, connected in inverse parallel, having output voltages v_p and v_n respectively, for the positive and negative converters. For a 3-phase output, 3 such circuits are required. Analysis is given here for one phase only, since the others differ only by an appropriate phase shift of $\pm 2\pi/3$.

The output voltage (v_p or v_n) is fabricated from consecutive segments of the 3 input voltage waveforms in order to best approximate the desired output voltage (Fig. 2.3). For example $v_p = v_1 - v_2$, then $v_p = v_1 - v_3$, then $v_p = v_2 - v_3$, etc. This can be expressed mathematically by means of existence functions h, where h = 0 or h = 1, and h is determined according to the method of output waveform fabrication, f_o, v_o (according to τ), and ϕ_o.

For a 3-pulse converter with output v_a and existence functions $h_k(\theta)$ as in Figure 2.4a, it is clear that each $h_k(\theta)$ is periodic and has a value of 1 for 1/3 of the input cycle for any α (α = constant) and 0 for the rest of the cycle. Therefore

$$v_a(\theta) = \sum_{k=1}^{3} \hat{v}_i \mathrm{Sin}[\theta_i-(k-1)\tfrac{2\pi}{3}]\ h_k[\theta_i-\alpha-(k-1)\tfrac{2\pi}{3}] \qquad (2.1a)$$

where

$$\hat{v}_i \mathrm{Sin}[\theta_i-(k-1)\tfrac{2\pi}{3}] \quad k = 1,2,3 \text{ are the 3 input voltages} \qquad (2.2)$$

and

$$h_k[\theta_i-\alpha-(k-1)\tfrac{2\pi}{3}] \quad k = 1,2,3 \text{ are the 3 existence functions} \qquad (2.3)$$

Likewise, for the 3-pulse converter with output v_b and existence functions $h'_k(\theta) = h_k(\theta-\pi)$

$$v_b(\theta) = -\sum_{k=1}^{3} \hat{v}_i \text{Sin}[\theta_i-(k-1)\tfrac{2\pi}{3}]\ h'_k[\theta_i-\alpha-(k-1)\tfrac{2\pi}{3}] \tag{2.1b}$$

Now, the 6-pulse bridge converter yields $v_p = v_a + v_b$, but in determining the Fourier coefficients for v_p, the Cos terms from v_a and v_b will cancel leaving

$$h_k[\theta_i-\alpha-(k-1)\tfrac{2\pi}{3}] = 2\sum_n b_n \text{Sin}[n(\theta_i-\alpha-(k-1)\tfrac{2\pi}{3})] \tag{2.4}$$

and

$$\sum_n b_n = \tfrac{\sqrt{3}}{\pi}[1 + \sum_{p=1}^{\infty}(-1)^p(\tfrac{1}{6p-1} + \tfrac{1}{6p+1})] \tag{2.5}$$

For example, for k = 1

$$h_1(\theta_i-\alpha) = \tfrac{2\sqrt{3}}{\pi}\text{Sin}(\theta_i-\alpha) + \sum_{p=1}^{\infty}(-1)^p\left[\tfrac{1}{6p\pm1}\text{Sin}[(6p\pm1)(\theta_i-\alpha)]\right] \tag{2.6}$$

Combining the 3 input voltages with their respective h functions, and using appropriate trigonometric identities gives

$$v_p(\theta) = \tfrac{2\sqrt{3}}{\pi}\hat{v}_i\left\{\tfrac{3}{2}\text{Cos}\alpha + \left[\sum_{p=1}^{\infty}(-1)^p \sum_{k=1}^{3}\tfrac{1}{6p\pm1}\left[\text{Sin}[\theta_i-(k-1)\tfrac{2\pi}{3}]\text{Sin}[(6p\pm1)(\theta_i-\alpha-(k-1)\tfrac{2\pi}{3})]\right]\right]\right\} \tag{2.7}$$

It is seen that the term containing Cosα is the desired DC output voltage and that the index p determines the characteristic harmonics and their amplitudes (for a 6-pulse converter with firing angle α).

By modulating α about $\pi/2$ ($0 \le \alpha \le \pi$) at a frequency f_o, the DC output voltage can be varied according to Cosα and can be considered as

an AC voltage with the same frequency f_o. This assumes continuous load current, as well as some means of alternating between the v_p and v_n converter banks when the polarity of the fundamental of the load current changes.

Now, the variation of α with time modifies the periodic nature of the existence functions (2.4) and of their coefficients (2.5), and since f_o and f_i are generally not related by an integer multiple, the standard method of Fourier analysis becomes unsuitable [16][17]. On the other hand, by treating the existence functions as periodic, but with a time-varying phase shift, the concept of the instantaneous Fourier transform can be used to derive the desired analytic expression.

Thus, in (2.7), the steady-state firing angle α is replaced by $\alpha = \pi/2 - f(\theta_o)$, where the modulating function $f(\theta_o)$ is in fact an arbitrary time-dependent phase shift. Substituting into (2.7) and simplifying gives

$$v_p(\theta) = \frac{3\sqrt{3}}{\pi}\hat{v}_i\left[\mathrm{Sin}[f(\theta_o)] + \sum_{p=1}^{\infty}\frac{1}{6p\pm1}\mathrm{Sin}[6p\theta_i+(6p\pm1)f(\theta_o)]\right] \qquad (2.8a)$$

Similarly, using $\alpha = -\pi/2 + f(\theta_o)$ gives the expression for v_n

$$v_n(\theta) = \frac{3\sqrt{3}}{\pi}\hat{v}_i\left[\mathrm{Sin}[f(\theta_o)] - \sum_{p=1}^{\infty}\frac{1}{6p\pm1}\mathrm{Sin}[6p\theta_i-(6p\pm1)f(\theta_o)]\right] \qquad (2.8b)$$

The choice of $f(\theta_o)$ largely determines the output voltage fundamental and its harmonic content. For a desired output voltage of $v_o = (3\sqrt{3}/\pi)\hat{v}_i r\mathrm{Sin}\theta_o$, the choice of $f(\theta_o) = \mathrm{Sin}^{-1}(r\mathrm{Sin}\theta_o)$ will yield the desired sinusoidal fundamental component. (This particular function for

$f(\theta_o)$ is referred to as the cosine wave method of control [17].)

Substitution of this modulating function into the expressions for v_p and v_n gives rise to the complex terms

$$\mathrm{Cos}[(6p\pm1)\mathrm{Sin}^{-1}(r\mathrm{Sin}\theta_o)] \tag{2.9a}$$

and

$$\mathrm{Sin}[(6p\pm1)\mathrm{Sin}^{-1}(r\mathrm{Sin}\theta_o)] \tag{2.9b}$$

which can be expressed as infinite-term Fourier series, and finite-term Fourier polynomials, respectively. The corresponding expressions for the coefficients, a_n and b_n will be functions of p, r and n, resulting in unwieldy expressions. These can be evaluated by computer and are tabulated in the literature [16][17]. Taking into account this specific choice of $f(\theta_o)$ then, gives the output of the positive converter as

$$v_p = \frac{3\sqrt{3}}{\pi}\hat{v}_i \left\{ r\mathrm{Sin}\theta_o + \frac{1}{2}\sum_{p=1}^{\infty} \left[+ \sum_{n=0}^{2n+1=6p+1} \frac{a(6p\pm1)_{2n+1}}{6p\pm1}\left(\mathrm{Sin}[6p\theta_i+(2n+1)\theta_o] - \mathrm{Sin}[6p\theta_i-(2n+1)\theta_o]\right) + \sum_{n=0}^{\infty} \frac{a(6p\pm1)_{2n}}{6p\pm1}\left(\mathrm{Sin}[6p\theta_i+2n\theta_o] + \mathrm{Sin}[6p\theta_i-2n\theta_o]\right)\right]\right\} \tag{2.10a}$$

and the output of the negative converter as

$$v_n = \frac{3\sqrt{3}}{\pi}\hat{v}_i \left\{ r\mathrm{Sin}\theta_o + \frac{1}{2}\sum_{p=1}^{\infty} \left[+ \sum_{n=0}^{2n+1=6p+1} \frac{a(6p\pm1)_{2n+1}}{6p\pm1}\left(\mathrm{Sin}[6p\theta_i+(2n+1)\theta_o] - \mathrm{Sin}[6p\theta_i-(2n+1)\theta_o]\right)\right.\right.$$

(continued...)

(...continued)

$$- \sum_{n=0}^{\infty} \frac{a(6p\pm1)_{2n}}{6p\pm1} \left[\mathrm{Sin}[6p\theta_i+2n\theta_o] + \mathrm{Sin}[6p\theta_i-2n\theta_o]\right]\Bigg\} \qquad (2.10b)$$

(The only difference being the sign reversal in the last summation.)

The final step is to account for the direction of current flow in the load, since this determines whether v_o is of the form v_p or v_n, at any instant, assuming that the thyristors carry current in only one direction. This can be expressed as

$$\begin{aligned} v_o &= v_p F_p(\theta_o) + v_n F_n(\theta_o) \\ &= v_p F_p(\theta_o) + v_n F_p(\theta_o-\pi) \end{aligned} \qquad (2.11)$$

where $F_p(\theta_o)$ is the bank selection signal, a unity amplitude square wave at the output frequency f_o.

Thus when $F_p(\theta_o) = 1$, $v_o = v_p$, and when $F_p(\theta_o) = 0$, $v_o = v_n$. In order to accommodate natural commutation, the phase of $F_p(\theta_o)$ must coincide with the phase of the load current fundamental ϕ_o. Expressing $F_p(\theta_o)$ and $F_n(\theta_o)$ as Fourier series gives

$$F_p(\theta_o) = \frac{1}{2} + \frac{2}{\pi} \sum_{m=0}^{\infty} \left[\frac{1}{2m+1} \mathrm{Sin}[(2m+1)(\theta_o+\phi_o)]\right] = \frac{1}{2} + F \qquad (2.12a)$$

and

$$\begin{aligned} F_n(\theta_o) &= F_p(\theta_o-\pi) \\ &= -\frac{1}{2} - \frac{2}{\pi} \sum_{m=0}^{\infty} \left[\frac{1}{2m+1} \mathrm{Sin}[(2m+1)(\theta_o+\phi_o)]\right] = \frac{1}{2} - F \end{aligned} \qquad (2.12b)$$

Combining (2.10), (2.11) and (2.12), and taking into consideration the minus sign difference between the last terms of (2.10a) and (2.10b), gives the desired analytic expression for the output voltage of a naturally commutated cycloconverter, composed of two 6-pulse bridge

converters:

$$v_o = \frac{3\sqrt{3}}{\pi}\hat{v}_i \left\{ r\,\mathrm{Sin}\theta_o + \frac{1}{2}\sum_{p=1}^{\infty} \left[\right. \right. \tag{2.13}$$

$$+ \sum_{n=0}^{2n+1=6p+1} \frac{a(6p\pm1)_{2n+1}}{6p\pm1} \left(\mathrm{Sin}[6p\theta_i+(2n+1)\theta_o] - \mathrm{Sin}[6p\theta_i-(2n+1)\theta_o] \right)$$

$$+ \frac{2}{\pi}\sum_{n=0}^{\infty}\sum_{m=0}^{\infty} \frac{1}{2m+1} \frac{a(6p\pm1)_{2n}}{6p\pm1} \left(+ \mathrm{Cos}[6p\theta_i+(2n-2m-1)\theta_o-(2m+1)\phi_o] \right.$$

$$- \mathrm{Cos}[6p\theta_i-(2n-2m-1)\theta_o+(2m+1)\phi_o]$$

$$- \mathrm{Cos}[6p\theta_i+(2n+2m+1)\theta_o+(2m+1)\phi_o]$$

$$\left. \left. + \mathrm{Cos}[6p\theta_i-(2n+2m+1)\theta_o-(2m+1)\phi_o] \right) \right] \Bigg\}$$

This expression is for one phase of the output. The other phases are shifted by $\pm 2\pi/3$. The first term is the desired output voltage and the rest are all harmonics, with the a_k coefficients as given in [16] and [17]. The first summation (over n) contains 4 Sin terms and the double summation (over n and m) contains 8 Cos terms, for 12 harmonic terms in total.

2.3.2 Graphical Interpretation of the Standard Output

The qualitative implications of these unwieldy equations are more clearly seen by plotting the results in three dimensions [18]. The 3-D plotting program used here greatly facilitates visualizing the interrelationships between the control parameters and the harmonic content of the output.

Considering firstly, the output of a phase-controlled rectifier,

one finds that the output harmonics are relatively simple, being multiples of the supply frequency and the pulse number (ie. $6nf_i$ for a 6-pulse rectifier). This was expressed mathematically in (2.7) where n, p and α determine the DC output voltage. For practical cycloconverters using natural commutation, the process of output voltage generation is essentially the same as for a phase controlled rectifier, except that there is now a continuous modulation of the phase angle α about the quiescent point $\alpha = \pi/2$, as in (2.8), and there is a switching between positive and negative rectifier banks every π radians at the output frequency f_o, as in (2.11). The depth of modulation of α determines the output to input voltage ratio r (which appears in (2.9)), and the frequency of modulation determines the frequency of the output voltage swings. The load current determines the angle ϕ_o at which current is transferred between positive and negative banks (2.12). For this reason, the output voltage harmonics are centered about the same basic harmonics of the corresponding 6-pulse rectifier (ie. $6nf_i$), but the continual variation of α at the output frequency f_o creates additional harmonics which beat at frequencies of $(6nf_i \pm (2m-1)f_o)$.

The variation of the average output voltage due to a time varying α, using the cosine control method, for the 6-pulse cycloconverter of Figure 2.2 is shown in Figure 2.3. The corresponding families of output harmonics are shown in Figure 2.5 and Figure 2.6.

In conjunction with the 3-D plots, the following observations can be made about the harmonic content of the naturally commutated cycloconverter output:

i) The unwanted frequency components (loosely referred to as

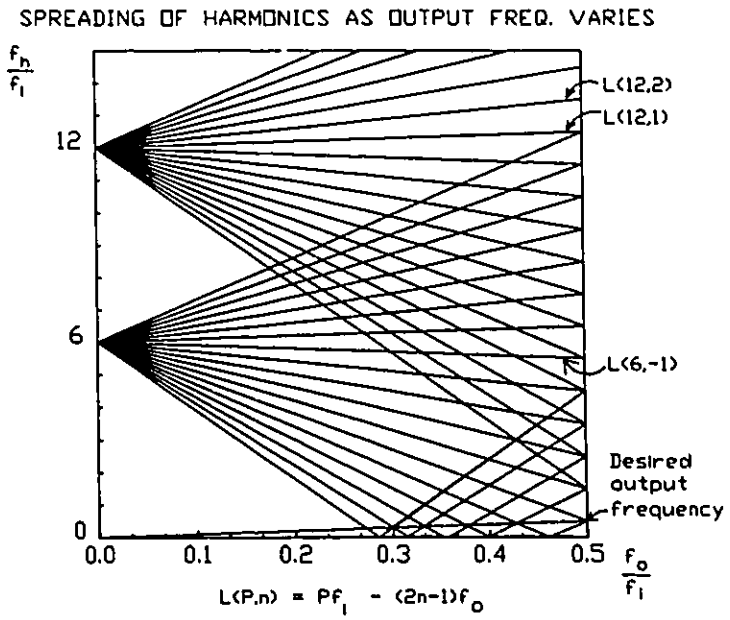

Figure 2.5 - OUTPUT HARMONICS OF A 6-PULSE CYCLOCONVERTER
The 3(2p-1) harmonic families have cancelled out.

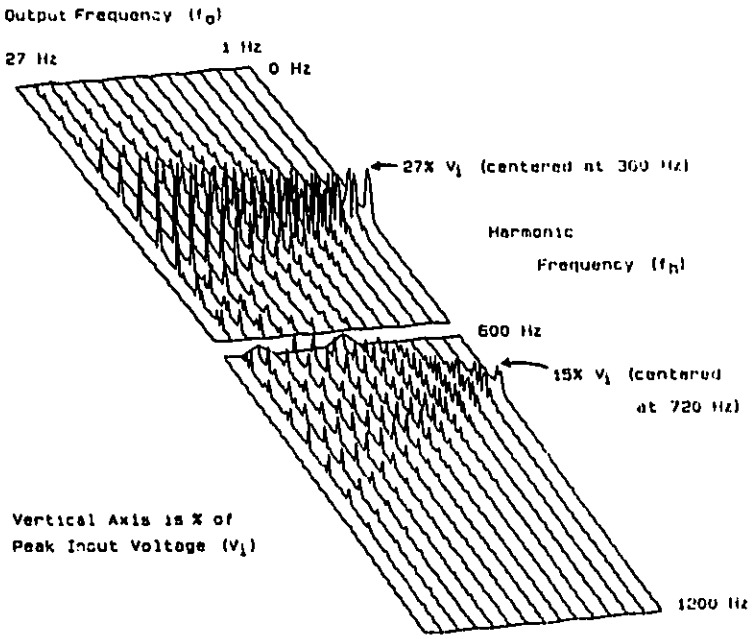

Figure 2.6 - 3-D PLOT OF 6-PULSE CYCLOCONVERTER HARMONIC SPECTRUM
Output frequency f_o = 1 to 27 Hz, r = 1, f_i = 60 Hz.

harmonics) vary in frequency, magnitude and phase as the output to input frequency ratio varies. However, they do follow 'lines' (as in Fig. 2.5) that have distinct characteristics.

ii) The 'spread' of the harmonic components in each family about their center frequency, $6nf_i$, is symmetric and is determined solely by the output to input frequency ratio. This is shown by the divergence of the lines from $6nf_i$ as f_o increases in Figure 2.5.

iii) The amplitude of each harmonic is constant along each line, but is affected by r and ϕ_o (as shown in Figure 2.7 and Figure 2.8). The lower side bands of the family $6f_i$ ($6nf_i$ with $n = 1$) are particularly bothersome because as f_o increases beyond $f_i/3$, they can intersect with the 5^{th} and 7^{th} harmonics of f_o as well as with the 11^{th} and 13^{th} harmonics. These are torque producing harmonics and can result in torque pulsations and unstable load operation.

iv) In general, reducing r increases the total energy content of the harmonics, but it also decreases the energy spread (Fig. 2.7). Therefore, the amplitude of harmonic lines near the center of each family increases in greater proportion as r is reduced. This aggravates the filtering problem by concentrating the harmonic energy in only a few bands. Fortunately, this also reduces interference with the 5^{th}, 7^{th}, 11^{th}, and 13^{th} load harmonics at small r, when the fundamental is also small.

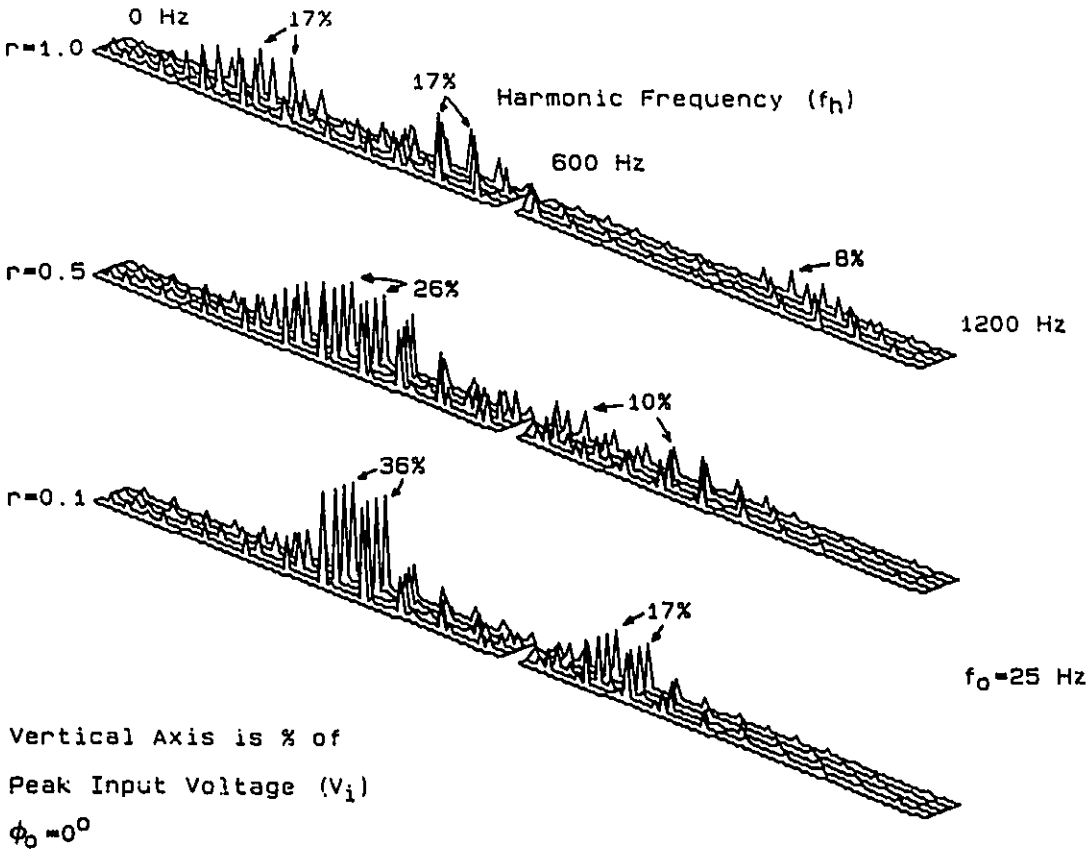

Figure 2.7 - VARIATION IN HARMONIC AMPLITUDE WITH OUTPUT VOLTAGE RATIO ($r = r$) - Reducing r increases the total amount of harmonic energy and concentrates it in a narrower band of frequencies.

NOTE: Each of the above 3 figures corresponds to output frequencies of 23, 25, 27, and 29 Hz. 'f_o = 25 Hz' therefore refers to the 'center' frequency of 25 Hz.

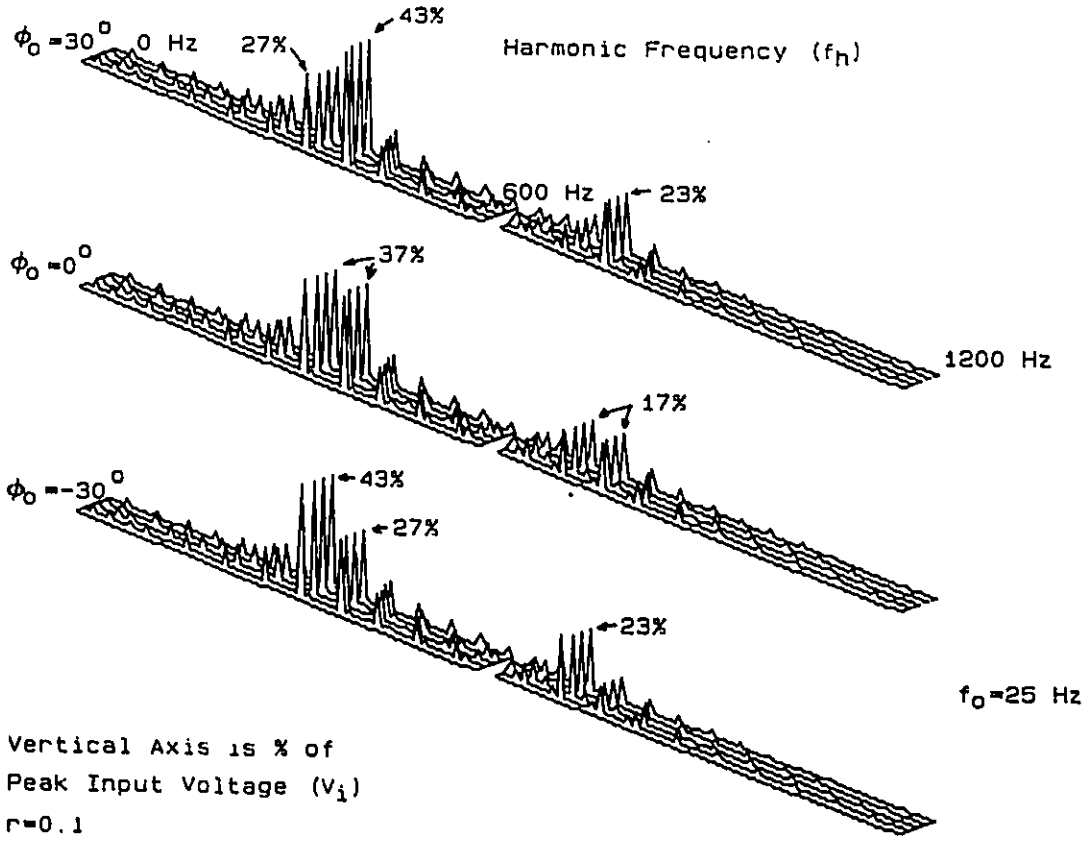

Figure 2.8 - VARIATION IN HARMONIC AMPLITUDE WITH LOAD CURRENT ANGLE (ϕ_o) - For lagging loads, $\phi_o < 0$ and the amplitude of the lower sideband harmonics increases with respect to the upper side band harmonics.
NOTE: Here again, 'f_o = 25 Hz' refers to the frequency of the 'center' line in each figure.

v) The polarity of the load current determines the choice of positive or negative converter operation at any instant. Additionally, each converter operates in the fast or slow switching modes according to whether v_o is increasing or decreasing. When v_p is in the fast switching mode, v_n is in the slow switching mode, and vice versa. However, the choice of v_p or v_n is determined by the load current angle ϕ_o, and so the percent of time that each converter operates in the fast or slow switching mode is dependent on ϕ_o.

The result is that for lagging loads ($\phi_o < 0$), the amplitude of the lower side bands

$$(6nf_i - (2m-1)f_o)$$

is higher than the amplitude of the upper side bands

$$(6nf_i + (2m-1)f_o)$$

since both converters operate longer in the slow switching mode (Fig. 2.8). This further aggravates interference of the output harmonics with the low (torque producing) harmonics of the load.

Considering the case of a motor load, to limit saturation in the iron cores the output voltage v_o (and thus r) is dictated by the motor speed (and therefore f_o). The output voltage and load (torque) conditions largely determine ϕ_o. As a result, the nature of the harmonic spectrum for a naturally controlled cycloconverter using standard control methods is strictly determined by the operating requirements of the load, and no control strategy is available to minimize or alter them

significantly.

This broad, load dependent nature of the harmonics, tends to defy practical filtering methods. At small r, the harmonic energy is concentrated in only a few large amplitude harmonics, requiring high component ratings and cost, to provide adequate filtering. On the other hand, since the harmonic frequencies shift greatly according to f_o, band pass filtering is also a very unwieldy solution.

2.4 Cycloconverter Harmonics with the New Jitter Control Method

2.4.1 Principles of the Jitter Method

Because of the very nature of the direct energy conversion process used in cycloconverters, harmonics can not be avoided. All that is required though, is that they be sufficiently controlled. Normally this means minimizing them or shifting them to other frequencies, but 'spreading' is also a legitimate solution.

For a given r, the total harmonic energy is essentially independent of the load angle ϕ_o or the spread about the lines $6nf_i$. Therefore, if additional harmonic components can be introduced in the converter output, without increasing the total harmonic energy produced, the possibility exists to reduce the peak amplitude of the largest components present, by redistributing the harmonic energy over a greater number of frequencies. The filtering problem can therefore be reduced or eliminated altogether.

The basic method is to introduce the additional angle δ into the firing angle of the thyristors, such that the basic $6nf_i$ pattern is broken up, thereby decreasing the amplitude of the harmonic components at

$$(6nf_i \pm (2m-1)f_o)$$

Since the power requirements necessitate natural commutation, PWM techniques are not possible. However, if the firing angle of alternate thyristors in the conduction sequence are advanced and retarded by the small angle δ, it will be shown that the average output voltage (the desired component, proportional to $r\mathrm{Sin}\theta_o$) will not be significantly affected, yet the harmonic content will be altered, producing a hitherto unattainable degree of freedom in the control of the cycloconverter. The desired improvement in harmonic performance can in fact be realized by an appropriate choice of δ, and this strategy is referred to as the Jitter method.

2.4.2 Derivation of the Jitter Control Method

With reference to Figure 2.4c, if a small angle δ is introduced into the firing angle α of the two 3-pulse converter groups, the expression for the modulating function $f(\theta_o)$ becomes

$$f(\theta_o) = \mathrm{Sin}^{-1}(r\mathrm{Sin}\theta_o) + \delta \qquad \text{for } v_a \text{ with } h(\theta) \tag{2.14a}$$

and

$$f'(\theta_o) = \mathrm{Sin}^{-1}(r\mathrm{Sin}\theta_o) - \delta \qquad \text{for } v_b \text{ with } h'(\theta) = h(\theta-\pi) \tag{2.14b}$$

Formerly, α was expressed (for v_a) as

$$\alpha = \frac{\pi}{2} - f(\theta_o) = \frac{\pi}{2} - \mathrm{Sin}^{-1}(r\mathrm{Sin}\theta_o) = \alpha_f$$

but now

$$\alpha = \frac{\pi}{2} - \mathrm{Sin}^{-1}(r\mathrm{Sin}\theta_o) - \delta$$

or simply

$$\alpha = \alpha_f - \delta$$

Therefore, $h_1(\theta_i-\alpha)$ (from (2.3) with k = 1) becomes $h_1(\theta_i-\alpha_f+\delta)$ for v_a and $h'(\theta_i-\alpha_f-\delta-\pi)$ for v_b. Expanding $h_1(\theta_i-\alpha_f+\delta)$ as a Fourier series gives

$$h_1(\theta_i-\alpha_f+\delta) = \frac{1}{3} + \sum_n \left[a_n\mathrm{Cos}[n(\theta_i-\alpha_f+\delta)] + b_n\mathrm{Sin}[n(\theta_i-\alpha_f+\delta)]\right] \quad (2.15)$$

or

$$h_1(\theta_i-\alpha_f+\delta) = \frac{1}{3} + \sum_n \left[a_n\left[\mathrm{Cos}[n(\theta_i-\alpha_f)]\mathrm{Cos}n\delta - \mathrm{Sin}[n(\theta_i-\alpha_f)]\mathrm{Sin}n\delta\right] + b_n\left[\mathrm{Sin}[n(\theta_i-\alpha_f)]\mathrm{Cos}n\delta + \mathrm{Cos}[n(\theta_i-\alpha_f)]\mathrm{Sin}n\delta\right]\right] \quad (2.16)$$

with $n = 2,4,8,10\ldots$ (for a_n), and $n = 1,5,7,11,13\ldots$ (for b_n). The coefficients b_n are given in (2.5) and the coefficients a_n are given as

$$\sum_n a_n = \frac{\sqrt{3}}{\pi}\sum_{p=1}^{\infty}(-1)^p\left[\frac{1}{3(2p-1)-1} + \frac{1}{3(2p-1)+1}\right] \quad (2.17)$$

However, when $h_1'(\theta_i-\alpha_f-\delta-\pi)$ is expanded, and then subtracted from $h_1(\theta_i-\alpha_f+\delta)$, to get v_p, as in

$$v_p = v_a + v_b = \sum_{k=1}^{3}\hat{v}_i\mathrm{Sin}[\theta_i-(k-1)\tfrac{2\pi}{3}] \times \left[h_k(\theta_i-(k-1)\tfrac{2\pi}{3} + \delta) - h_k'(\theta_i-(k-1)\tfrac{2\pi}{3} - \pi + \delta)\right] \quad (2.18)$$

the Cos terms no longer all cancel as they did in (2.4). Thus, $h_1(\theta_i-\alpha)$ now becomes

$$h_k(\theta_i-\alpha) = \frac{2\sqrt{3}}{\pi}\left\{\mathrm{Cos}\delta\,\mathrm{Sin}[\theta_i-\alpha_f-(k-1)\tfrac{2\pi}{3}]\right. \tag{2.19}$$

$$+\sum_{p=1}^{\infty}(-1)^p\left[\frac{\mathrm{Cos}[(6p\pm1)\delta]}{6p\pm1}\,\mathrm{Sin}[(6p\pm1)(\theta_i-\alpha_f-(k-1)\tfrac{2\pi}{3})]\right.$$

$$\left.\left.-\frac{\mathrm{Sin}[(3(2p-1)\pm1)\delta]}{3(2p-1)\pm1}\,\mathrm{Sin}[(3(2p-1)\pm1)(\theta_i-\alpha_f-(k-1)\tfrac{2\pi}{3})]\right]\right\}$$

Combining (2.19) with the 3 input voltages as in (2.1), gives

$$v_p = \frac{3\sqrt{3}}{\pi}\hat{v}_i\left\{\mathrm{Cos}\delta\,\mathrm{Sin}f(\theta_o)\right.$$

$$+\sum_{p=1}^{\infty}\frac{\mathrm{Cos}[(6p\pm1)\delta]}{6p\pm1}\left[\mathrm{Sin}[6p\theta_i+(6p\pm1)f(\theta_o)]\right]$$

$$\left.+\sum_{p=1}^{\infty}\frac{\mathrm{Sin}[3(2p-1)\pm1)\delta]}{3(2p-1)\pm1}\left[\mathrm{Cos}[3(2p-1)\theta_i+(3(2p-1)\pm1)f(\theta_o)]\right]\right\} \tag{2.20a}$$

The expression for v_n is

$$v_n = \frac{3\sqrt{3}}{\pi}\hat{v}_i\left\{\mathrm{Cos}\delta\,\mathrm{Sin}f(\theta_o)\right.$$

$$-\sum_{p=1}^{\infty}\frac{\mathrm{Cos}[(6p\pm1)\delta]}{6p\pm1}\left[\mathrm{Sin}[6p\theta_i-(6p\pm1)f(\theta_o)]\right]$$

$$\left.+\sum_{p=1}^{\infty}\frac{\mathrm{Sin}[3(2p-1)\pm1)\delta]}{3(2p-1)\pm1}\left[\mathrm{Cos}[3(2p-1)\theta_i-(3(2p-1)\pm1)f(\theta_o)]\right]\right\} \tag{2.20b}$$

With $f(\theta_o) = \mathrm{Sin}^{-1}(r\mathrm{Sin}\theta_o)$ as before, complex expressions result that must be simplified using infinite-term Fourier series and finite-term Fourier polynomials. These are the same as in (2.9), but with the addition of

$$\mathrm{Cos}[(3(2p-1)\pm1)\mathrm{Sin}^{-1}(r\mathrm{Sin}\theta_o)] \tag{2.21a}$$

and

$$\mathrm{Sin}[(3(2p-1)\pm1)\mathrm{Sin}^{-1}(r\mathrm{Sin}\theta_o)] \tag{2.21b}$$

Substitution into (2.20) gives

$$v_p = \frac{3\sqrt{3}}{\pi}\hat{v}_i \left[A + \frac{1}{2}\sum_{p=1}^{\infty}(B + C + D + E)\right] \tag{2.22a}$$

$$v_n = \frac{3\sqrt{3}}{\pi}\hat{v}_i \left[A + \frac{1}{2}\sum_{p=1}^{\infty}(B + C - D - E)\right] \tag{2.22b}$$

where

$$A = r\text{Cos}\delta\ \text{Sin}\theta_o \tag{2.23a}$$

$$B = \sum_{n=0}^{2n+1=6p+1} K_1 \left(\text{Sin}[6p\theta_i+(2n+1)\theta_o] - \text{Sin}[6p\theta_i-(2n+1)\theta_o]\right) \tag{2.23b}$$

$$C = \sum_{n=0}^{2n=3(2p-1)+1} K_2 \left(\text{Cos}[3(2p-1)\theta_i+2n\theta_o] + \text{Cos}[3(2p-1)\theta_i-2n\theta_o]\right) \tag{2.23c}$$

$$D = \sum_{n=0}^{\infty} K_3 \left(\text{Sin}[6p\theta_i+2n\theta_o] + \text{Sin}[6p\theta_i-2n\theta_o]\right) \tag{2.23d}$$

$$E = \sum_{n=0}^{\infty} K_4 \left(\text{Cos}[3(2p-1)\theta_i+(2n+1)\theta_o] - \text{Cos}[3(2p-1)\theta_i-(2n+1)\theta_o]\right) \tag{2.23e}$$

and where

$$K_1 = \frac{a(6p\pm1)_{2n+1}}{6p\pm1}\ \text{Cos}[(6p\pm1)\delta] \tag{2.24a}$$

$$K_2 = \frac{a(3(2p-1)\pm1)_{2n}}{3(2p-1)\pm1}\ \text{Sin}[(3(2p-1)\pm1)\delta] \tag{2.24b}$$

$$K_3 = \frac{a(6p\pm1)_{2n}}{6p\pm1}\ \text{Cos}[(6p\pm1)\delta] \tag{2.24c}$$

$$K_4 = \frac{a(3(2p-1)\pm1)_{2n+1}}{3(2p-1)\pm1}\ \text{Sin}[(3(2p-1)\pm1)\delta] \tag{2.24d}$$

and the a_k coefficients are the same as in [16] and [17].

Considering, finally, the bank switching function $F_p(\theta_o)$ as in (2.12), v_p and v_n can be combined to give, after cancelling terms, the

output for one phase of the naturally commutated 6-pulse bridge cycloconverter, with Jitter control, as

$$v_o = \frac{3\sqrt{3}}{\pi}\hat{v}_i \left[A + \frac{1}{2}(B + C) + F(D + E)\right] \tag{2.25}$$

where A, B, C, D and E are defined in (2.23) and F is from (2.12). This expands to give

$$\begin{aligned} v_o = \frac{3\sqrt{3}}{\pi}\hat{v}_i \Bigg\{ & r\cos\delta\sin\theta_o + \frac{1}{2}\sum_{p=1}^{\infty}\Bigg[\\ & + \sum_{n=0}^{2n+1=6p+1} K_1 \sin[6p\theta_i \pm (2n+1)\theta_o] + \sum_{n=0}^{2n=3(2p-1)+1} K_2 \cos[3(2p-1)\theta_i \pm 2n\theta_o] \\ & + \frac{2}{\pi}\sum_{n=0}^{\infty}\sum_{m=0}^{\infty}\frac{1}{2m+1}\Big[+ K_3\cos[6p\theta_i + (2n-2m-1)\theta_o - (2m+1)\phi_o] \\ & \qquad - K_3\cos[6p\theta_i + (2n+2m+1)\theta_o + (2m+1)\phi_o] \\ & \qquad + K_3\cos[6p\theta_i - (2n+2m+1)\theta_o - (2m+1)\phi_o] \\ & \qquad - K_3\cos[6p\theta_i - (2n-2m-1)\theta_o + (2m+1)\phi_o] \\ & \qquad + K_4\sin[3(2p-1)\theta_i + (2n+2m+2)\theta_o + (2m+1)\phi_o] \\ & \qquad - K_4\sin[3(2p-1)\theta_i + (2n-2m)\theta_o - (2m+1)\phi_o] \\ & \qquad - K_4\sin[3(2p-1)\theta_i - (2n-2m)\theta_o + (2m+1)\phi_o] \\ & \qquad + K_4\sin[3(2p-1)\theta_i - (2n+2m+2)\theta_o - (2m+1)\phi_o]\Big]\Bigg]\Bigg\} \end{aligned} \tag{2.26}$$

The first term is the fundamental, or desired component, of the output voltage. Note that, both '±' terms in K_1 to K_4 must be considered for each Cos or Sin term in this expression. After taking into account all the '±' terms therefore, there are 24 harmonic terms; 4 from each of the first 2 summations (over n), and 16 from the last summation (over n and m).

2.4.3 Interpretation of the Jitter Output

From Section 2.3.1, recall that when 3-pulse converters are configured to give converters with higher pulse numbers, certain families of harmonics exactly cancel, while the remaining families do not change in amplitude.

As an example, consider a 6-pulse bridge converter composed of two series-connected 3-pulse converters, where SCR's 1,3,5 produce v_a and SCR's 2,4,6 produce v_b as shown in Figure 2.2 and Figure 2.4a. In this case, v_a and v_b sum to give v_p, the output of the positive current converter (Fig. 2.4b). For a steady state, or DC, output, if the respective 3-pulse converters are fired such that

$$\alpha_p + \alpha_n = 180^o \tag{2.27}$$

then the harmonic families

$$3(2n-1)f_i$$

will exactly cancel and the output will be as shown in Figure 2.4b. This is the standard method of control for a 6-pulse converter. To understand the Jitter control method, consider the effect of jittering the firing angle 'to and fro' by δ, effectively shifting the phase angle of each converter either forward or backwards. Thus, if

$$\alpha_p' = \alpha_p + \delta \tag{2.28a}$$

and

$$\alpha_n' = \alpha_n - \delta \tag{2.28b}$$

then

$$\alpha_p' + \alpha_n' = 180^o \tag{2.29}$$

and the average output voltage remains the same. However the $3(2n-1)f_i$ families will no longer be exactly 180^o out of phase and won't completely cancel each other. The $6nf_i$ pattern is broken and harmonic energy is again present in the output in the families $3(2n-1)f_i$. The waveform will now be as in Figure 2.4c.

Since the two 3-pulse converter groups are not controlled with $\alpha_p + \alpha_n = 180^o$ (2.27), the harmonic terms in the families $6nf_i$ also experience phase shifts between their constituent terms, and as a result, there is a reduction in their amplitudes as well. This is the heart of the Jitter method; by phase shifting the two 3-pulse groups slightly with respect to each other, phase shifts are introduced which reduce the amplitudes of the standard 6-pulse harmonic families by more than the amplitudes of the reintroduced (or now not quite cancelled) 3-pulse harmonic families. This is the desired result.

Examination of the $Cos\delta$ and $Sin\delta$ terms in (2.24) and (2.26) show how for small δ (ie. 10^o) the effect on the fundamental, or wanted output component, is slight. However, the $6f_i$ families are reduced by 34% or 64% from their normal 6-pulse amplitudes, while the newly introduced $3(2p-1)$ families are only 34% of their normal 3-pulse amplitude (which would be present in separate 3-pulse converters). With $\delta = 0$, K_2 and K_4 become zero and (2.26) reduces to the standard cyclo-converter output of (2.13).

If the value of δ becomes large, then the fundamental amplitude decreases according to $Cos\delta$, as would be expected for a phase-shift voltage control scheme, and the $3(2p-1)f_i$ harmonic families soon predominate, as in a 3-pulse system. Further, for a naturally commutated

cycloconverter, the practical value of δ must be restricted to the range during which natural commutation can occur. A value of 30^{o} is a reasonable upper limit, but 15^{o} is appropriate to minimize the effect on the fundamental. On the other hand, if the cycloconverter input voltage $\hat{v}_i$ is raised by the percentage $\cos\delta$, then there will be no change in $\hat{v}_o$ with the Jitter method.

Figure 2.9 shows the harmonics present using Jitter control with $f_o = 25$ Hz and $\delta = 10^{o}$. Comparison with Figure 2.7 shows clearly the reduction in the amplitude of the largest harmonics, and the more even distribution of the harmonic energy across the spectrum.

The problem of the lower side band harmonics, which occur in the range of the lower order harmonics of the output frequency (i.e. $5f_o$, $7f_o$, $11f_o$, $13f_o$), is accentuated somewhat by the introduction of the $3(2p-1)f_o$ harmonic families. Another novel control method, referred to as 'frequency hopping', has been developed for the case of the double fed motor to prevent the lower side band frequencies

$$6nf_i - (2n-1)f_o$$

from interfering with the torque producing harmonics of the output frequency. This method is well suited to dealing with interference by the $3(2p-1)f_i$ family as well, and as such, strikes directly at the practical upper frequency limitation of the naturally commutated cycloconverter (see Section 4.3).

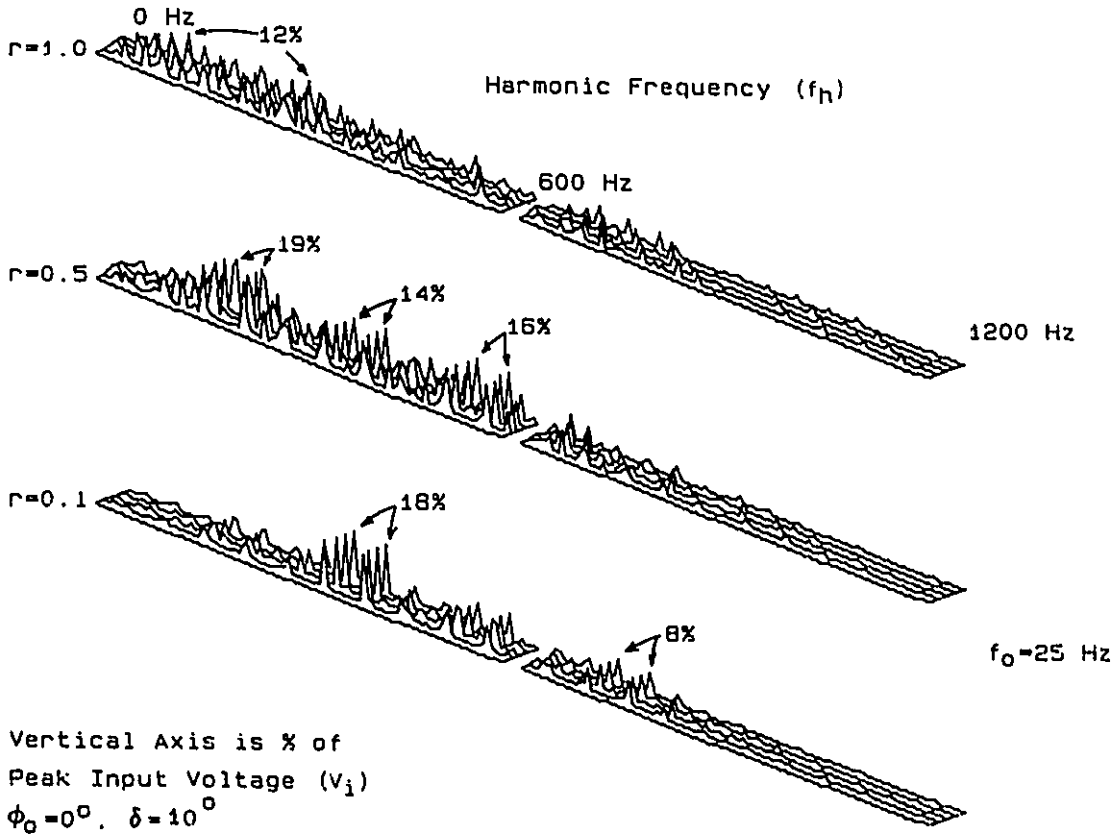

Figure 2.9 - CYCLOCONVERTER OUTPUT SPECTRUM WITH JITTER CONTROL
The small jitter angle δ effectively spreads the output harmonics over a greater number of frequencies, reducing both the total and peak harmonic energy.
NOTE: r = r, and f_o = 25 Hz refers to the 'center' line in each the three figures.

2.5 Summary

With normal firing control methods for naturally commutated cycloconverters, the frequencies and amplitudes of the unwanted harmonic energy components vary with frequency, and are essentially determined by the operating requirements of the load. Filtering is generally impractical due to the high powers involved and the frequency variation of the harmonics themselves.

By introducing a small 'Jitter' in the firing control circuit, the firing angle of the thyristors (in alternate 3-pulse banks) can be varied by the small angle δ. This has little affect on the desired output voltage but effectively spreads the harmonic energy over more frequency components in the spectrum. This very desirable effect reduces the filtering requirements of the cycloconverter.

CHAPTER 3

DOUBLE FED MOTOR THEORY

3.1 Introduction - Rotating Machine Analysis

Common to all rotating machines is the air gap between the stator and rotor circuits, which permits relative motion to exist between their respective magnetic circuits. Whenever an incremental rotation of the rotor circuits will reduce the total flux linkage in the machine, then a mechanical torque will be present between the stator and rotor. By continual mechanical realignment of the conduction paths in the rotor, or by changing the phase angle of the electrical currents that produce the magnetic fluxes, it is possible to continually advance the angle where the minimum reluctance occurs. As a consequence, the rotating machine is able to maintain a constant torque while rotating, and thereby continuously convert power between electrical and mechanical forms.

Rotating machines also make possible the direct transformation of electrical energy from one frequency to another. Within the air gap, the relative motion between the air gap flux and some of the windings of the machine results in a time varying flux, whose frequency is, in part, proportional to the relative motion between the flux and the conductors.

The fluxes can be generated by either constant or time varying electric currents, and this leads to the different classes of machine; the DC, the AC synchronous, and the AC asynchronous (induction) machines.

Traditionally, each of these machines is analyzed in a somewhat different manner. Although this has been expedient for various reasons (ie. simplicity), the resulting equations and system models appear quite different. Much work has been done to unify the theory and to represent all rotating machines with a common model. Without going into detail at this point (since it is outside the scope of this thesis), it is sufficient to note merely that, with respect to what occurs within the air gap, all rotating machines are simplifications of a general case: the double fed wound rotor machine (DFM).

The double fed motor can have currents of independent frequency supplied to the stator and rotor windings. In general, their magnitudes and phase can also be varied, and electrical power can be supplied to (or taken from) either (or both) of the stator and rotor circuits. This allows for the greatest freedom of control and for the maximum energy conversion capability for a given machine size.

As discussed in Chapter 1, the development of static variable frequency power supplies, with ever increasing ratings, has led to great improvements in the control of both AC and DC machines. There are many cases though, where the high harmonic content at low frequency, the limited frequency range, or the inability to precisely control the phase of the rotating electric flux impose limits on drive power or performance.

Chapter 1 outlined how application of two cycloconverters to a

double fed wound rotor machine presents a unique opportunity to advance the limits of control, power and/or economy in traction drive systems. Chapter 2 dealt with an analysis of cycloconverter output harmonics and a novel method to minimize them, thus improving performance. It is expedient now to look at the theory of the double fed motor and to analyze the production of torque and flux in relation to the terminal conditions; namely the stator and rotor voltages, the stator and rotor currents, and the rotor speed.

In addition, a powerful interactive plotting program (DFMPLT) was written to simulate the double fed motor, and to serve as a design tool for developing suitable control equations. Section 3.3 describes this program and focuses on the graphical interpretation of the results, using the circle diagram of the double fed motor. This leads to development of the rotating flux equation and implications on the controllability of the DFM system. These will be discussed in Chapter 4.

3.2 DFM Equivalent Circuit and Torque Expression

3.2.1 Definition of Terms

subscript 1 = stator
subscript 2 = rotor

For stator coils 1a, 1b and 1c:

r_1 = stator resistance
ℓ_{s1} = stator self-inductance
m_1 = stator mutual inductance
$\ell_1 \triangleq \ell_{s1} - m_1$ = stator cyclic inductance
u_{1a}, u_{1b}, u_{1c} = balanced 3-phase stator voltages
i_{1a}, i_{1b}, i_{1c} = balanced 3-phase stator currents

For rotor coils 2a, 2b and 2c:

r_2 = rotor resistance
ℓ_{s2} = rotor self-inductance
m_2 = rotor mutual inductance
$\ell_2 \Delta \ell_{s2} - m_2$ = rotor cyclic inductance
u_{2a}, u_{2b}, u_{2c} = balanced 3-phase rotor voltages
i_{2a}, i_{2b}, i_{2c} = balanced 3-phase rotor currents

Also

$m_{ij}(\theta)$ = stator-rotor mutual inductance (see Figure 3.1)
$\hat{m}$ = proportionality constant
θ = rotor angle (mechanical, of coil 1a w/respect to coil 2a)
θ_o = rotor initial position (mechanical)
ω, Ω = stator,rotor angular frequency (electrical)
F_1, F_2 = stator,rotor electrical frequency (in Hz)
Ω_s = rotor angular velocity (electrical)
W = rotor speed (in electrical rps)
n = rotor speed (mechanical rpm)
$s \Delta \Omega/\omega = F_2/F_1$ = slip
P = the number of poles
Γ = torque developed

$\hat{i}_1$, $\hat{i}_2$ = peak stator,rotor current
δ_i = angle between stator and rotor current phasers
$\hat{u}_1$, $\hat{u}_2$ = peak stator,rotor voltage
$\psi = \delta_v$ = angle between the stator and rotor voltage phasers (also referred to as the pseudo torque angle)
Φ = flux in a coil
V_1, V_2 = stator,rotor voltage phasers
I_1, I_2 = stator,rotor current phasers
R_1, R_2 = stator,rotor resistance (per phase)
X_1, X_2 = stator,rotor self-inductance (per phase)
X_m = stator-rotor mutual inductance (per phase)
α = stator electrical phase angle
β = rotor electrical phase angle
$P_1 = \phi_1$ = angle between the stator voltage and current
$P_2 = \phi_2$ = angle between the rotor voltage and current

3.2.2 Derivation of the DFM Equivalent Circuit

The following is a summary of the DFM model equations developed in my Master's thesis [3]. They are included here for completeness, along with a qualitative interpretation of their implications.

The analysis assumes balanced steady state operation, sinusoidal

voltages and currents (with linear flux-current relationships) and negligible iron losses. Although this is never the case in reality, it greatly facilitates modelling of the DFM system, and the determination of its basic operating characteristics. (More accurate non-linear models can later be applied, if necessary, for control purposes.) On this basis, the stator and rotor self and mutual inductances, and the stator-rotor mutual inductances, are all defined. In addition, the stator-rotor mutual inductances are assumed to vary as the cosine of the angle θ between any two coils. This gives rise to the relationships found in Figure 3.1. (For $P \neq 2$, replace θ by $\frac{P}{2}\theta$, where θ is the mechanical rotor angle.)

		Stator Coil i		
		1a	1b	1c
Rotor Coil j	2a	$m_{aa} = \hat{m}\cos\theta$	$m_{ba} = \hat{m}\cos(\theta - \frac{2}{3}\pi)$	$m_{ca} = \hat{m}\cos(\theta + \frac{2}{3}\pi)$
	2b	$m_{ab} = \hat{m}\cos(\theta + \frac{2}{3}\pi)$	$m_{bb} = \hat{m}\cos\theta$	$m_{cb} = \hat{m}\cos(\theta - \frac{2}{3}\pi)$
	2c	$m_{ac} = \hat{m}\cos(\theta - \frac{2}{3}\pi)$	$m_{bc} = \hat{m}\cos(\theta + \frac{2}{3}\pi)$	$m_{cc} = \hat{m}\cos\theta$

(for P = 2)

Figure 3.1 - STATOR-ROTOR MUTUAL INDUCTANCE $m_{ij}(\theta)$

Example: $m_{ab} = m_{1a2b}(\theta) = \hat{m}\cos(\theta + \frac{2}{3}\pi)$

The stator and rotor voltages are known, and are assumed to be controllable in frequency, magnitude and phase. The resultant currents in the stator and rotor are to be determined, as well as the resulting torque over the entire speed range.

There exists in any polyphase machine, a fixed relationship between the stator and rotor electrical frequencies and the angular velocity of the rotor. This is true whether the rotor currents are induced at the slip frequency, as in an induction machine, created by a rotating DC field, as in a synchronous machine, or produced by an external polyphase supply, as is possible with a wound rotor induction machine.

As it applies to the wound rotor induction machine, the term 'induction' is really a misnomer, in so far as it implies that the rotor currents are 'induced' by the flux variations cutting the rotor windings due to the rotor slip. This is true for an induction machine, since these induced currents provide power to the rotor windings and maintain the rotor field. On a double fed machine though, the rotor power is independently supplied, apart from interaction with the rotating fluxes. If the fundamental components of the stator and rotor rotating fields are synchronized, then the DFM is more appropriately termed a 3-phase excited synchronous machine.

When the DFM is synchronized, the stator and rotor currents combine to produce a fundamental flux which is sinusoidally distributed around the air gap (according to the number of pole pairs) and which rotates at a frequency proportional to the stator supply frequency. The corresponding rotor angular speed will be proportional to the sum (or difference) of the stator and rotor electrical frequencies. That is

$$\Omega_s = \omega - \Omega \tag{3.1}$$

In terms of n, the rotor rpm, this relationship is scaled by the number of poles P to give

$$n = 60 \frac{2}{P} \frac{\Omega_s}{2\pi} = 60 \frac{2}{P} \frac{\omega - \Omega}{2\pi} = 60 \frac{2}{P} W \tag{3.2}$$

Since $\omega = 2\pi F_1$, $\Omega = 2\pi F_2$ and $\Omega_s = 2\pi W$, the rotor speed can also be expressed in terms of its mechanical frequency (in electrical degrees) as

$$W = F_1 - F_2 \tag{3.3}$$

The basis of these frequency relationships is the requirement that the phase angle between the stator and rotor fluxes must also be constant to produce a steady torque (at any speed). Therefore, the rotor position θ must be known in order to coordinate the stator and rotor fluxes. The rotor position is related to the stator and rotor angular frequencies by the relationship

$$\frac{d\theta}{dt} = \frac{2}{P} (\omega - \Omega) = \frac{2}{P} \Omega_s \tag{3.4}$$

For $P = 2$, after integrating, the rotor angular position θ is given as

$$\theta = (\omega - \Omega)t + \theta_o \tag{3.5}$$

or

$$\theta = \alpha - (\beta + \psi) + \theta_o \tag{3.6}$$

where $\alpha = \omega t$ and $\beta + \psi = \Omega t$ are the phase angles of the stator and rotor voltages, and θ_o compensates for the rotor offset at $t = 0$ and/or the offset due to the position of the angular transducer used to sense θ (Section 5.4.3).

The stator and rotor voltages are defined as:

$$u_{1a} = \hat{u}_1 \cos(\omega t) \qquad \text{(where } u_{1a} = \Delta \bar{u}_1 \text{ also)} \tag{3.7a}$$

$$u_{1b} = \hat{u}_1 \cos(\omega t - \tfrac{2}{3}\pi) \tag{3.7b}$$

$$u_{1c} = \hat{u}_1 \cos(\omega t + \tfrac{2}{3}\pi) \tag{3.7c}$$

$$u_{2a} = \hat{u}_2 \cos(\Omega t + \psi) \tag{3.8a}$$

$$u_{2b} = \hat{u}_2 \cos(\Omega t + \psi - \tfrac{2}{3}\pi) \tag{3.8b}$$

$$u_{2c} = \hat{u}_2 \cos(\Omega t + \psi + \tfrac{2}{3}\pi) \tag{3.8c}$$

where

$\hat{u}_1$, $\hat{u}_2$ - peak stator, peak rotor voltage respectively

ψ - phase shift between the stator and rotor supply voltages at t = 0

Using the cyclic inductances, the instantaneous voltage across stator coil '1a' can be expressed in terms of the stator and rotor currents as

$$u_{1a} = r_1 i_{1a} + \frac{d}{dt}\ell_1 i_{1a} + \frac{d}{dt}\left(m_{aa} i_{2a} + m_{ab} i_{2b} + m_{ac} i_{2c}\right) \tag{3.9a}$$

and across rotor coil '2a' as

$$u_{2a} = r_2 i_{2a} + \frac{d}{dt}\ell_2 i_{2a} + \frac{d}{dt}\left(m_{aa} i_{1a} + m_{ba} i_{1b} + m_{ca} i_{1c}\right) \tag{3.10a}$$

The other stator and rotor voltage equations (3.9b), (3.9c), (3.10b), (3.10c) are similar, except for phase shifts of $2\pi/3$ and $4\pi/3$ as in (3.7) and (3.8).

The stator and rotor currents are similarly defined as:

$$i_{1a} = \hat{i}_1 \cos(\omega t - \phi_1) \tag{3.11a}$$

$$i_{1b} = \hat{i}_1 \cos(\omega t - \phi_1 - \tfrac{2}{3}\pi) \tag{3.11b}$$

$$i_{1c} = \hat{i}_1 \cos(\omega t - \phi_1 + \tfrac{2}{3}\pi) \tag{3.11c}$$

$$i_{2a} = \hat{i}_2 \cos(\Omega t + \psi - \phi_2) \tag{3.12a}$$

$$i_{2b} = \hat{i}_2 \cos(\Omega t + \psi - \phi_2 - \tfrac{2}{3}\pi) \tag{3.12b}$$

$$i_{2c} = \hat{i}_2 \cos(\Omega t + \psi - \phi_2 + \tfrac{2}{3}\pi) \tag{3.12c}$$

where

$\hat{i}_1$, $\hat{i}_2$ - peak stator, peak rotor current respectively

ϕ_1, ϕ_2 - the phase shift between the stator voltage and current and between the rotor voltage and current respectively

Substituting the rotor current expressions (3.12) into the stator voltage equations (3.9) and using $\theta + \Omega t = \omega t + \theta_o$ from (3.5) transforms the rotating mutual inductance terms ($m_{aa} i_{2a}$ of Figure 3.1

ctc.) into the stationary stator reference frame. Likewise, substituting the stator current expressions (3.11) into the rotor voltage equations (3.10) and using (3.5) transforms the stationary mutual inductance terms ($m_{aa}i_{1a}$ etc.) into the rotating rotor reference frame. This gives

$$u_{1a} = r_1 i_{1a} + \frac{d}{dt}\ell_1 i_{1a} + \frac{d}{dt}\frac{3}{2}\hat{m}\hat{i}_2\cos(\omega t + \psi - \phi_2 + \theta_o) \qquad (3.13a)$$

$$u_{2a} = r_2 i_{2a} + \frac{d}{dt}\ell_2 i_{2a} + \frac{d}{dt}\frac{3}{2}\hat{m}\hat{i}_1\cos(\Omega t - \phi_1 - \theta_o) \qquad (3.14a)$$

Then, substituting the stator and rotor current expressions (3.11) and (3.12) into the respective stator and rotor voltage equations (3.13) and (3.14) yields, for coils '1a' and '2a'

$$u_{1a} = r_1\hat{i}_1\cos(\omega t - \phi_1) + \frac{d}{dt}\left[\ell_1\hat{i}_1\cos(\omega t - \phi_1) + \frac{3}{2}\hat{m}\hat{i}_2\cos(\omega t + \psi - \phi_2 + \theta_o)\right] \qquad (3.15a)$$

$$u_{2a} = r_2\hat{i}_2\cos(\Omega t + \psi - \phi_2) + \frac{d}{dt}\left[\ell_2\hat{i}_2\cos(\Omega t + \psi - \phi_2) + \frac{3}{2}\hat{m}\hat{i}_1\cos(\Omega t - \theta_o - \phi_1)\right] \qquad (3.16a)$$

It is desirable to transform the rotor equations (3.16) from the rotor frequency Ω to the stator frequency ω so that all the currents can be represented on a single phaser diagram at the stator frequency ω. This transformation seems to eliminate the rotational effect of the air gap though, along with the corresponding mechanical-electrical power conversion that takes place. This is taken into account by treating the reactive and passive components of the system differently, so as to introduce a term that represents the mechanical energy transferred by the shaft.

In (3.15) and (3.16), the cosine terms represent the circuit parameters which are frequency sensitive. For these, a change from Ω to ω merely requires a scaling factor of Ω/ω. That is, adjusting the rotor voltage proportional to the new rotor frequency results in the same reactive rotor current magnitudes and the same resultant torque component. On the other hand, the resistive elements require no transformation or scaling. However, the mechanical power is proportional to the slip s and since $s = \Omega/\omega$, it is clear that this is the same scaling factor that is required to transform the reactive elements of the system to the stator frequency. Therefore, multiplying all the rotor terms by s yields a fictitious rotor voltage u_2/s. When applied to the resistive terms, this results in a new power term, with the difference representing the mechanical shaft power. Therefore, considering u_1 and u_2 to represent the stator and rotor voltages respectively, the per phase representation of the double fed motor is

$$u_1 = r_1\hat{i}_1\cos(\omega t - \phi_1) + \frac{d}{dt}\left[\ell_1\hat{i}_1\cos(\omega t - \phi_1) + \frac{3}{2}\hat{m}\hat{i}_2\cos(\omega t + \psi - \phi_2 + \theta_o)\right] \tag{3.17}$$

and

$$\frac{u_2}{s} = \frac{r_2}{s}\hat{i}_2\cos(\omega t + \psi - \phi_2 + \theta_o) + \frac{d}{dt}\left[\ell_2\hat{i}_2\cos(\omega t + \psi - \phi_2 + \theta_o) + \frac{3}{2}\hat{m}\hat{i}_1\cos(\omega t - \phi_1)\right] \tag{3.18}$$

Using $\Omega t = \omega t + \theta_o$ (from (3.5), with $\theta = 0$) gives

$$u_2' = \hat{u}_2\cos(\omega t + \psi + \theta_o) \tag{3.19}$$

and similarly, from (3.12a)

$$i_2' = \hat{i}_2\cos(\omega t + \psi - \phi_2 + \theta_o) \tag{3.20}$$

In terms of phasers, using the stator voltage $\bar{u}_1$ (3.7a) as a reference, the rotor quantities can now be expressed at the stator frequency ω as

$$\frac{\bar{u}_2'}{s} = \frac{\bar{u}_2''}{s} e^{j(\theta_o + \psi)} = \frac{\bar{u}_2}{s} e^{j\theta_o} \tag{3.21}$$

and

$$\bar{i}_2' = \bar{i}_2 e^{j\theta_o} \tag{3.22}$$

This, then, gives the basic single-phase model for the double fed machine (Fig. 3.2) as:

$$\bar{u}_1 = (r_1 + j\omega\ell_1)\bar{i}_1 + \frac{3}{2}\hat{m}j\omega\bar{i}_2' \tag{3.23}$$

$$\frac{\bar{u}_2'}{s} = (\frac{r_2}{s} + j\omega\ell_2)\bar{i}_2' + \frac{3}{2}\hat{m}j\omega L\bar{i}_1 \tag{3.24}$$

It is convenient to use the following transformations (3.25)

$$\begin{aligned} V_1 &= \bar{u}_1 & V_2 &= K\bar{u}_2' \\ I_1 &= \bar{i}_1 & I_2 &= \frac{1}{k}\bar{i}_2' \\ R_1 &= r_1 & R_2 &= k^2 r_2 \\ X_1 &= \omega(\ell_1 - \frac{3}{2}k\hat{m}) & X_2 &= \omega(k^2\ell_2 - \frac{3}{2}k\hat{m}) \\ X_m &= \frac{3}{2}k\hat{m}\omega & k &= K \end{aligned} \tag{3.25}$$

and the model is now given by Figure 3.3, (3.26) and (3.27) [3].

$$V_1 = \left(R_1 + j(X_1 + X_m)\right)I_1 + jX_m I_2 \tag{3.26}$$

$$\frac{V_2}{s} = \left(\frac{R_2}{s} + j(X_2 + X_m)\right)I_2 + jX_m I_1 \tag{3.27}$$

3.2.3 Derivation of the DFM Torque Expression

The torque expression is developed from the basic torque

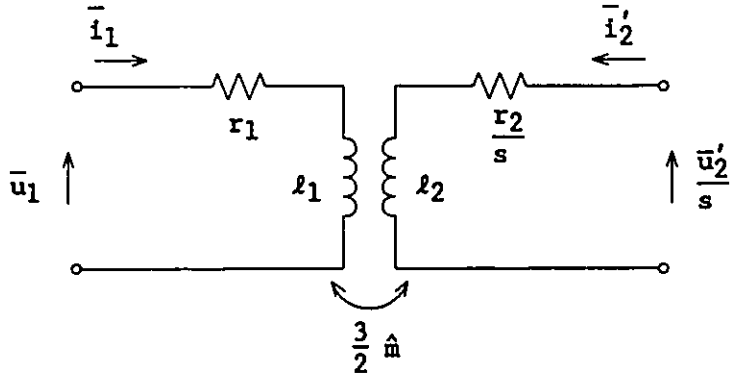

Figure 3.2 - EQUIVALENT CIRCUIT FOR THE DOUBLE FED MACHINE

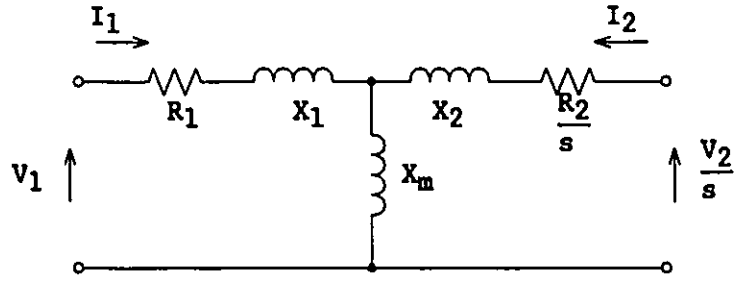

Figure 3.3 - MODIFIED EQUIVALENT CIRCUIT FOR THE DFM

relationship

$$\gamma = i \frac{\partial \Phi}{\partial \theta} \tag{3.28}$$

where γ is the incremental torque, due to the virtual movement $d\theta$ of a coil carrying current i, and Φ is the flux linking the coil.

The steady-state voltage u_{2a} across rotor coil '2a' is

$$u_{2a} = \hat{u}_2 \cos(\Omega t + \psi) = (r_2 + \ell_2 \frac{d}{dt}) i_{2a} + \frac{d\Phi_{2a1}}{dt} \tag{3.29}$$

where

$$\Phi_{2a1} = \frac{3}{2} \hat{m}\hat{i}_1 \cos(\Omega t - \theta_o - \phi_1) \tag{3.30}$$

is the flux in rotor coil '2a' due to the currents in the stator coils (1a, 1b, and 1c). But $\omega t - \theta = \Omega t - \theta_o$, from (3.5), and noting that

$$\frac{d\Phi_{2a1}}{dt} = \frac{\partial \Phi_{2a1}}{\partial t} + \frac{d\theta}{dt} \frac{\partial \Phi_{2a1}}{\partial \theta} \tag{3.31}$$

then (3.29) becomes, after simplification, the steady state voltage expressed in terms of the incremental movement $d\theta$ of the rotor. Thus

$$u_{2a} = r_2 i_{2a} + \ell_2 \frac{di_{2a}}{dt} - \Omega \frac{\partial \Phi_{2a1}}{\partial \theta} \tag{3.32}$$

Now the torque on rotor coil '2a' is

$$\gamma_{2a1} = i_{2a} \frac{\partial \Phi_{2a1}}{\partial \theta} \tag{3.33}$$

where Φ_{2a1} is the flux in rotor coil '2a' due to the currents in the 3 stator coils. Therefore, the total torque Γ on all three rotor coils combined is

$$\Gamma = \gamma_{2a1} + \gamma_{2b1} + \gamma_{2c1} \tag{3.34}$$

In terms of power, multiplying both sides of (3.32) by the coil current

i_{2a} gives

$$i_{2a}u_{2a} = (i_{2a})^2 r_2 + i_{2a}\ell_2 \frac{di_{2a}}{dt} - \Omega\gamma_{2a1} \tag{3.35}$$

Summing (3.35) with similar expressions for $i_{2b}u_{2b}$ and $i_{2c}u_{2c}$ gives, after simplification, the torque equation for the double fed motor.

$$\Gamma = \frac{3}{2} \frac{r_2\hat{i}_2^2 - \hat{u}_2\hat{i}_2\cos\phi_2}{\Omega} \tag{3.36}$$

This shows that the torque Γ is in fact determined by

$$\Gamma = \frac{\text{rotor joule losses - elect. power entering the rotor}}{\text{rotor angular frequency}} \tag{3.37}$$

The synchronous power $\omega\Gamma$ is therefore

$$\omega\Gamma = \frac{3}{2}\left(\hat{i}_2^2[\frac{r_2}{s}] - [\frac{\hat{u}_2}{s}]\hat{i}_2\cos\phi_2\right) \tag{3.38}$$

In terms of stator quantities (taking into account the reversal of sign when referring torque to the stator reference frame) the torque can also be expressed as

$$\omega\Gamma = \frac{3}{2}\left(\hat{u}_1\hat{i}_1\cos\phi_1 - \hat{i}_1^2 r_1\right) \tag{3.39}$$

In this manner, the steady-state torque in the double fed machine can be calculated from the terminal voltages and currents.

3.3 Double Fed Motor Circle Diagram

Section 3.3.1 reviews the double fed motor circle diagram and the basic relationships between the operating point and the developed torque and speed of the machine. Being a graphical method, the circle

diagram is outdated as a useful computational tool for motor design or control purposes. However, for developing an intuitive grasp of the complex relationships between voltages, currents, frequencies, speed and torque in the double fed machine, it is without equal. For this reason, an interactive plotting program has been developed (Section 3.3.2) to study these relationships. Section 3.3.3 provides an interpretation of the results.

3.3.1 Derivation of the DFM Circle Diagram and the DFM Torque Line

The standard circle diagram can be extended for the double fed machine by using superposition, since the model was derived assuming linearity. This is shown in Figure 3.4, with the following observations.

Circle C1 is the locus of the current vector I_{1s}, the stator current resulting from the stator voltage, as the slip s is varied from $-\infty$ to $+\infty$. The center and radius of C1 are determined from (3.26) and (3.27) with the rotor voltage $V_2 = 0$, as in a single fed induction machine. The stator voltage V_1 scales both axis equally, and for each value of slip there exists a unique point on the locus of C1. This point determines the speed of the rotor and is called the basepoint BP.

For the double fed case, the rotor voltage V_2 is non-zero and introduces a second stator current component I_{1r}, the stator current due to the rotor voltage. The magnitude of I_{1r} is determined by the magnitude of the rotor voltage V_2 and its phase is determined by the relative phase angle δ_v ($\delta_v \Delta \psi$) between the stator and rotor voltages.

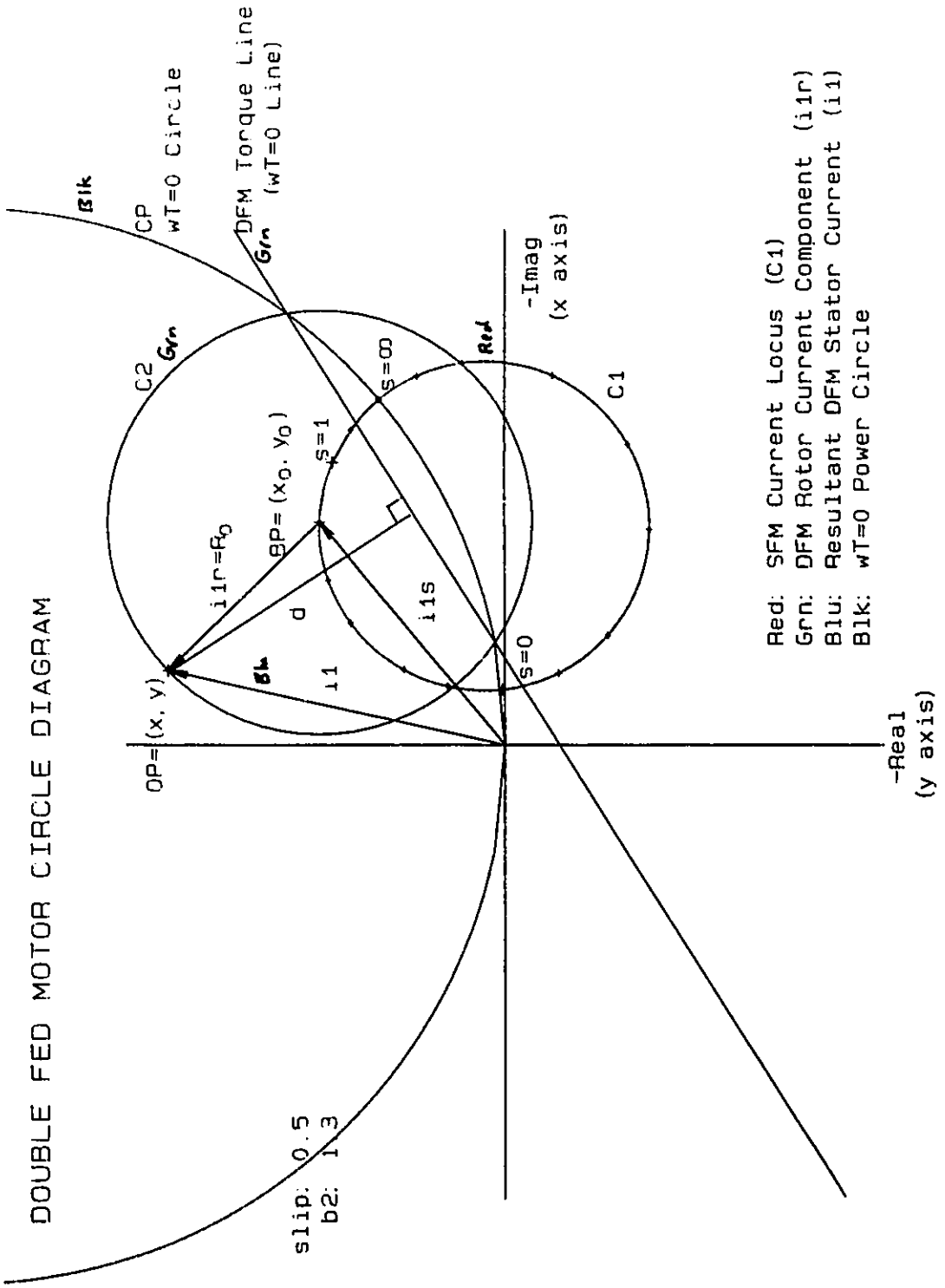

Figure 3.4 - DOUBLE FED MOTOR CIRCLE DIAGRAM - The basepoint BP varies with the slip s, the radius $|I_{1r}|$ varies with V_2, and the operating point OP varies with δ_v.

The operating point OP is at the tip of the stator current vector I_1 and is on the locus C2 with center BP (the basepoint). The stator current $I_1 = I_{1s} + I_{1r}$ lags the stator voltage by the angle P_1 ($P_1 = \phi_1$). For the single fed motor, $V_2 = 0$, and the operating point and the basepoint are one and the same (unless external resistance is added to the rotor circuit, then the rotor terminal voltage V_2 is no longer zero).

The torque line for the double fed machine is similar to that of a single fed induction machine in that the developed torque is proportional to the perpendicular distance from the operating point to the torque line. This can be expressed as a function of OP and BP where OP = (x,y) and BP = (x_o,y_o). Note that the coordinate system is rotated 90^o counter clockwise (CCW) as is customary in some texts. Therefore, the point (x,y) on the diagram corresponds to the current components (-Imaginary, + Real).

From Figure 3.4, the operating point (x,y) can be expressed in terms of the locus C2 using the following substitutions;

$$(x - x_o)^2 + (y - y_o)^2 - R_o^2 = 0 \tag{3.40a}$$

or

$$x^2 + y^2 = 2(x_o x + y_o y) + (R_o^2 - x_o^2 - y_o^2) \tag{3.40b}$$

$$y = \hat{I}_1 \cos\phi_1 \tag{3.41a}$$

$$x^2 + y^2 = \hat{I}_1^2 \tag{3.41b}$$

where

$$R_o = |I_{1r}|$$

$$\hat{V}_1 = |V_1| \qquad \hat{V}_2 = |V_2| \tag{3.42}$$

$$\hat{I}_1 = |I_1| \qquad \hat{I}_2 = |I_2|$$

and

$\frac{3}{2}$ = converts single phase power to 3-phase power and rms values to peak values

From (3.39) the air gap, or synchronous, power $\omega\Gamma$ can also be expressed graphically, in terms of the locus of the input power circle CP, by noting that

$$\omega\Gamma = \frac{3}{2}\left[\hat{V}_1\hat{I}_1\cos\phi_1 - \hat{I}_1^2R_1\right] \tag{3.43}$$

or

$$\omega\Gamma = \frac{3}{2}\left[V_1y - (x^2 + y^2)R_1\right] \tag{3.44}$$

In standard form this becomes

$$x^2 + \left(y - \frac{V_1}{2R_1}\right)^2 - \left(\frac{V_1}{2R_1}\right)^2 + \frac{\omega\Gamma}{R_1} = 0 \tag{3.45}$$

and for $\omega\Gamma = 0$, this circle has center $(0, \frac{V_1}{2R_1})$ and radius $\frac{V_1}{2R_1}$ as shown in Figure 3.4. From geometrical considerations [19], the radical axis between C2 and CP is found by substituting (3.40b) and (3.41a) into (3.45) to give

$$\omega\Gamma = \frac{3}{2}(-2R_1)\left[x_ox + (y_o - \frac{V_1}{2R_1})y + \frac{1}{2}(R_o^2 - x_o^2 - y_o^2)\right] \tag{3.46}$$

For $\omega\Gamma = 0$, (3.46) becomes (3.47), the line of zero torque

$$0 = x_ox + (y_o - \frac{V_1}{2R_1})y + \frac{1}{2}(R_o^2 - x_o^2 - y_o^2) \tag{3.47}$$

which is the torque line Γ for the double fed machine. The perpendicular distance d of any point OP = (x,y) on C2, the locus of I_1, from the torque line is

$$d = \frac{x_ox + (y_o - \frac{V_1}{2R_1})y + \frac{1}{2}(R_o^2 - x_o^2 - y_o^2)}{\left[x_o^2 + (y_o - \frac{V_1}{2R_1})^2\right]^{1/2}} \tag{3.48}$$

Substituting (3.48) into (3.46) gives the air gap power at the operating point OP as

$$\omega\Gamma = \frac{3}{2}\,(-2R_1)\,d\left[x_o^2 + \left(y_o - \frac{V_1}{2R_1}\right)^2\right]^{1/2} \qquad (3.49)$$

This expression for $\omega\Gamma$ is the same as the torque line for the single fed motor, except that the circle C2, with center BP = (x_o,y_o), has been used in place of the circle C1, with center (x_c,y_c), and radius R_c. C1 and CP are both constant for all slip and so the radical axis of C1 and CP (3.45) is invariant to changes in slip and passes through the points s = 0 and s = ∞ on C1. For the double fed case, BP (the center of C2) moves with the slip, and so the torque line Γ is not constant. Figure 3.5 shows the variation of Γ with slip, and the correspondence to the single fed motor torque line Γ_{SFM} when $V_2 = 0$. Then, for any point OP = BP (ie. with s = 1), the magnitude of the developed torque Γ will be the same, whether considering the perpendicular distance from Γ_{SFM} to OP, or from Γ_{DFM} to OP. Although the distances d_1 and d_2 are different, the square root term in (3.49) has coefficients (x_o,y_o) versus the single fed coefficients (x_c,y_c) and so $\Gamma_{DFM} = \Gamma_{SFM}$ as expected.

Several general observations can be made at this point concerning the torque-speed characteristic of the double fed machine.

Firstly, the sign of d determines if the machine is motoring or generating. When OP is above the torque line, d is negative, $\omega\Gamma > 0$, and the double fed machine is motoring. For OP below the torque line, d is positive, $\omega\Gamma < 0$ and the machine is generating.

Secondly, the basepoint BP, and therefore the steady state speed

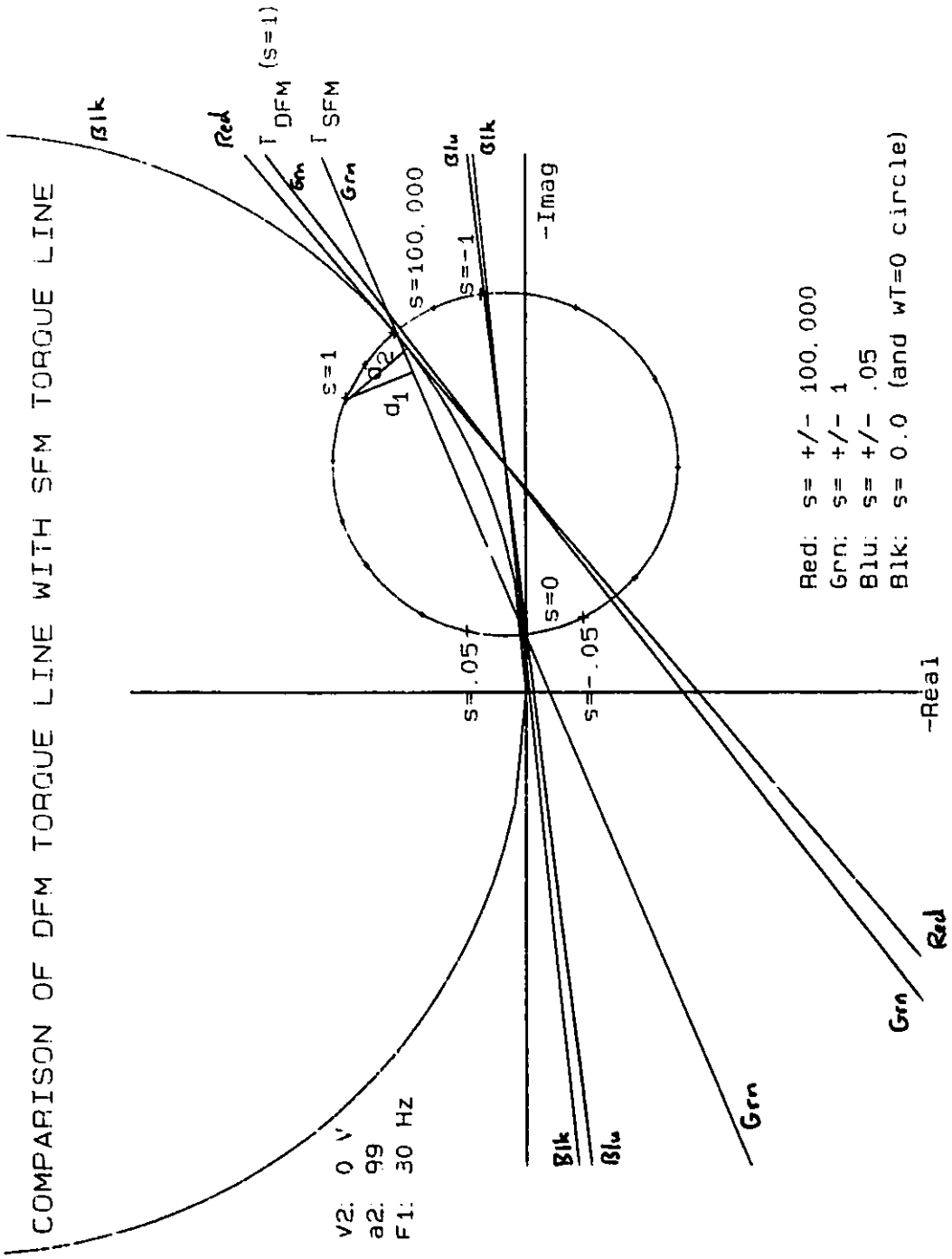

Figure 3.5 - COMPARISON OF THE DFM TORQUE LINE WITH THE SFM TORQUE LINE - The slope of Γ_{DFM} varies with the slip s and shifts vertically with the magnitude of $|V_2|$.

of the double fed machine, are strictly determined by the stator frequency F_1 and the rotor to stator frequency ratio s (slip $s = F_2/F_1$). However, when the electrical torque does not equal the shaft mechanical torque, then the rotor speed will increase or decrease. As this happens, F_1 or F_2 must be simultaneously adjusted in frequency and phase to maintain synchronization of the rotating fluxes in the air gap and thus produce a steady, non-zero torque. Since the relation $W = F_1 - F_2$ (3.3) does not contain any phase information, by itself it is not a sufficient criterion for stable control of the DFM.

The manner in which phase information is used to control the field synchronization and provide for stable operation will be discussed in Section 4.2. It is appropriate first though, to review the results obtained from the DFMPLT simulation program in Sections 3.3.2 and 3.3.3, and see how the stator and rotor voltages are used to control the operating point OP.

3.3.2 DFMPLT Program

3.3.2.1 Purpose and Overview

The program DFMPLT was developed to study the interrelationships between the numerous control variables of the double fed machine, the resultant current vectors, and the developed torque under all possible operating conditions. DFMPLT (DFM plot) is fully menu driven and has the

following features:

i) The circular loci C1, C2, C3, and C4 (derived from I_{1s}, I_{1r}, I_{2s}, and I_{2r} respectively) can all be drawn independently, as functions of the parameters, basepoint and operating point of the system.

ii) Specific current vectors can be drawn as well for I_1, I_{1s}, I_{1r}, I_2, I_{2s}, and I_{2r}. These can be drawn offset from the origin if necessary for extra clarity.

iii) The torque line Γ can be drawn for any operating condition.

iv) Independent lines, vectors, and circles can be drawn, using parametric, R-θ, or interactive representations. These aid in determining geometric relationships between elements in the diagram. (Note: a vector is simply a line with a direction arrow at one end.)

v) For any given stator frequency F_1, stator voltage V_1, and rotor voltage V_2, the basepoint BP and operating point OP can be selected according to the rotor speed (W), the slip (s), or the angle between the stator and rotor voltage vectors (δ_v). This provides the most useful information for studying the operating conditions of the DFM system.

vi) All motor parameters can be read from a parameter data file and altered if necessary. Inductive elements can be entered as inductances or reactances (L_mode or X_mode respectively).

vii) The stator and rotor voltages, V_1 and V_2, can be set independently or can be scaled according to the respec-

tive stator or rotor frequency.

viii) Color graphics allows plotting in any of seven colors, with sequential color selection possible for consecutive plotting of sets of curves.

ix) An optional logging feature creates a '.LOG' file which saves the current screen drawing commands. The log file may be replayed at any time to recreate the screen image and minimizes having to redraw complex images or repetitive sections (such as axes and labels). There is no limit to the number of log files that can be created.

x) An optional plotter feature sends the current screen drawing commands to the plotter for color hardcopy of the screen image. Logging files can also be plotted when replayed to the screen. Default or manual pen color selection are possible.

xi) The screen limits can be rescaled for any magnitude of voltages and currents.

xii) Optional markers (small '+' marks) can be displayed at preset values of slip to provide a visual scale for the slip values. These are presently set for slip = ±100,000, ±2, ±1, ±0.5, ±0.3, ±0.2, ±0.1, ±0.05, and 0.0.

xiii) Internal values of voltage, current and slip can be optionally sent to a printer while the curves are being drawn. This provides numeric values to check the results and to complement the graphical information.

xiv) The graphics screen can be reviewed (or cleared) and labels

can be placed anywhere on the image. Logging and plotting features also apply to the labels.

xv) DOS commands may be entered from within DFMPLT. This allows on-line editing of the log files without exiting from the program.

The main menu options, along with brief descriptions, are listed in Figure 3.6.

```
        DOUBLE FED MOTOR CIRCLE DIAGRAM PLOTTING PACKAGE

  P - Set Parameters (also, Set Variables, and Data Display Mode)
  C - Draw Circles (Locus of Current Vectors, Interactive, etc.)
  L - Draw Lines (Torque Lines, Current Vectors, etc.)
  F - File Logging (Create, Replay & Append, Edit,
                    Close, Toggle Logging On/Off)
  R - Review the Graphics Display (and Add Labels if desired)
  W - Clear Graphics Display (Wipe)
  E - Set Limits (Extents) of Graphics Display
  B - Set Basepoint (Stator/Rotor from s, W etc.)
  O - Set Operating Point (Stator/Rotor from δv etc.)
  D - Execute DOS Command(s)
  M - Toggle Slip Markers On/Off
  T - Toggle Plotter On/Off
ESC - Exit DFMPLT
```

Figure 3.6 - DFMPLT MAIN MENU OPTIONS

3.3.2.2 DFM Parameters and Automatic Scaling Feature

From the main menu, the DFM parameters and control variables can be modified. The following per phase values are used in L_mode (3.25), where p (as part of a variable name) denotes a parameter read in from the parameter file (ie. pr_1 = parameter value of r_1):

$$R_1 = pr_1 \qquad R_2 = (pk)^2 \times pr_2$$

$$L_1 = p\ell_1 \qquad L_2 = p\ell_2$$

$$L_m = p\hat{m} \tag{3.50}$$

$$X_1 = 2\pi F_1(p\ell_1 - \frac{3}{2} \times pk \times p\hat{m})$$

$$X_2 = 2\pi F_1(pk^2 \times p\ell_2 - \frac{3}{2} \times pk \times p\hat{m})$$

$$X_m = \frac{3}{2} \times 2\pi F_1 \times p\hat{m}$$

In this case, the values of X_1, X_2, and X_m will be rescaled according to the current stator frequency F_1. If reactance values for a specific stator frequency are known, then the parameters can be evaluated in X_mode, if desired, as:

$$R_1 = pr_1 \qquad R_2 = pr_2$$

$$L_1 = 0 \qquad L_2 = 0$$

$$L_m = 0 \tag{3.51}$$

$$X_1 = pX_1 \qquad X_2 = pX_2$$

$$X_m = p\hat{m} \qquad k = 1$$

These values are valid only while the same stator frequency is used.

In both cases, the slip s is calculated on the basis of the stator frequency F_1 and the current rotor speed W, using

$$s = (1 - \frac{W}{F_1}) \tag{3.52}$$

and is then rounded to the nearest discrete value. W is then updated on the basis of F_1 and the rounded value of slip. This allows the slip to be quantized into a limited number of values and permits the impedance parameters to be precalculated.

The DFM impedances are then calculated as:

$$Z_1 = R_1 + jX_1 \tag{3.53a}$$

$$Z_m = jX_m \tag{3.53b}$$

$$Z_2(\text{slipindex}) = \frac{R_2}{s(\text{slipindex})} + jX_2 \tag{3.53c}$$

where

$s(\text{slipindex}) = \text{slip}$

$\text{slipindex} = (1,2,3,\ldots 154)$

and

$$\det(\text{slipindex}) = Z_1 + Z_2(\text{slipindex}) + \frac{Z_1 Z_2(\text{slipindex})}{Z_m} \tag{3.53d}$$

The stator and rotor voltages are generally scaled according to their respective frequency to prevent saturation at low frequencies, and to maintain a constant level of flux in the machine. The equations to do so are:

$$V_1 = a_1 + b_1 F_1 \tag{3.54a}$$

$$V_2 = a_2 + b_2(F_1 - W) \tag{3.54b}$$

where

a1, a2, b1, b2 are settable parameters

and from (3.3)

$$F_2 = (F_1 - W) = F_1 \times s(\text{current value of slipindex}) \tag{3.55}$$

Although F_1 does not change, unless specifically modified using the parameter command, V_1 and V_2 will be adjusted according to (3.54) as the basepoint varies due to changes in W or slip. If it is necessary to set V_1 (or V_2) independently of (3.54), the operator sets $a_1 = 99$ (or $a_2 = 99$). The program then sets b_1 (or b_2) to zero and sets a_1 to pV_1 (or a_2 to pV_2). This effectively overrides the automatic voltage scaling of (3.54) and V_1 (or V_2) will remain at the parameter values despite changes in F_1 and F_2.

3.3.2.3 Determination of the Basepoint and Operating Point

For a given set of parameters and control variables, there is exactly one operating point in the machine. Yet each operating point is not unique and can be reached by many combinations of the control variables (V_1, V_2, δ_v, and F_1). The best way to describe the DFM operating state, is in terms of the rotor speed W and the developed torque Γ.

Since DFMPLT can draw the stator currents (I_1, I_{1s}, I_{1r}) and the rotor currents (I_2, I_{2s}, I_{2r}) for each state of operation, this leads to two distinct sets of curves, each with a basepoint BP and an operating point OP. Although drawn separately, these both represent the same operating state. Changing one BP changes the other BP and changing one OP changes the other OP. A typical set of stator and rotor current loci are shown in Figure 3.7 along with the stator and rotor current components. As with a transformer, I_1 and I_2 nearly cancel out, the difference being due to the magnetizing current.

The basepoint(s) and operating point(s) are set from the main menu. A stator/rotor submenu option merely dictates which point will be drawn on the screen. The basepoint can be set according to the desired slip value s or rotor speed W, and the operating point can be set according to the stator-rotor voltage phase offset δ_v. (If it is necessary to change F_1, then the Parameter command is used first.)

When s or W are input, the other variable (W or s) is adjusted according to (3.55) and the voltages are rescaled according to (3.54). In this way, the simulation program parallels the available rotor speed

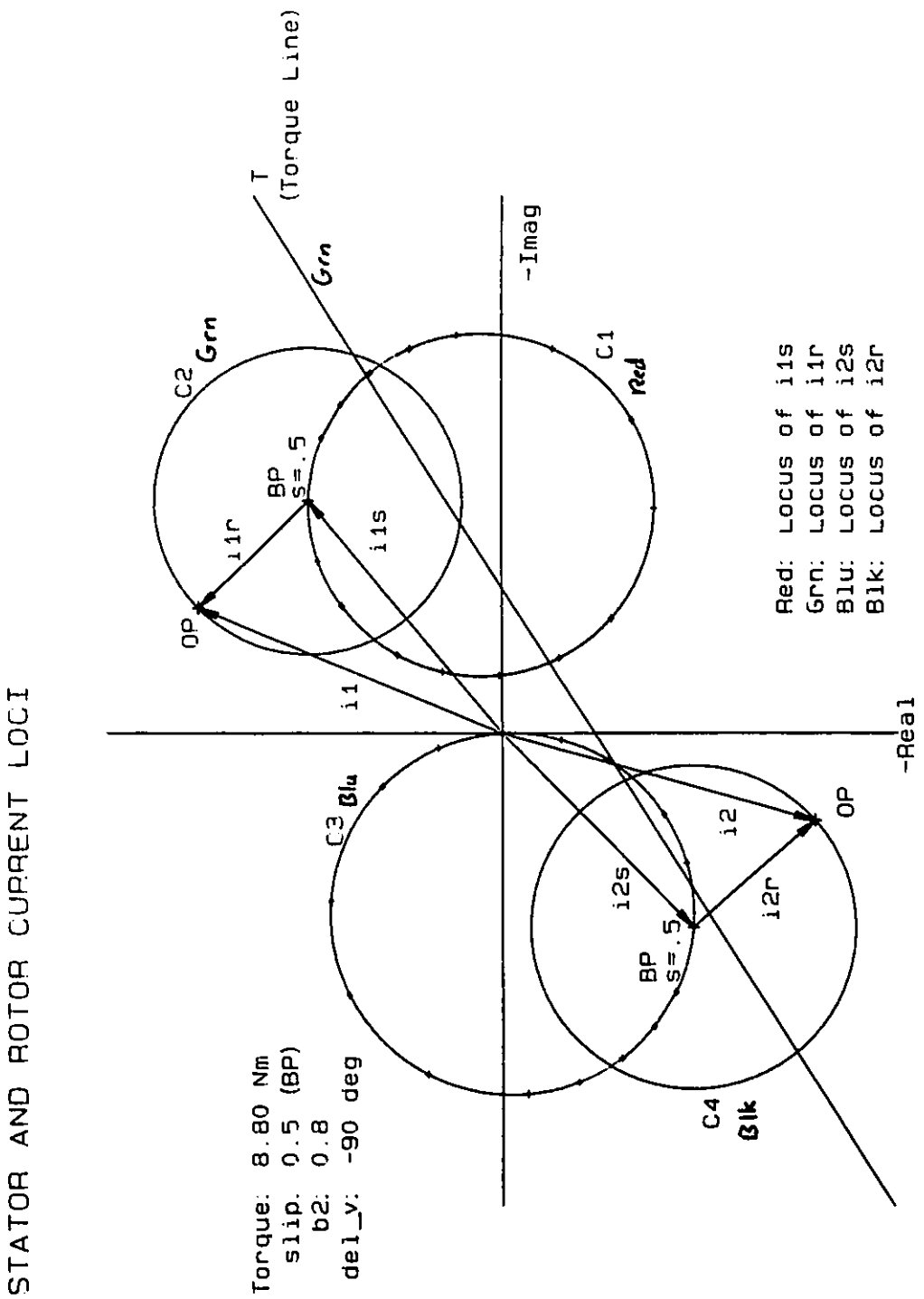

Figure 3.7 - STATOR AND ROTOR CURRENT LOCI - The rotor BP and OP correspond exactly to those of the stator (ie. there is only one BP and OP, but two representations).

information and the control variables which are present in the actual DFM drive hardware developed in this thesis (Chapter 5).

Every change in BP or OP causes the current vectors to be recalculated as well as the stator and rotor current phase angles P_1 and P_2. The most recent value of P_1, P_2, δ_v, δ_i and Γ are each displayed in the lower left corner of the graphics screen, for reference (But they aren't sent to the plotter). The relationship between these variables is

$$\delta_v = P_1 - P_2 + \delta_i \tag{3.56}$$

where δ_i is the internal angle between the stator and rotor current phasers, as well as the angle between the rotating mmf vectors due to the magnetizing flux (See Sections 3.3.3 and 4.2).

3.3.2.4 DFMPLT Plotting Options

The circle and line drawing options in the main menu are used to plot the desired curves, and their submenus are listed in Figures 3.8 and 3.9. From the line drawing menu, the current vectors can be drawn, according to the menu of Figure 3.10.

The current vectors, for the circles C1 to C4, are derived from (3.26) and (3.27) as

$$I_1 = I_{1s} + I_{1r} \tag{3.57a}$$

$$I_2 = I_{2s} + I_{2r} \tag{3.57b}$$

where

$$I_{1s} = V_1 \frac{1 + Z_2/Z_m}{\det Z} \tag{3.57c}$$

CIRCLE DRAWING MENU

C1 - Draw the Locus of I_{1s} (as s is varied from $-\infty$ to $+\infty$)
C2 - Draw the Locus of I_{1r}, for a given BP
(as δ_v is varied from $\delta_v = 0^o$ to $\delta_v = 360^o$)
CS - Draw a Set of C2 Curves (for a Predetermined Set of BP's)
C3 - Draw the Locus of I_{2s} (as s is Varied from $-\infty$ to $+\infty$)
C4 - Draw the Locus of I_{2r}, for a given BP
(as δ_v is varied from $\delta_v = 0^o$ to $\delta_v = 360^o$)
CR - Draw a Set of C4 Curves (for a Predetermined Set of BP's)
P - Draw a Parametric Circle
(of the form $(x - x_o)^2 + (y - y_o)^2 - R^2 = 0$)
I - Draw a Circle Interactively (by moving the cursor to the center and then to a point on the circumference)

Figure 3.8 - CIRCLE DRAWING MENU OPTIONS

LINE DRAWING MENU

T - Draw the Torque Line
C - Draw a Current Vector (I_1, I_{1s}, I_{1r}, etc., see below)
I - Draw a Line Interactively (from one cursor position to a 2nd)
X - Draw a Line from (x_1,y_1) to (x_2,y_2)
M - Draw a Line from (x_1,y_1) according to (R,θ)
A - Draw a Parametric Line of the form: $Ax + By + C = 0$
V - Toggle Between Vector and Line Drawing Modes
R - Review the Graphics Display (and add Labels if desired)

Figure 3.9 - LINE DRAWING MENU

CURRENT VECTOR MENU

I_{1s} - Draw the Component of I_1 due to the Stator Voltage V_1
I_{1r} - Draw the Component of I_1 due to the Rotor Voltage V_2
I_1 - Draw the Stator Current Vector ($I_1 = I_{1s} + I_{1r}$)
I_{2s} - Draw the Component of I_2 due to the Stator Voltage V_1
I_{2r} - Draw the Component of I_2 due to the Rotor Voltage V_2
I_2 - Draw the Rotor Current Vector ($I_2 = I_{2s} + I_{2r}$)
I - Set (or Clear) Interactive Offset for the Current Vectors
L - Restore Last Interactive Stator (or Rotor) Current Offset
V - Toggle Between Vector and Line Drawing Modes
M - Toggle Between Stator and Rotor Modes (for BP & OP display)

Figure 3.10 - CURRENT VECTOR DRAWING MENU

$$I_{1r} = \frac{V_2}{s}\,\frac{-1}{\det_Z} \tag{3.57d}$$

$$I_{2s} = V_1\,\frac{-1}{\det_Z} \tag{3.57e}$$

$$I_{2r} = \frac{V_2}{s}\,\frac{1 + Z_1/Z_m}{\det_Z} \tag{3.57f}$$

and Z_1, Z_2, Z_m and $\det_Z$ are given in (3.53).

The torque line (3.47) is derived from (3.46), with $\omega\Gamma = 0$. The torque line is dependent on the basepoint BP and $|I_{1r}|$, the radius of C2, as given by |OP - BP|. Since the screen display is rotated 90° CCW (according to convention), then the coordinates of BP and OP are given by (x_o,y_o) and (x,y) respectively, with

$$x_o = \text{-Imaginary (BP)} \tag{3.58a}$$

$$y_o = \text{Real (BP)} \tag{3.58b}$$

$$x = \text{-Imaginary (OP)} \tag{3.59a}$$

$$y = \text{Real (OP)} \tag{3.59b}$$

The torque line can then be expressed in screen coordinates as

$$Ax + By + C = 0 \tag{3.60}$$

where

$$A = x_o \tag{3.61a}$$

$$B = y_o - \frac{\hat{V}_1}{2R_1} \tag{3.61b}$$

$$C = \frac{1}{2}(R_o^2 - x_o^2 - y_o^2) \tag{3.61c}$$

$$\hat{V}_1 = (a_1 + b_1F_1) \qquad \text{from (3.54a)} \tag{3.61d}$$

$$R_o = |I_{1r}| = |OP - BP| = \left[(x - x_o)^2 + (y - y_o)^2\right]^{1/2} \tag{3.61e}$$

$$OP = (x,y) \tag{3.61f}$$

$$BP = (x_o,y_o) \tag{3.61g}$$

Before plotting any circle or line, DFMPLT prompts for the color. The color can be specified from a submenu, taken from a default value, or incremented automatically to the next color in a sequence. This enhances the clarity of the plots greatly.

Throughout the program, menus prompt the user with all the available options. However, it is not necessary to use the arrow keys and enter key to select a menu option; single key commands also work for each function, making the program very quick to use.

The ability, as well, to execute DOS commands from within DFMPLT is very convenient, since one can easily examine, edit, and merge log files using the screen editor, without having to exit from DFMPLT.

3.3.3 Interpretation of the DFM Circle Diagram

The following sets of curves show the interrelationships between the control variables (V_1, V_2, δ_v, F_1) and the DFM currents.

Changing the stator voltage V_1 (while keeping F_1 constant) results in a linear scaling of C1 and C3, the stator and rotor current vector loci due to the stator voltage alone (Fig. 3.11). The components of I_1 and I_2 due to the rotor voltage (I_{1r} and I_{2r}, respectively) remain unchanged, yet since the basepoint is shifted, the curves C2 and C4 (not shown) are similarly shifted. The torque line moves vertically upward as V_1 is decreased, generally reducing the distance d of OP from Γ and thus reducing the developed torque, as one might expect.

In a similar manner, decreasing the stator frequency F_1, while

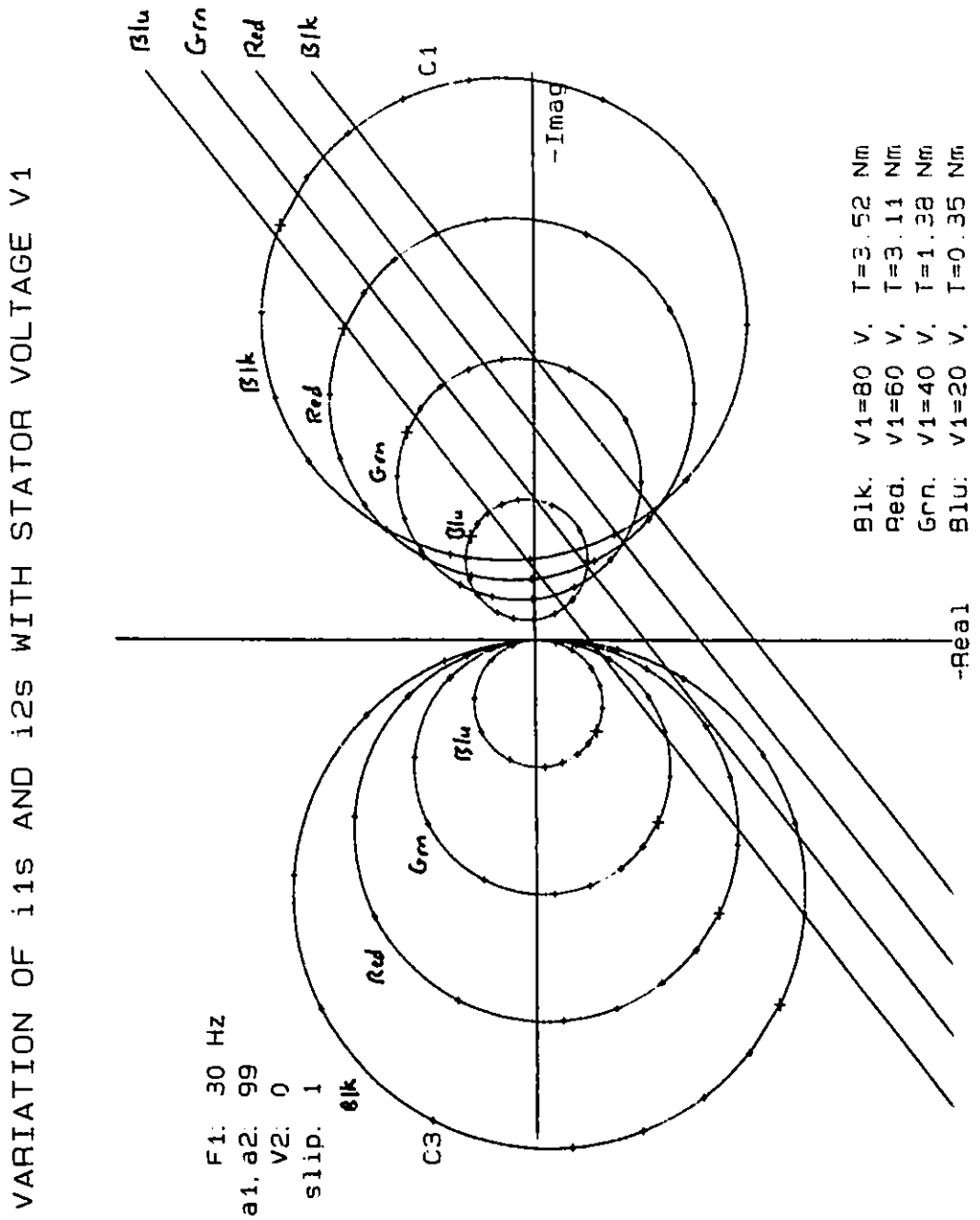

Figure 3.11 - VARIATION OF I_{1s} AND I_{2s} WITH THE STATOR VOLTAGE V_1
If F_1 is constant, the flux level varies with V_1.
The torque line shifts vertically with changes in V_1.

keeping V_1 constant, causes the radius of C1 and C2 to become large. This corresponds to saturation of the iron unless the stator voltage is decreased simultaneously. When the linear approximation of (3.54) is used, the diameter of C1 and C3 remain fairly constant (Fig. 3.12). However, the slip values are shifted towards the point s = 0 and the current vectors I_{1s} and I_{1r} decrease substantially for the same value of slip. This can be compensated for by adjusting V_2 or δ_v, as noted below, to maintain the torque and keep the speed $W = F_1 - F_2$ constant.

The relationship between δ_v and the torque Γ is shown in Figure 3.13. In this case, since the rotor voltage V_2 and the basepoint BP are kept constant, C2 does not change and so the torque line is invariant for all δ_v. (This is to be expected, because the torque line Γ was derived as the radical axis of the two circles C1 and C2). The perpendicular distance d (shown for $\delta_v = -45^o$), and thus the developed torque, now vary according to the sinusoidal relation

$$d = d_o + R_o \mathrm{Sin}(\delta_v + \delta_o) \tag{3.62}$$

R_o is the magnitude of I_{1r}, given by (3.61e), and is dependent on $|V_2|$ and s. δ_o is the stator-rotor voltage phase difference that produces an I_{1r} which is parallel to Γ and oriented towards the origin. d_o is the perpendicular distance from BP to Γ, and is found from (3.48) with $(x,y) = (x_o,y_o)$. That is

$$d_o = \frac{\frac{1}{2}(R_o^2 + x_o^2 + y_o^2) - \frac{V_1}{2R_1} y_o}{\left[x_o^2 + (y_o - \frac{V_1}{2R_1})^2\right]^{1/2}} \tag{3.63}$$

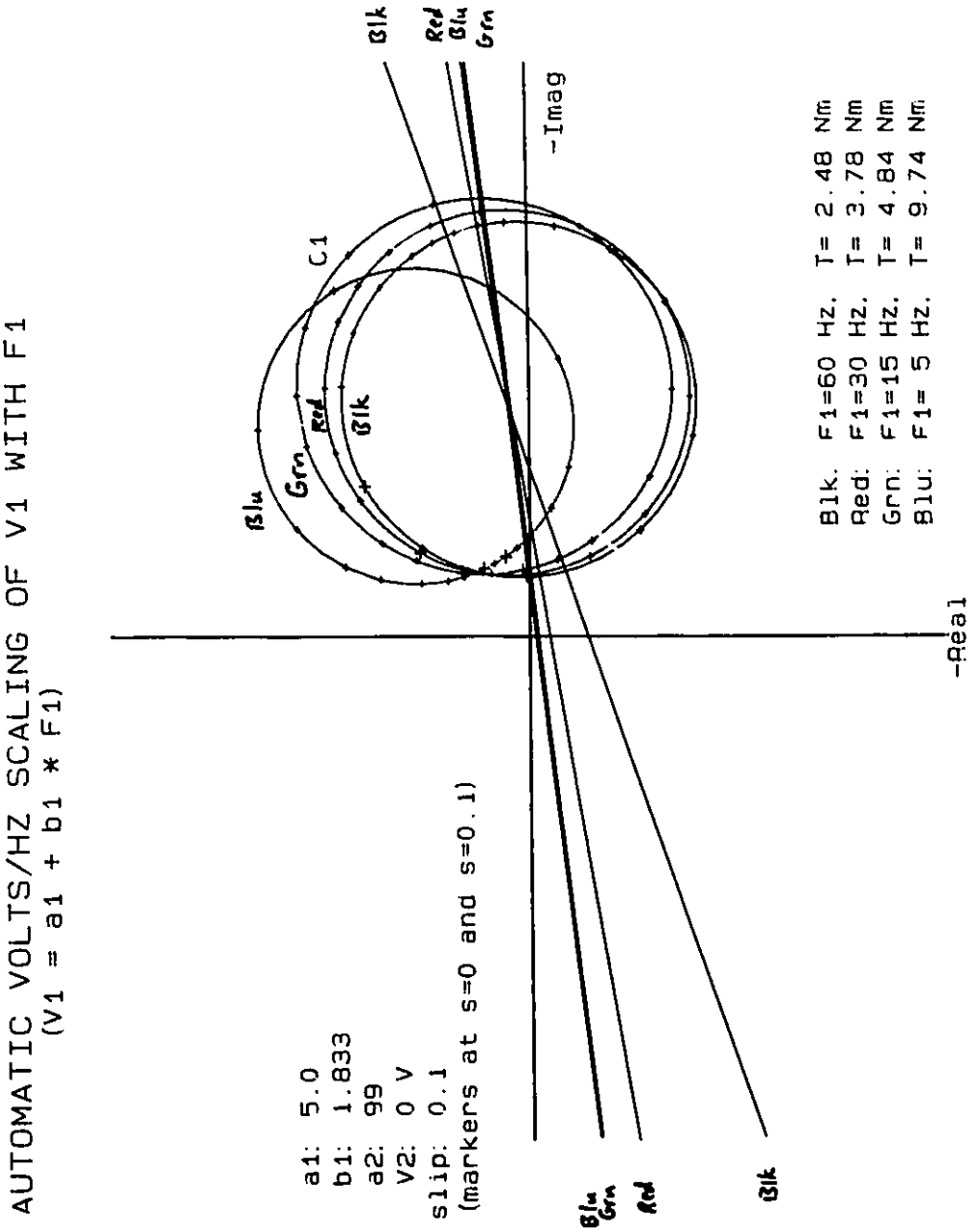

Figure 3.12 - AUTOMATIC VOLTS/HZ SCALING OF V_1 WITH F_1
The values of a_1 and b_1 are chosen to maintain a relatively constant level of flux in the machine.

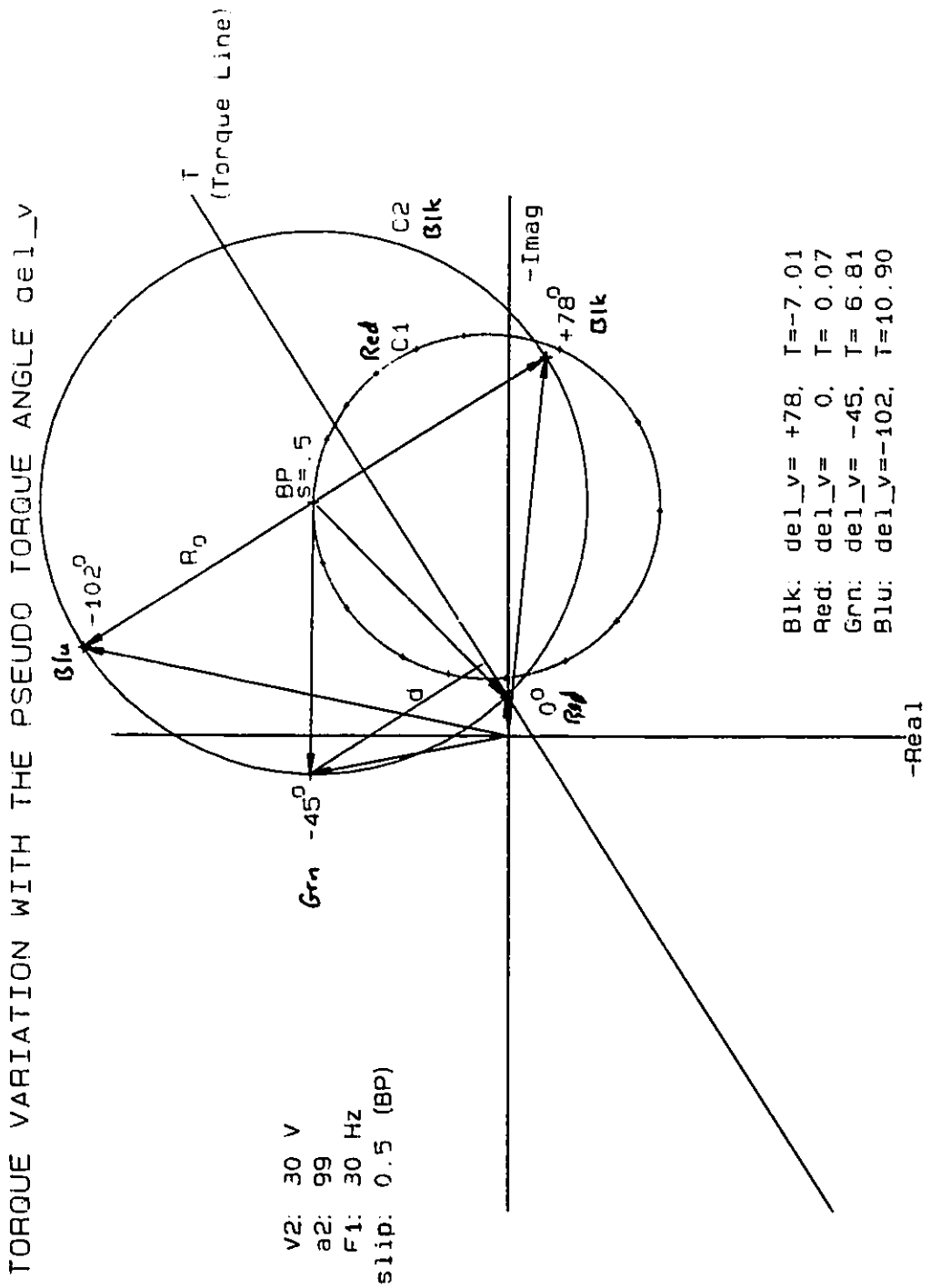

Figure 3.13 - TORQUE VARIATION WITH THE PSEUDO TORQUE ANGLE δ_v
The torque varies sinusoidally with δ_v according to the relationship $d = d_o + R_o \sin(\delta_v + \delta_o)$.

or

$$d_o = \frac{\frac{1}{2}|I_{1s}|^2 + \frac{1}{2}|I_{1r}|^2 - \frac{V_1}{2R_1} y_o}{\left[x_o^2 + (y_o - \frac{V_1}{2R_1})^2\right]^{1/2}} \tag{3.64}$$

Note that for points above the torque line, $d < 0$ and the torque is positive. Therefore, $d < 0$ corresponds to when the basepoint BP is above Γ and $\delta_V < 0$ will give a negative result for the Sin term, as shown in Figure 3.13. This sinusoidal relationship between the voltage phase difference δ_V and the developed torque will be utilized in Section 4.2 to control the torque of the DFM drive.

The maximum motoring torque occurs where the tangent to C2 is parallel to the torque line Γ, and d_o is positive (ie. where $\delta_V = -102^o$ in Fig. 3.13). The largest generating torque occurs when δ_V is shifted by 180^o from this point (ie. $\delta_V = 78^o$), the other point on C2 where the tangent is parallel to Γ.

Increasing the rotor voltage V_2 from zero, increases the radius of C2 (or C4) as shown in Figure 3.14. The torque line keeps the same slope but moves upward as the rotor voltage increases. The net result, for δ_V near -90^o and BP at $s = .5$, is an increase in the distance d from OP to the resultant torque line, and thus an increase in the torque. However, the magnitude of the increase varies with δ_V. For example, with δ_V near 0^o, and V_2 small, the torque is relatively small and positive. But as V_2 increases, the torque decreases and becomes negative near $V_2 = 40$ V. For δ_V near 90^o, the torque is small, decreases to zero, and then becomes large and negative when V_2 is increased from 0 to 40 V. This variation in torque, as V_2 is varied, is dependent upon the operating point OP, as determined by the magnitude of V_2 and its phase angle relative to V_1 (ie. δ_V).

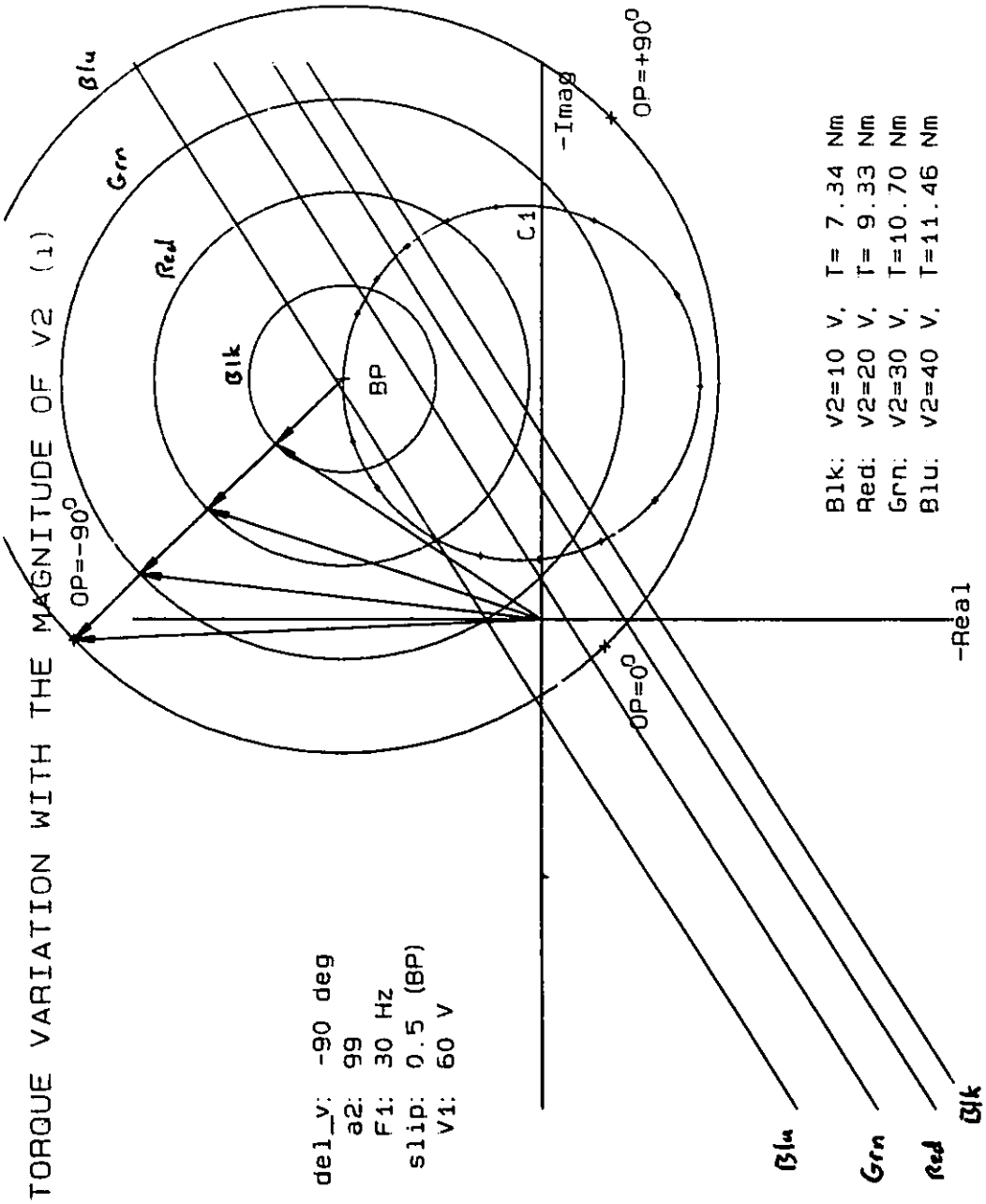

Figure 3.14 - TORQUE VARIATION WITH THE MAGNITUDE OF $|V_2|$ (i) The exact effect of changing $|V_2|$ depends on the pseudo torque angle δ_v.

The basepoint BP also modifies the relationship between the developed torque and the operating point because, as BP moves around the circle C1, the slope of the torque line varies (Figure 3.5), and the distance d_o changes. This means that the torque control algorithm must be modified according to the value of s. In addition, the torque line shifts vertically with increases in the magnitude of V_2. Therefore, d_o and δ_o (3.62) are functions of slip, $|V_2|$, and δ_v.

When the slip is negative, the torque line takes on the same values as for positive slip, with the point of symmetry being s = 0. That is, $\Gamma(s) = \Gamma(-s)$ for all values of s. The radius of C2, though, is larger for negative values of s than for positive values. Figure 3.15 shows the same terminal conditions as Figure 3.14, except that the slip is now s = -.5. The corresponding values of I_{1r} are larger for s = -.5 than for s = .5. None-the-less, the maximum motoring torque is smaller because BP(s=-.5) lies below the torque line. As s approaches s = -1, the distance d_o from BP to Γ decreases and the maximum value of motoring torque increases for a given magnitude of V_2. This shows that the largest motoring torques are available for $s > 0$.

As the slip approaches zero, the rotor frequency decreases and the rotor voltage required to produce the same magnitude of I_{1r} also decreases. Figure 3.16 shows the case where s = 0. The blue circle, where C2 has V_2 = 40 V, shows that a large positive or negative torque may be obtained, depending on δ_v (the phase of V_2 with respect to V_1). δ_v also has a large affect on the stator input power factor.

For example, when $\delta_v = -180^o$, as shown in Figure 3.16, the developed torque is near its maximum and the stator input power factor,

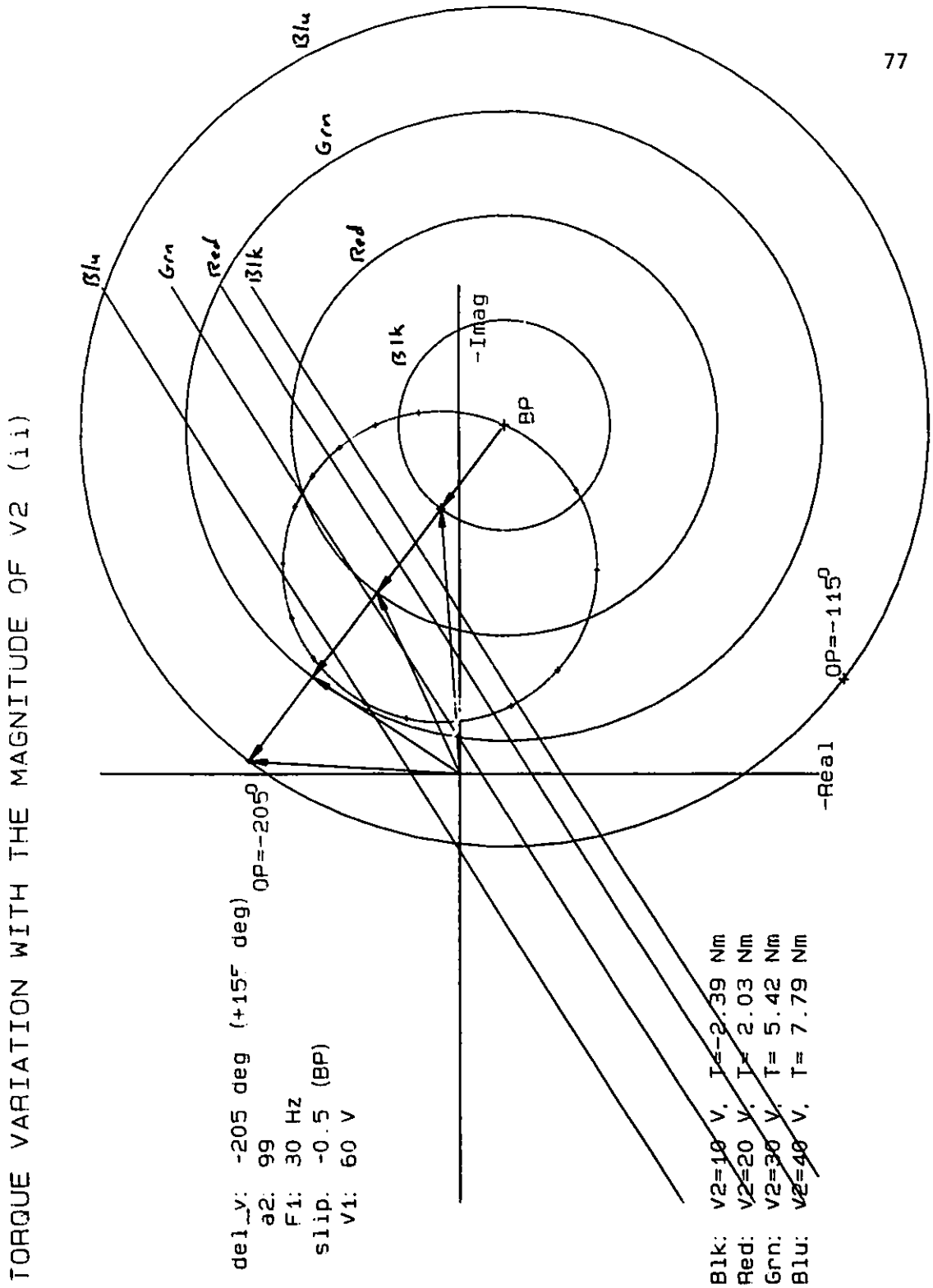

Figure 3.15 - TORQUE VARIATION WITH THE MAGNITUDE OF $|V_2|$ (ii)
The angle δ_o shifts greatly with BP, as shown here for s = -.5 (as compared to s = +.5 in Fig. 3.14).

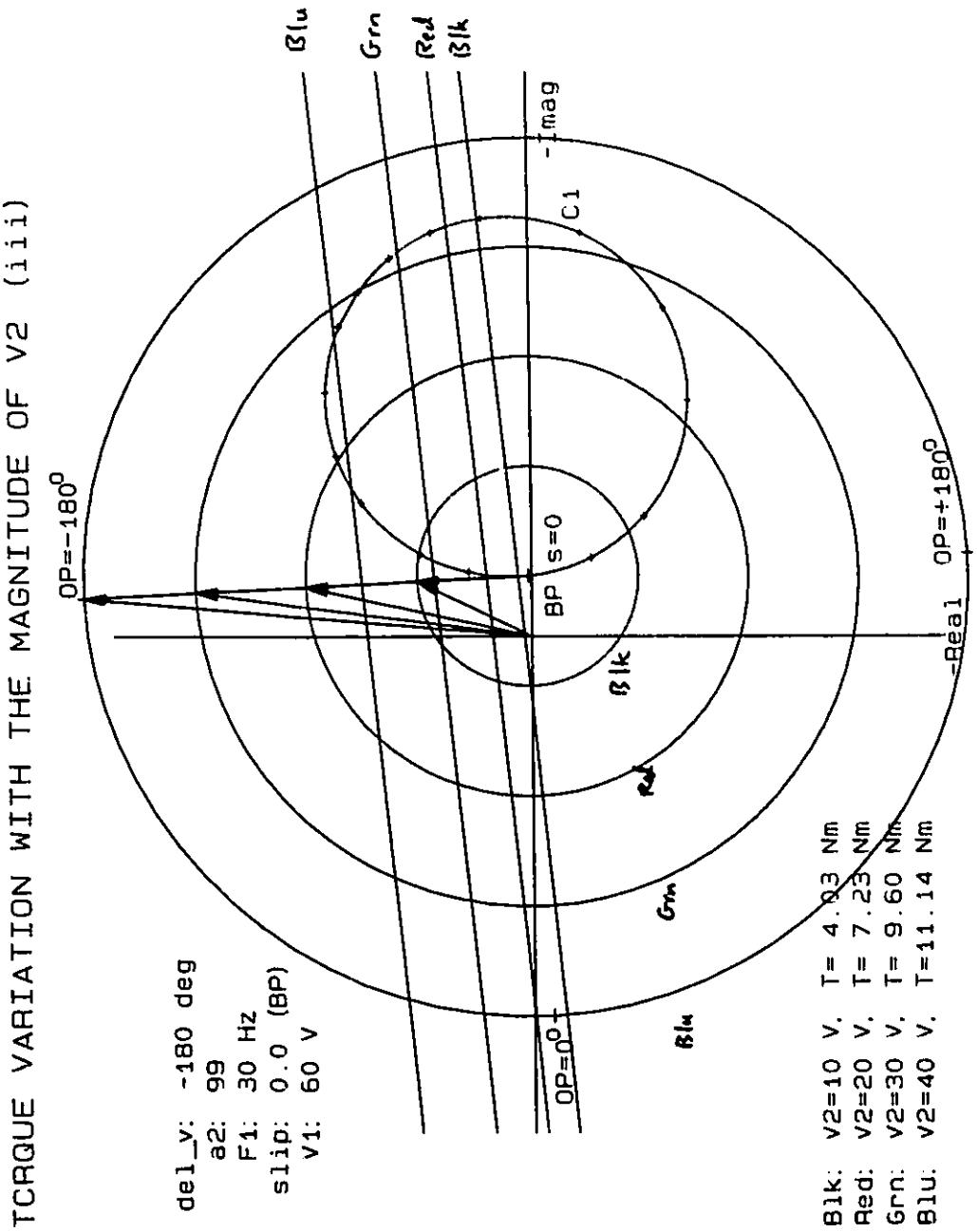

Figure 3.16 - TORQUE VARIATION WITH THE MAGNITUDE OF $|V_2|$ (iii)
δ_v has a large effect on the input power factor.
(eg. with s = 0 and $\delta_v \approx -170^0$, $\cos\phi_1 = 1$)

$\cos\phi$, is near unity ($\delta_v \approx -170^\circ$ gives $\cos\phi_1 = 1$). At the same time ϕ_2 is also close to unity since I_1 and I_2 are nearly in phase opposition and V_2 lags V_1 by 180° ($\delta_v = -180^\circ$). On the other hand, with δ_v near 170°, the maximum generating torque is produced and both stator and rotor power factors are near unity.

If δ_v is chosen $\approx 0^\circ$, then the stator power factor is 0 and the stator supplies lagging VARS to the input lines. The rotor power factor is also close to 0, since ϕ_2 is near $+90^\circ$. This situation is similar to the case of an overexcited synchronous generator, and the DFM can be used for power factor correction [20].

As the slip moves away from zero, it is still possible to control the input power factor via δ_v, but the rotor power factor will not be near unity. Reasonable power factor compensation is still possible though, because if the slip is not too large, the rotor power, and thus the rotor reactive power, will be small with respect to the stator power, and the combined stator and rotor power factor can be improved.

In general, the ability to control the magnitude and phase of the rotor voltage, makes it possible to control the torque and input power factor of the DFM, at any speed. The particular control strategy that is implemented will depend on the desired performance of the drive system. For example, one very useful control scheme involves decoupling the torque and flux producing components of V_2, providing independent control of both torque and power factor. The control principles of the double fed motor are developed more fully in Chapter 4, including the rotating flux equation necessary for stable control.

CHAPTER 4

DOUBLE FED MOTOR CONTROL PRINCIPLES

4.1 Cycloconverter Operating Constraints and DFM Implications

Any variable frequency power conversion scheme has inherent limitations that dictate the most desirable mode of operation. This section outlines both the constraints and the flexibility of a cycloconverter driven DFM system.

The cycloconverter is ideally suited for high power frequency conversion, when the input to output frequency ratio is relatively large (ie. greater than 3). The output harmonic spectrum described in Chapter 2, is concentrated at the frequencies $6nf_i$ when the output frequency f_o is zero. As f_o increases, the harmonics appear at frequencies $6nf_i \pm (2m-1)f_o$ and vary in frequency with f_o. As f_o increases, the frequency of the lower sideband harmonics decreases, leading to parasitic torques, when they occur at the frequencies $5f_o$, $7f_o$, $11f_o$ and $13f_o$. This is minimized if the cycloconverter is operated with $f_o < f_i/3$. However, the double fed drive allows these frequencies to be completely avoided, by 'hopping' around them, and operation up to $f_o = f_i/2$ and higher becomes possible (Section 4.3).

The amplitude of the sideband harmonics generally decreases as m

increases, so that most of the harmonic energy is contained in the terms with m = 1 to m = 6. For lagging loads, the lower sidebands have larger amplitude than the upper sidebands, increasing the potential for subharmonics and torque producing harmonics. The input power factor also decreases as ϕ_o increases, making it preferable to operate the load at unity power factor if at all possible.

It is also desirable to operate a cycloconverter at the highest possible output voltage v_o (ie. with r = 1) because, as the output voltage decreases, the total harmonic energy increases, and the input power factor decreases. Of course, this is constrained by the need to correlate v_o with f_o and prevent saturation of the iron in the motor.

The double fed motor provides an elegant solution to this problem because, with the double fed motor, the freedom to choose F_1 and F_2 independently of W (as long $F_1 - F_2 = W$), makes it possible to operate both cycloconverters with relatively high output voltages and frequencies, even at standstill. In this way, smooth high torque is possible over the entire speed range.

Another factor that must be considered when developing a cycloconverter drive system, is that the cycloconverter is neither a controlled current device (as in a current source inverter) nor a controlled voltage device (as in a voltage source inverter). The cycloconverter inputs are similar to conventional voltage sources, but they vary sinusoidally, have a stiffness which is determined by the source impedance, and their frequency is relatively low when compared to typical PWM inverter frequencies (ie. 60 Hz versus 500 to 1000 Hz). Also, since the cycloconverter employs natural commutation, it is not

possible to turn off the load current, but only to delay the point at which it is turned on for the next half cycle of load current.

The powerflow equation for the double fed machine (neglecting iron losses, and friction and windage losses) is

$$\frac{3}{2}\left[\hat{u}_1\hat{i}_1\cos\phi_1 - \hat{i}_1^2 r_2\right] - \frac{3}{2}\left[\hat{u}_2\hat{i}_2\cos\phi_2 - \hat{i}_2^2 r_2\right] = \Omega_s\Gamma \qquad (4.1)$$

The first term in brackets represents the electrical power, at frequency ω, supplied to the stator, minus the stator joule losses. The second term in brackets corresponds to the electrical power, at frequency Ω, supplied to the rotor, minus the rotor joule losses. There is only one torque Γ in the machine, but it yields three different power terms in (4.1) depending on the frequency (ω, Ω or Ω_s), with which it is associated.

From (4.1) therefore, the mechanical power delivered out via the shaft $\Omega_s\Gamma$ can be expressed as

$$\omega\Gamma - \Omega\Gamma = \Omega_s\Gamma \qquad (4.2)$$

Considering that $s = \Omega/\omega$, this can also be expressed as

$$\omega\Gamma - s\omega\Gamma = \Omega_s\Gamma \qquad (4.3)$$

or

$$(1-s)\omega\Gamma = \Omega_s\Gamma \qquad (4.4)$$

Equation (4.3) shows that the rotor converter need only have a power rating proportional to the slip range over which the drive is designed to be operated at. In contrast to normal sub/supersynchronous cascades (where the slip range is usually limited to $+.5 \geq s \geq -.5$), the rotor convertor in the DFM drive must have the same power rating as the stator converter, since it is necessary to produce rated torque at standstill.

Likewise, when operating at twice synchronous speed (s = -1), both converters also need to supply the full rated power $\omega\Gamma$. At full speed (s = -1) and rated torque therefore, the DFM power balance equation is

$$\Omega_s\Gamma = (1-s)\omega\Gamma = 2\omega\Gamma \qquad (4.5)$$

and each cycloconverter need only be rated at half of the maximum drive power. This simplifies the power handling requirements and cost of each cycloconverter for a specified drive size. On the other hand, it doubles the maximum drive capacity for a given power of cycloconverter.

4.2 Field Synchronization in the Airgap and Torque Angle Control

4.2.1 Stability and Field Oriented Control

Independent control of torque and flux in DC motor drive systems allows them to achieve excellent dynamic performance, limited only by the ability of the armature controller to regulate the armature current [21]. Similar performance from AC drives requires independent, or decoupled, control of the torque and flux producing components of the rotating mmf.

In general, the production of constant non-zero torque in AC machines requires that the stator and rotor components of the airgap mmf rotate synchronously with respect to each other. This is readily achieved for synchronous motor drives by using the rotor position to control the stator current angle, as in self-commutated synchronous drives (also known as brushless DC drives). Since the airgap mmf has a

fixed angle with respect to the rotor, it is possible to provide a self-synchronizing drive that will not fall out of step. In addition, power factor and torque can be controlled by the magnitude of the rotor field and by the stator current amplitude and phase angle [22][23].

For induction motor drives, the situation is more complicated, since there is no convenient way of controlling the phase angle of the rotor current vector. However, the principles of field oriented control [21][24][25][26] enable the torque and flux producing components of the stator current to be identified and controlled in such a way as to provide decoupled, or independent, control of the torque and flux. Since the flux time constant is relatively long, it is usually kept constant in the short term, and excellent dynamic performance is achieved by manipulating the torque producing component of the current only.

When applied to the double fed motor, the situation is similar to that of the synchronous machine, since the angle of the rotor current vector and its resultant mmf vector are known precisely. On the other hand, the situation is also like the induction machine since the airgap field is rotating with respect to both the stator and rotor windings, and operation below and above synchronous speed is possible. (Synchronous speed in this case is a variable quantity, proportional to the stator frequency ω.)

The requirement for synchronously rotating stator and rotor current vectors is fulfilled by the frequency relationship $W = F_1 - F_2$ (3.3). However, the resultant torque and power factor are also dependent on the precise phase angle δ_V between the stator and rotor voltage phasers. Section 3.3.3 examined how the terminal variables V_1, V_2, F_1,

and δ_v interact to give the torque Γ for different values of slip. Since the cycloconverters are not controlled current devices, the control hardware utilizes δ_v (instead of δ_i) to control the DFM drive. This will be examined in more detail in the following section, but two other items must be noted first.

Concerning stability, a rotating power converter is in a stable equilibrium when the developed electrical torque is equal and opposite to the mechanical shaft torque. If the equilibrium is stable, any perturbation will create a restoring torque sufficient to return the system to its previous state, or move it to a slightly different, but stable, equilibrium. For example, a small load increase results in an increase in δ for a synchronous motor, or in a slight increase in slip for an induction motor. Both machines are stable until the shaft torque increases to the value of the pullout torque, or breakdown torque, respectively. At this point, the restoring torque is not sufficient to restore either system to its previous state, nor to maintain it at a new equilibrium, and both motors will slow down and stop.

Upon closer examination though, the behavior of the two machines in this situation is quite different. Since the stator and rotor fluxes of the induction motor always remain synchronized (because of the induction action), the induction motor torque drops off smoothly, even while the machine slows down and stalls. In the synchronous machine, when the pullout torque in exceeded, the stator and rotor components of the airgap flux no longer rotate at the same (synchronous) speed. If the effect of any damper windings is neglected, the net torque will drop abruptly to zero, becoming a large oscillating torque, but with no DC

component.

Since the double fed motor has externally imposed stator and rotor currents of independent frequency, it behaves as a synchronous motor and develops no net torque when the stator and rotor mmf's are not rotating at the same speed. When controlled using open loop frequency commands for F_1 and F_2 though, there is no mechanism to synchronize the phase of the rotating mmf's, and therefore it is unstable.

A phase-based approach, however, such as that implied by (3.6), will ensure field synchronization at all speeds, including during transients when the phase between F_1 and F_2 changes to compensate for a change in load torque. For this case, if the developed torque does not exactly balance the shaft torque, then a small speed change, similar to that of an induction machine, will take place. If the new slip results in a torque balance, the system will again be in equilibrium, although at a different speed. It is now merely a matter of using an outer speed control loop to modify the terminal parameters to give the desired torque. The response time of the developed torque, to commands from the speed error signal, determines the dynamic performance of the DFM drive system.

Field oriented control schemes for AC drives result in high performance drives with rapid response to changes in torque commands or load torque. The term 'field oriented' usually implies controlling the phase angle of the current vectors to achieve complete decoupling between the torque and flux components of the rotating airgap mmf [24].

Since fast dynamic performance is not generally a requirement of traction drives (unless related to the control of wheel slip), decoupled

field oriented control has not been applied to the DFM drive system developed in this research. The present control algorithm is field oriented in the general sense though, in that it is phase-based, and thus self-synchronizing. Decoupled field oriented control is a natural extension of what has been done to date.

4.2.2 DFM Torque Control

Stable operation of the double fed motor requires phase synchronization of the stator and rotor mmf vectors. In steady state operation, this also implies phase synchronization of the stator and rotor voltage vectors. This is equivalent to equation (3.6) where ψ is the stator-rotor voltage phase shift. This expression, repeated here with ψ replaced by δ_v, is illustrated by Figure 4.1 for several cases of sub and supersynchronous motoring and generating. From (3.6)

$$(\theta - \theta_o) = \alpha - \beta - \delta_v \tag{4.6}$$

Rearrangement gives

$$\beta = \alpha - (\theta - \theta_o) - \delta_v \tag{4.7}$$

α, the phase angle of the stator voltage, is basically the integral of the stator frequency F_1. $(\theta-\theta_o)$ corresponds to the rotor position (in electrical degrees) and can be obtained from a simple shaft encoder. Therefore, if δ_v is constant, the phase angle of the rotor voltage β will be fixed in the airgap with respect to α, and a steady torque will be developed. The magnitude of this torque though, is a function of δ_v and is the key to developing the DFM torque control algorithm.

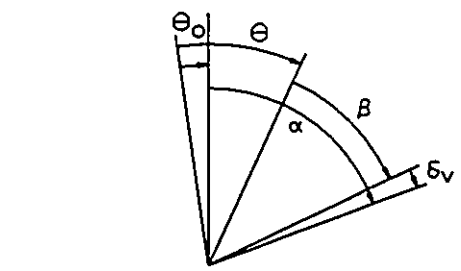

At all times, $(\Theta-\Theta_o) = \alpha-\beta-\delta_v$

Subsynchronous Motoring
with δ_v small

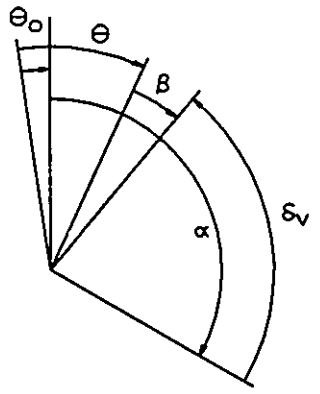

Subsynchronous Motoring
with δ_v near -90^o

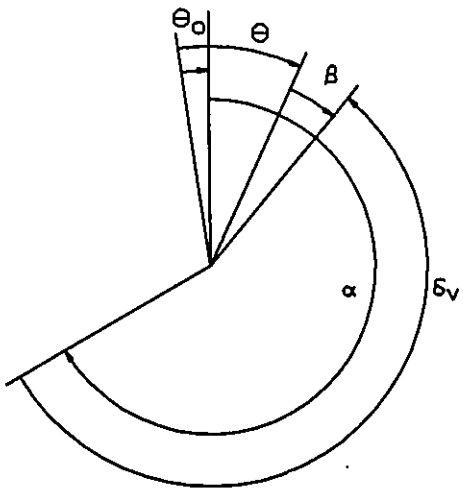

Supersynchronous Motoring
with δ_v near -205^o

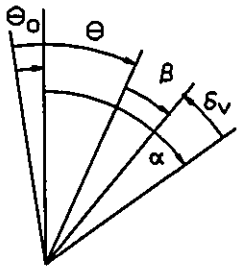

Supersynchronous Generating
with δ_v near -15^o

Definitions

Θ = Rotor Position (elec. deg.)
Θ_o = Rotor Shaft Offset
α = Stator Voltage Angle
β = Rotor Voltage Angle
δ_v = Pseudo Torque Angle
(also the phase shift between V_1 and V_2)

Figure 4.1 - PHASE SYNCHRONIZATION OF THE ROTATING STATOR AND ROTOR VOLTAGE VECTORS - Steady torque is developed when $\beta = \alpha - (\theta - \theta_o) - \delta_v$ is maintained.

Analysis of the DFM circle diagram in Section 3.3.3 showed that the electrical torque (which is proportional to d) is a function of $(\delta_v + \delta_o)$, plus a certain torque offset proportional to d_o (as in (3.47) and (3.62)). Since $(\delta_v + \delta_o)$ is analogous to δ, the internal (torque) angle in a synchronous machine, δ_v will be referred to as the pseudo torque angle of the double fed machine.

For any given set of values for V_1, V_2, F_1 and slip s (or W) the basepoint $BP = (x_o, y_o)$ is fixed, and the torque can be expressed by (3.49) as a linear function of d. That is

$$\Gamma = \frac{3}{2} \frac{-2R_1}{\omega} \left[x_o^2 + (y_o - \frac{\hat{V}_1}{2R_1})^2 \right]^{1/2} \times d \tag{4.8}$$

or

$$\Gamma = K_{BP} \times det_{BP} \times d \tag{4.9}$$

where

$$K_{BP} = \frac{3}{2} \frac{-2R_1}{\omega} \tag{4.10}$$

and

$$det_{BP} = \left[x_o^2 + (y_o - \frac{\hat{V}_1}{2R_1})^2 \right]^{1/2} \tag{4.11}$$

K_{BP} and det_{BP} are both functions of the basepoint (x_o, y_o), but they are not affected by the values of V_2 and δ_v. The magnitude and phase of the rotor voltage can therefore be used to control the torque of the DFM machine. The perpendicular distance d from the operating point (x,y), on C2, to the torque line Γ can be expressed graphically as

$$d = d_o + R_o \sin(\delta_v + \delta_o) \tag{4.12}$$

Equations (3.57d) and (3.61e) show that R_o is proportional to the rotor voltage V_2, and d_o is given by (3.63). Thus

$$R_o = |I_{1r}| = \left| \frac{V_2}{s} \frac{-1}{det_Z} \right| = \left[(x - x_o)^2 + (y - y_o)^2 \right]^{1/2} \tag{4.13}$$

and

$$d_o = \frac{\frac{1}{2}(R_o^2 + x_o^2 + y_o^2) - \frac{\hat{V}_1}{2R_1} y_o}{det_{BP}} \tag{4.14}$$

d_o gives the torque offset for a particular basepoint and varies with R_o^2 according to

$$d_o = D_1 + \frac{1}{2} \frac{R_o^2}{det_{BP}} \tag{4.15}$$

with

$$D_1 = \frac{\frac{1}{2}(x_o^2 + y_o^2) - \frac{\hat{V}_1}{2R_1} y_o}{det_{BP}} \tag{4.16}$$

D_1 is constant for any given basepoint (x_o,y_o).

In (4.8) the value of δ_o determines for what value of δ_v that d will be a negative maximum. Therefore, the angle δ_o is called the torque angle offset. From Section 3.3.3, it was also noted that the torque maximum occurs at the operating point OP = (x,y) where the tangent to OP is parallel to the torque line Γ. However, since the slope of Γ varies with the basepoint (ie. the slip, or the rotor speed), the slope of the tangent for Γ_{max} also shifts.

In addition, the point $OP_d = (x_d,y_d)$, where $\delta_v = 0^o$, also varies with the slip. This is clear from Figures 3.13, 3.14 and 3.15 where the operating point corresponding to $\delta_v = 0^o$ (labeled '$OP=0^o$') shifts widely as the slip varies. Control of the torque requires knowing the value of δ_o at the current basepoint. This can easily be determined from the basepoint (x_o,y_o) and OP_d. Referring to Figure 4.2, the slope m_δ of the line OP_dBP, from OP_d to BP, is

$$m_\delta = \frac{y_o - y_d}{x_o - x_d} \tag{4.17}$$

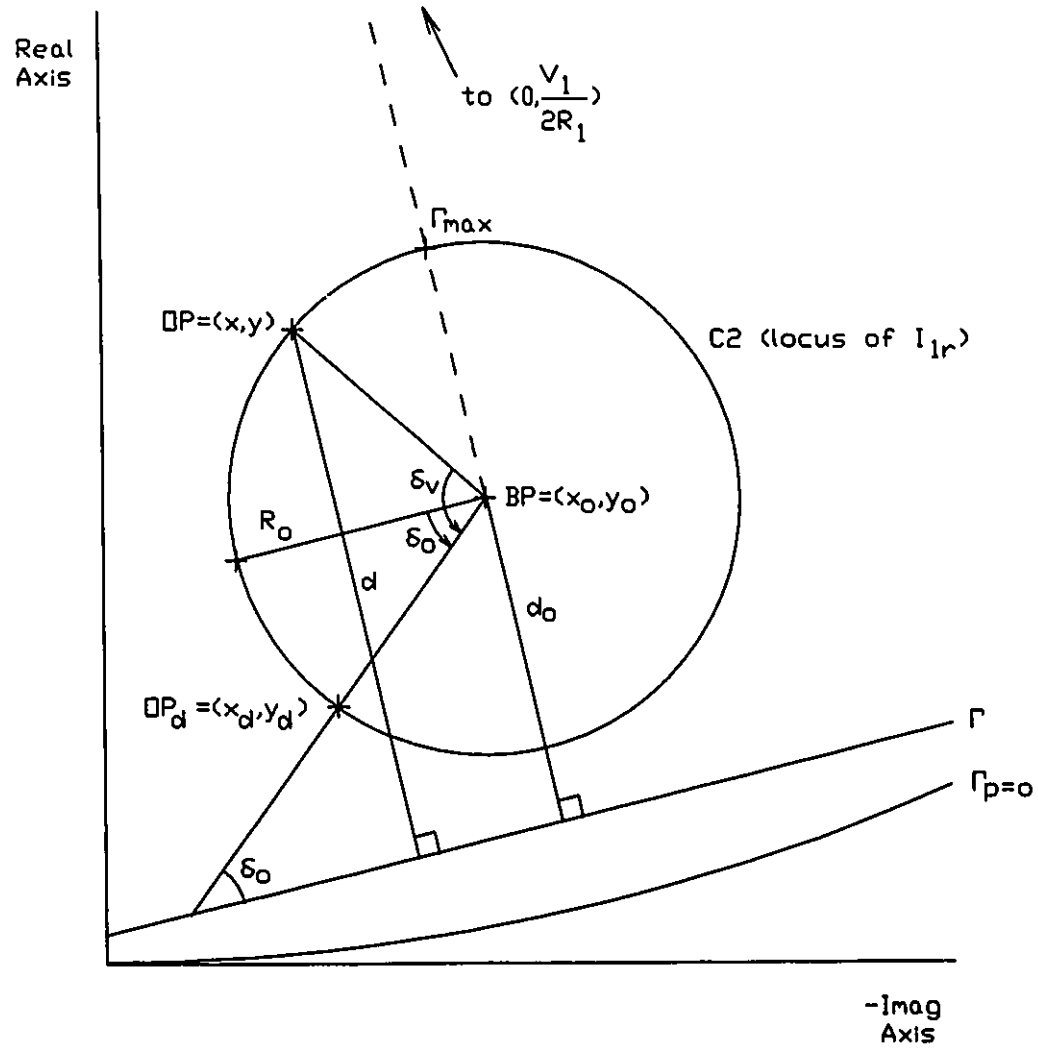

Figure 4.2 - DETERMINATION OF δ_o AND d_o FROM BP AND OP
The slope m_Γ is a function of the BP, and the slope m_δ is found using BP and OP_d (with $\delta_v = 0^o$).

The slope of the torque line, from simple geometrical considerations [27], is given by

$$m_\Gamma = \frac{x_o}{y_o - \frac{\hat{V}_1}{2R_1}} \tag{4.18}$$

Therefore, the torque angle offset δ_o is given by

$$\delta_o = \tan^{-1}(m_\delta) - \tan^{-1}(m_\Gamma) \tag{4.19}$$

and the maximum motoring torque, for any given basepoint, will occur at the angle where

$$\delta_v + \delta_o = -90^o \tag{4.20a}$$

or simply

$$\delta_v = -(\delta_o + 90^o) \tag{4.20b}$$

The maximum generating torque is likewise found to be where

$$\delta_v = -(\delta_o - 90^o) \tag{4.21}$$

4.2.3 DFM Torque Control Using δ_v

From the above considerations, a torque control algorithm can be derived using the pseudo torque angle δ_v, that does not require knowledge of the DFM currents. This is very useful, since no current sensors are needed to determine the phase angle of the 3-phase stator and rotor current vectors.

Figure 4.3 shows a block diagram of the proposed δ_v torque control algorithm. The operation of this system is as follows.

The stator and rotor cycloconverters are each controlled in terms of their output voltage magnitude (V_1 or V_2) and voltage phase

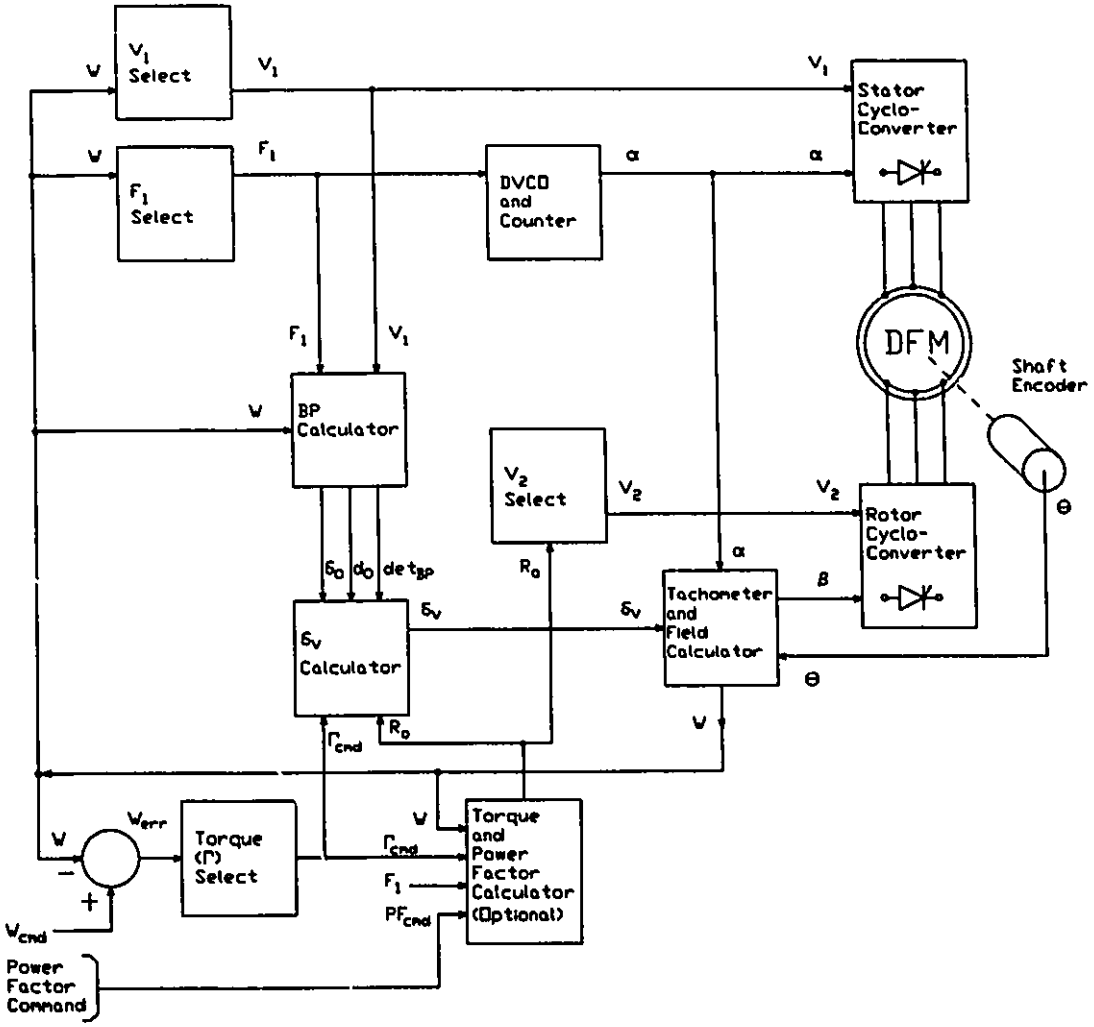

Figure 4.3 - BLOCK DIAGRAM OF THE PROPOSED δ_V CONTROL ALGORITHM No current sensors are required to achieve stable, field oriented (ie. self-synchronized) control.

angle (α or β). Optional current phase angle inputs P_1 and P_2 can be used to modify the natural bank switching angle of the cycloconverters if desired (Section 5.5.4.2).

Volts/Hz control is applied to the stator cycloconverter to maintain constant flux as the stator frequency varies. The V_1 Select and F_1 Select blocks implement one of several different algorithms chosen; to optimize the cycloconverter power factor, reduce the magnitude of the cycloconverter output harmonics, or avoid specific frequencies that create parasitic torques in the double fed motor (Section 4.3).

Phase synchronization and stable operation are ensured by the rotor field angle calculator (FC in the TFC block) which maintains $\beta = \alpha - \theta - \delta_v$ (4.7). Note: Since the rotor shaft offset θ_o can be nulled out by modifying δ_v, θ_o is not shown in the Figure.

From the F_1 command, a wide range digitally controlled VCO and counter generate the stator voltage angle α, and the effective stator frequency, since

$$\frac{d\alpha}{dt} = \omega = 2\pi F_1 \tag{4.22}$$

In a similar manner, the derivative of β yields

$$\frac{d\beta}{dt} = \Omega = 2\pi F_2 \tag{4.23}$$

From (3.4)

$$\frac{d\theta}{dt} = \frac{2}{P}(\omega - \Omega) = \frac{2}{P}\Omega_s = \frac{2}{P}2\pi W \tag{4.24}$$

and therefore $W = F_1 - F_2$ as desired (3.3).

The heart of the control system centers on the δ_v calculator, which determines the pseudo torque angle δ_v, which results in the

desired torque. This is readily calculated in the following steps:

i) From F_1, W and V_1, the basepoint BP = (x_o, y_o) is calculated, and then used to find d_o, δ_v and det_{BP}.

ii) R_o is determined by the effective rotor frequency $F_2 = F_1 - W$, or by a separate Torque and Power Factor Calculator.

iii) The speed error is used to calculate the necessary torque command in the Torque Select block. This block includes automatic ramping of the speed, if desired, for controlled acceleration and deceleration.

iv) The δ_v calculator then uses the values d_o, δ_o, det_{BP}, W, Γ_{cmd} and R_o to give the required stator-rotor voltage phase shift δ_v. This offset is acted upon by the field calculator, which controls the instantaneous phase relationship between β and α, according to δ_v and the instantaneous rotor angle θ.

The control can be implemented totally in software, or by a combination of dedicated hardware and software. At this point, it will be assumed that the software inputs are the set speed W_{cmd} (from the operator) and the actual rotor speed W (from the shaft encoder and associated logic). The software outputs are V_1, V_2, F_1 and δ_v (P_1 and P_2 are optional). Therefore the hardware determines δ and β, and generates all the firing pulses for both cycloconverters, with very little software overhead. (Supervisory functions such as overcurrent detection, short circuit protection, and system monitoring are not shown.) Detailed calculations are as follows.

The software determines F_1 and V_1, based on the actual rotor speed W and the F_1 selection algorithm. F_1 and $|V_1|$ are output to the hardware which generates α, and runs the stator cycloconverter open loop. According to F_1 the slip is determined as

$$s = 1 - \frac{W}{F_1} \tag{4.25}$$

and Z_1, Z_2, Z_m and $\det_Z$ are calculated using (3.50) and (3.52).

From V_1 and s, I_{1s} and the basepoint $BP = (x_o, y_o)$ are calculated using (3.57c)

$$BP = (x_o, y_o) = I_{1s} = V_1 \frac{1 + Z_2/Z_m}{\det_Z} \tag{4.26}$$

where it is assumed that the angle of V_1 is 0^o (ie. V_1 is the reference phasor). The basepoint determinant $\det_{BP}$ and basepoint constant K_{BP} are then found using (4.10) and (4.11).

$$K_{BP} = \frac{3}{2} \frac{-2R_1}{\omega} = -\frac{3}{2} \frac{R_1}{\pi F_1} \tag{4.27}$$

and

$$\det_{BP} = \left[x_o^2 + (y_o - \frac{\hat{V}_1}{2R_1})^2 \right]^{1/2} \tag{4.28}$$

$|V_2|$ is chosen according to W and the torque select algorithm. (This could be based on; volts/Hz control (using $F_2 = F_1 - W$), or torque and power factor considerations that are in turn functions of the speed, torque and power factor commands.) Given $|V_2|$ then, (3.57a) and (3.57d) give

$$|I_{1r}| = \left| \frac{V_2}{s} \frac{-1}{\det_Z} \right| \tag{4.29}$$

For any δ_v, the operating point OP is found from

$$OP = (x,y) = I_1 = (x_o, y_o) + I_{1r} \tag{4.30}$$

and from (3.61e)

$$R_o = \left[(x - x_o)^2 + (y - y_o)^2\right]^{1/2} \tag{4.31}$$

This is true for any (x,y) on C2, but it is convenient to choose $\delta_v = 0^o$ so that $(x,y) = (x_d,y_d) = OP_d$. The torque offset distance d_o is then found from (4.14) as

$$d_o = \frac{\frac{1}{2}(R_o^2 + x_o^2 + y_o^2) - \frac{\hat{V}_1}{2R_1} y_o}{det_{BP}} \tag{4.32}$$

To find the torque angle offset, it is necessary to know the angle between the torque line Γ and I_{1r} when $\delta_v = 0^o$ (Figure 4.2). Thus, from (4.29) with $\delta_v = 0^o$, $OP_d = (x_d,y_d)$ and

$$m_\delta = \frac{y_o - y_d}{x_o - x_d} \tag{4.33}$$

and

$$m_\Gamma = \frac{x_o}{y_o - \frac{\hat{V}_1}{2R_1}} \tag{4.34}$$

Then

$$\delta_o = \tan^{-1}(m_\delta) - \tan^{-1}(m_\Gamma) \tag{4.35}$$

The speed error is determined from

$$W_{err} = W_{cmd} - W \tag{4.36}$$

and serves as input to the Torque Select block, which yields the torque command Γ_{cmd}. Then from (4.27), (4.28), (4.31), (4.32), and (4.35) the pseudo torque angle is

$$\delta_v = \sin^{-1}\left[\frac{1}{R_o}\left(\frac{\Gamma_{cmd}}{K_{BP} \times det_{BP}} - d_o\right)\right] - \delta_o \tag{4.37}$$

The software then outputs δ_v, and the hardware performs

$$\beta = \theta - \alpha - \delta_v \tag{4.38}$$

to give synchronized operation at the desired torque. The rotor angle θ (and the corresponding speed W) is therefore the only variable necessary to achieve field oriented (ie. self synchronizing) torque and speed control of the double fed machine.

4.3 Avoidance of Harmonic Torques by Frequency Hopping

4.3.1 Cycloconverter Harmonic Producing Torques

In Chapter 2, the Jitter control method was introduced to minimize the dominant harmonics of the cycloconverter output. This approach reduced the harmonics that are produced at frequencies of $6nf_i \pm (2m-1)f_o$ at the expense of reintroducing some of the $3(2n-1)f_i$ harmonics. This effectively spreads the harmonic energy over a larger number of frequencies and minimizes the energy at any one frequency. In this way, the Jitter method allows a measure of control over the output harmonics, independent of the load operating conditions.

The application of two cycloconverters to a double fed motor provides an even greater degree of freedom than this though. It is now possible, at certain output frequencies, to avoid producing specific output harmonics, by 'hopping' around those frequencies. For a single fed drive, the motor speed f_o determines exactly the output frequency of the cycloconverter. With a double fed motor however, the motor speed only determines the difference frequency that must exist between F_1 and F_2 according to (3.1) and (3.3). That is, $W = F_1 - F_2$, and for any speed

W it is now possible to choose F_1 and F_2 so that neither cycloconverter operates at a frequency that produces large torque harmonics.

As an example, consider the case where the stator frequency F_1 is fixed and the motor speed W is increasing (ie. the load torque is less than the developed torque). To ensure synchronization of the rotating mmfs in the airgap, the rotor frequency F_2 is automatically decreased as the motor speed W increases, maintaining the necessary phase relationship (Sections 4.2.1 and 5.4.4). However, when F_1 is incremented (or decremented), the control circuit causes an immediate decrease (or increase) in F_2 of the same amount , so that the rotor frequency Ω_s (and W) remains the same.

Assume now, that F_1 is constant, W is increasing, and F_2 is decreasing. Then, just before F_2 reaches a frequency that produces undesirable harmonics of a large amplitude, F_1 is increased by a small amount, on the order of .5 to 1.5 Hz. Simultaneously, the control hardware decreases F_2 by the same amount, causing F_2 to 'hop' over the undesirable frequency. Since the undesirable frequencies are known, it is possible to always choose F_1 such that the stator and rotor cycloconverters never generate large torque producing harmonics, regardless of the motor speed or load condition. This is a very attractive feature of the double fed drive system, and allows the output frequencies of the cycloconverters to go substantially higher than is normally possible.

4.3.2 DFM Response to Frequency Hopping

Before implementing such a scheme, it is important to consider the response of the DFM to sudden changes in the stator and rotor frequencies. From Figure 3.12 (Section 3.3.3), it is seen that changing F_1 will alter the slip scale of C1 and shift the basepoint BP of C2. This results in a corresponding change in the developed torque and will eventually lead to a change in the rotor speed.

However, the mechanical time constant of the rotor is approximately an order of magnitude longer than the electrical time constants of the torque producing currents. Therefore, the rotor speed W can be considered to be constant in the time interval immediately after any change in F_1. Similarly, the phase angle control circuit of the rotor cycloconverter is an order of magnitude shorter than the time constant of the stator and rotor currents. This means that a change in the control variable F_1, causes an immediate change in the effective rotor frequency F_2.

At the same time, changes can be made in the control variables V_1, V_2 and δ_v to maintain the desired torque in the airgap, despite the change in the speed of the synchronously rotating mmf. The mechanical inertia of the rotor serves to smooth out any brief fluxuations in the developed torque.

Figures 4.4, 4.5 and 4.6 show how F_2 is adjusted to maintain a constant speed W when F_1 is changed. The step changes shown in F_1 are larger than actually required, but they serve to enhance the clarity of the diagrams. Note, also, that F_2 is not specifically controlled or

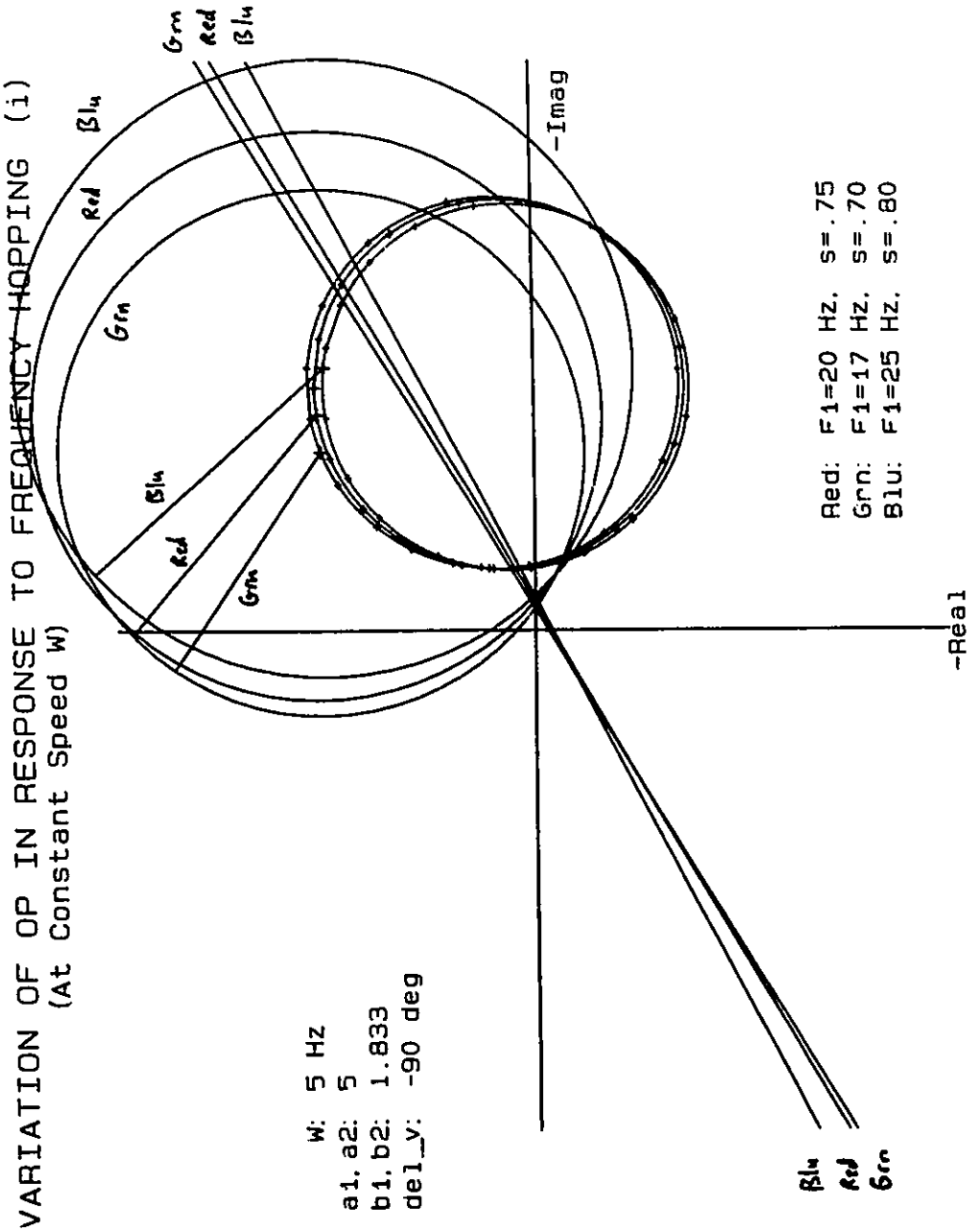

Figure 4.4 - VARIATION OF THE OPERATING POINT OP IN RESPONSE TO FREQUENCY HOPPING (i) - A small step change in F_1 does not produce a large variation in the developed torque Γ.

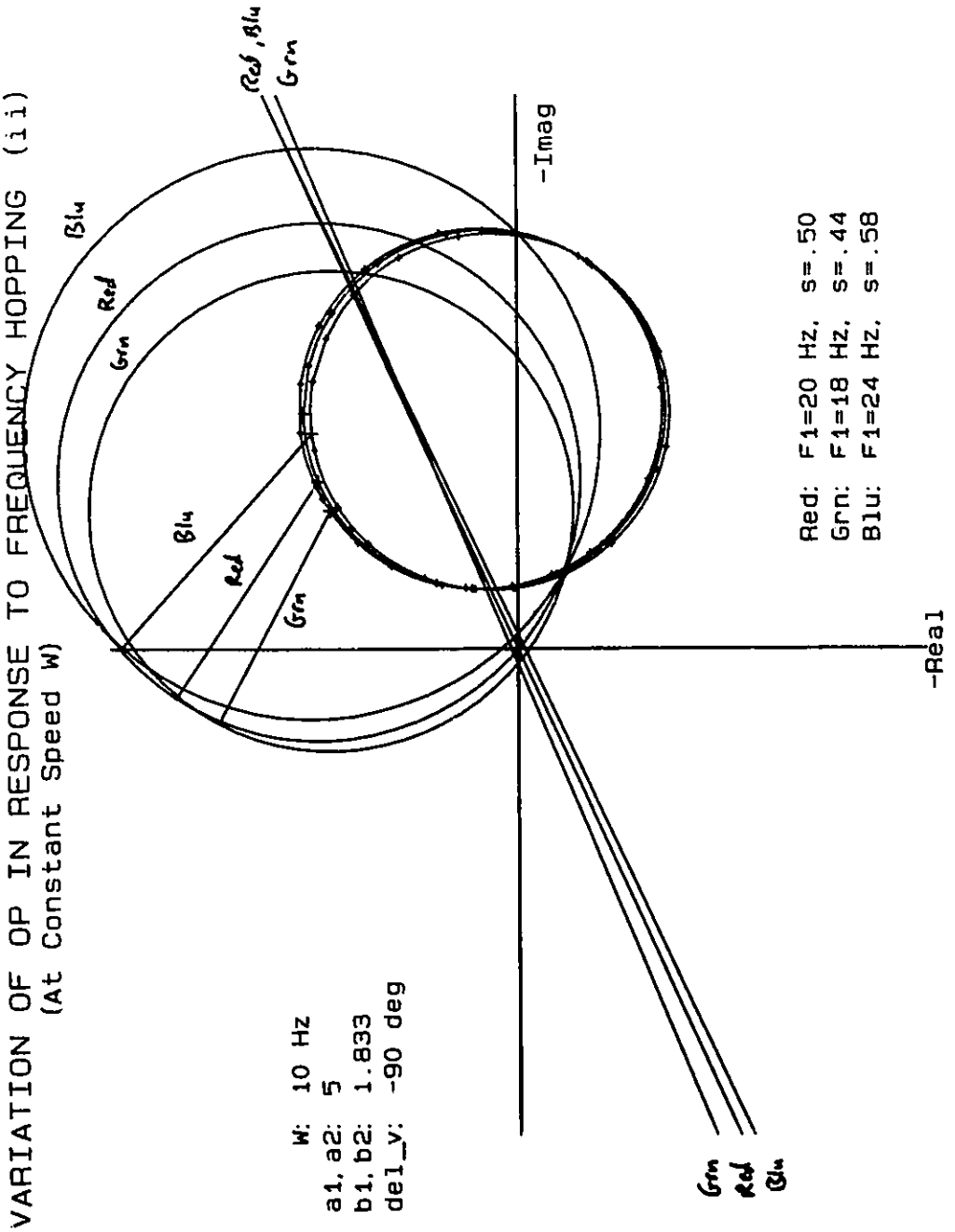

Figure 4.5 - VARIATION OF THE OPERATING POINT OP IN RESPONSE TO FREQUENCY HOPPING (ii) - Simultaneous variation of δ_v, with the step change in F_1, allows the torque to be maintained precisely.

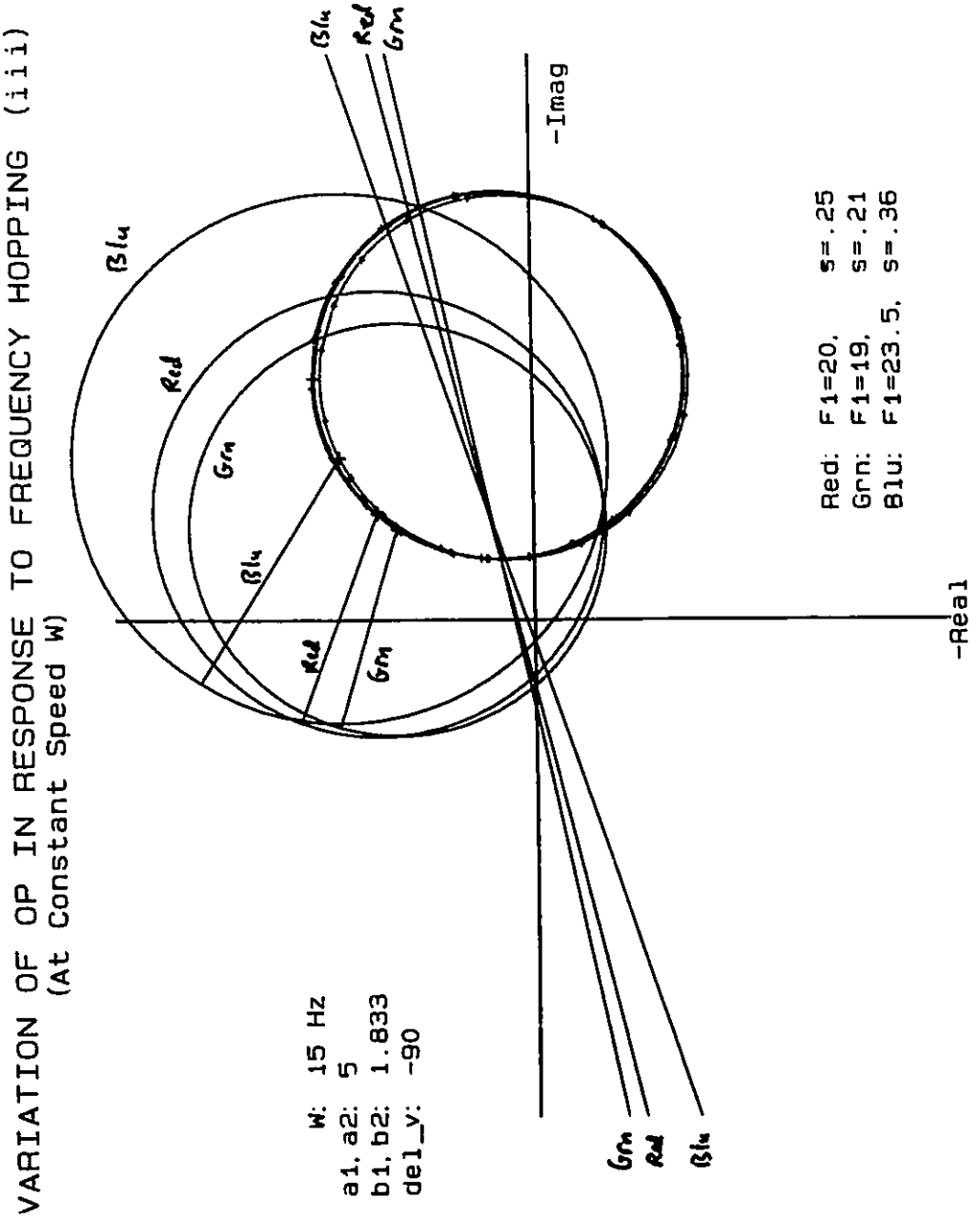

Figure 4.6 - VARIATION OF THE OPERATING POINT OP IN RESPONSE TO FREQUENCY HOPPING (iii) - The mechanical inertia of the rotor insures that the rotor speed W is constant during the step change.

specified in the Figures. It is implied though by the value of slip s, since $s = F_2/F_1$.

Since it is possible to adjust V_1, V_2 and δ_v when F_1 is changed, these simulation results from DFMPLT, show that frequency hopping is a viable control option for the double fed motor. A specific control strategy will now be derived to avoid the cycloconverter harmonics which generate the major parasitic torques.

4.3.3 Hopping Algorithm for Choosing the Stator Frequency F_1

Chapter 2 showed how the cycloconverter harmonics vary in frequency and amplitude as the output frequency f_o varies. Figures 2.1 and 2.5 show the 'lines' which the harmonics follow as f_o changes. The undesirable output frequencies can be derived from the intersection of the harmonic lines of Figure 2.5 and specific harmonics of the output frequency; the 5^{th}, 7^{th}, 11^{th} and 13^{th}. These values are found from equating

$$6nf_i \pm (2m-1)f_o \qquad n = 1,2 \qquad m = 1,2... \tag{4.39}$$

with

$$nf_o \qquad n = 1,5,7,11,13 \tag{4.40}$$

This is shown graphically in Figure 4.7. It is seen that the intersection of the torque producing harmonic lines (the 5^{th}, 7^{th}, 11^{th}, & 13^{th} harmonics of the desired output frequency) only intersect the families $6nf_i \pm (2m-1)f_o$ at a limited number of discrete values. Generally, these values are approximately 2 Hz apart and it is therefore

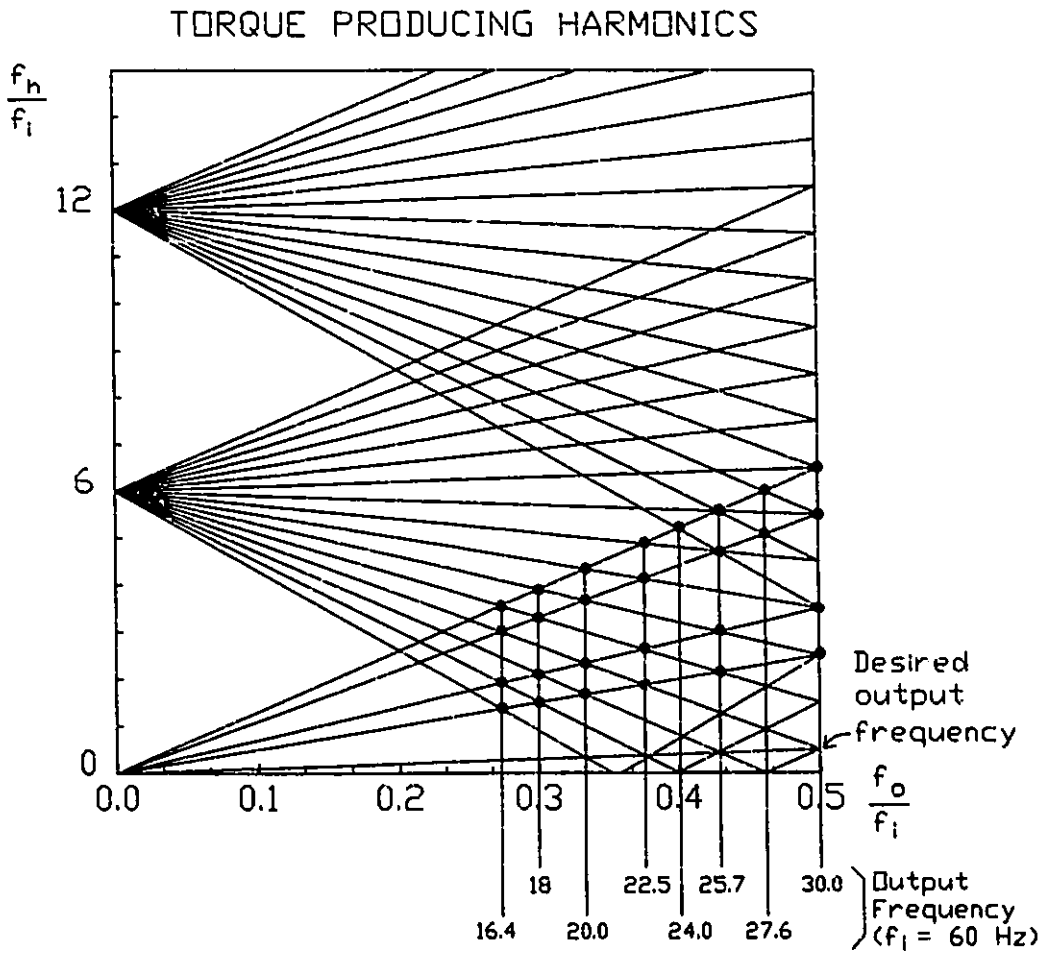

Figure 4.7 - DETERMINATION OF THE OUTPUT FREQUENCIES WHICH PRODUCE HARMONIC TORQUES - Harmonic torques occur at the intersection points of the lines $6nf_i \pm (2m-1)f_o$ (with n = 1,2; m = 1,2...) and the lines nf_o (with n = 1,5,7,11,13...).

quite easy to avoid them. Only the harmonic lines up to m = 9, and n = 2 have been considered. The others lie above the frequencies of interest or are not large enough to have any effect.

Figure 4.8 expresses the relationship $W = F_1 - F_2$ for all four quadrants of operation. In this diagram, the x and y axes correspond to the stator and rotor frequencies F_1 and F_2, and the infinite set of parallel diagonals represent lines of constant speed W. For any speed, the combination of F_1 and F_2 determines the basepoint, or slip, of the machine. It is possible to move the basepoint ($W = F_1 - F_2$) instantly along any line of constant speed. This is due to the much shorter time constant of the stator and rotor field currents when compared to the rotor mechanical time constant.

For a given stator frequency F_1, the magnitude of F_2 is changed automatically to compensate for any change in rotor speed, and the basepoint moves vertically. A step change in F_1, on the other hand, appears as a diagonal jump along one of the lines of constant speed. When F_1 is increased (decreased), the trajectory is upward to the right (downward to the left). The magnitude of the change in F_1 is limited by the capabilities of the torque control scheme (Section 4.2.3), to compensate via V_1, V_2 and δ_v for the torque variation that would otherwise occur.

From Section 4.1, to minimize harmonic generation and to maximize the input power factor, it is desirable to simultaneously keep the cycloconverter output voltage high, and output frequency low. This conflicts with the usual constant volts/Hz ratio control used to prevent saturation of the motor, and a so compromise must be made.

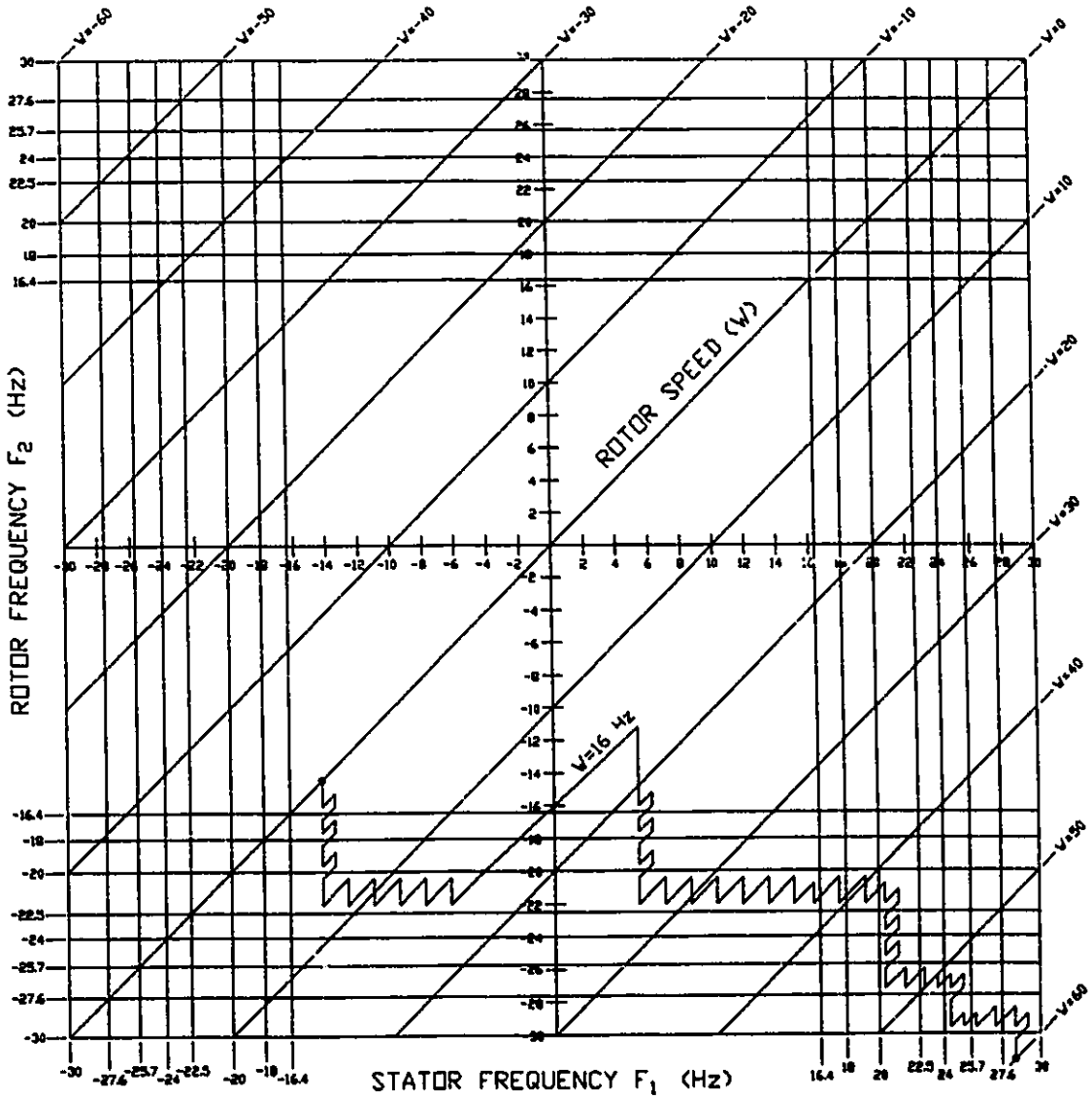

Figure 4.8 - FREQUENCY HOPPING TRAJECTORY FOR THE DOUBLE FED MOTOR
Step changes in F_1 result in diagonal motion along the lines of constant speed W, and undesirable output frequencies (of F_1 or F_2) can thus be avoided.

A possible trajectory, from W = 0 to W = 60 Hz, is also shown in Figure 4.8. Initially, both cycloconverters are operating near -15 Hz with V_1 and V_2 determined by (3.54) and the torque control algorithm of Section 4.2.3. Assuming the torque is positive, W will increase and F_1 will be stepped up and then down, three times in succession, so that the rotor cycloconverter avoids the output frequencies 16.4, 18 and 20 Hz. At W = 8 Hz, F_1 then alternates between 13 and 15 Hz until W = 16 Hz and then is moved quickly through its low frequency, low voltage region to +6 Hz. At this point the stator frequency continues to be stepped up and down for the rest of the trajectory until W = 60 Hz.

Several points are of interest. First, the trajectory can be chosen to include subsynchronous and supersynchronous operation, or supersynchronous operation only. The choice is determined by the tradeoff of between the required load torque and the input power factor as incorporated into the control algorithm. Secondly, as W approaches 60 Hz, there is less and less freedom to choose the basepoint, since both cycloconverters are operating near their maximum output frequency.

From the considerations of this chapter and the previous one, it is clear that the double fed motor, using two separately controlled cycloconverters, is a very attractive approach for use in high power traction drives. The next two chapters document the hardware and software developed to implement a working DFM drive system of this type.

CHAPTER 5

DOUBLE FED MOTOR DRIVE HARDWARE

5.1 Introduction and Overview

The DFMDRV hardware, shown in Figure 5.1, performs three basic functions:

i) In response to the computer control signals V_1, V_2, F_1, P_1, P_2, B_1 and B_2, the control circuits generate firing pulses for the cycloconverters to run the motor at its desired speed and torque.

ii) Continuous monitoring of the bank current zero crossings, and the rotor angle θ, provide feedback information for control of the firing pulses, synchronized with the actual rotor position.

iii) Protection is provided against steady-state overload conditions and transient short circuits. This also includes an automatic short circuit reset provision to facilitate development and calibration of the hardware.

The DFM control principles outlined in Chapters 3 and 4 require a precise knowledge of the rotor shaft position θ. This is obtained

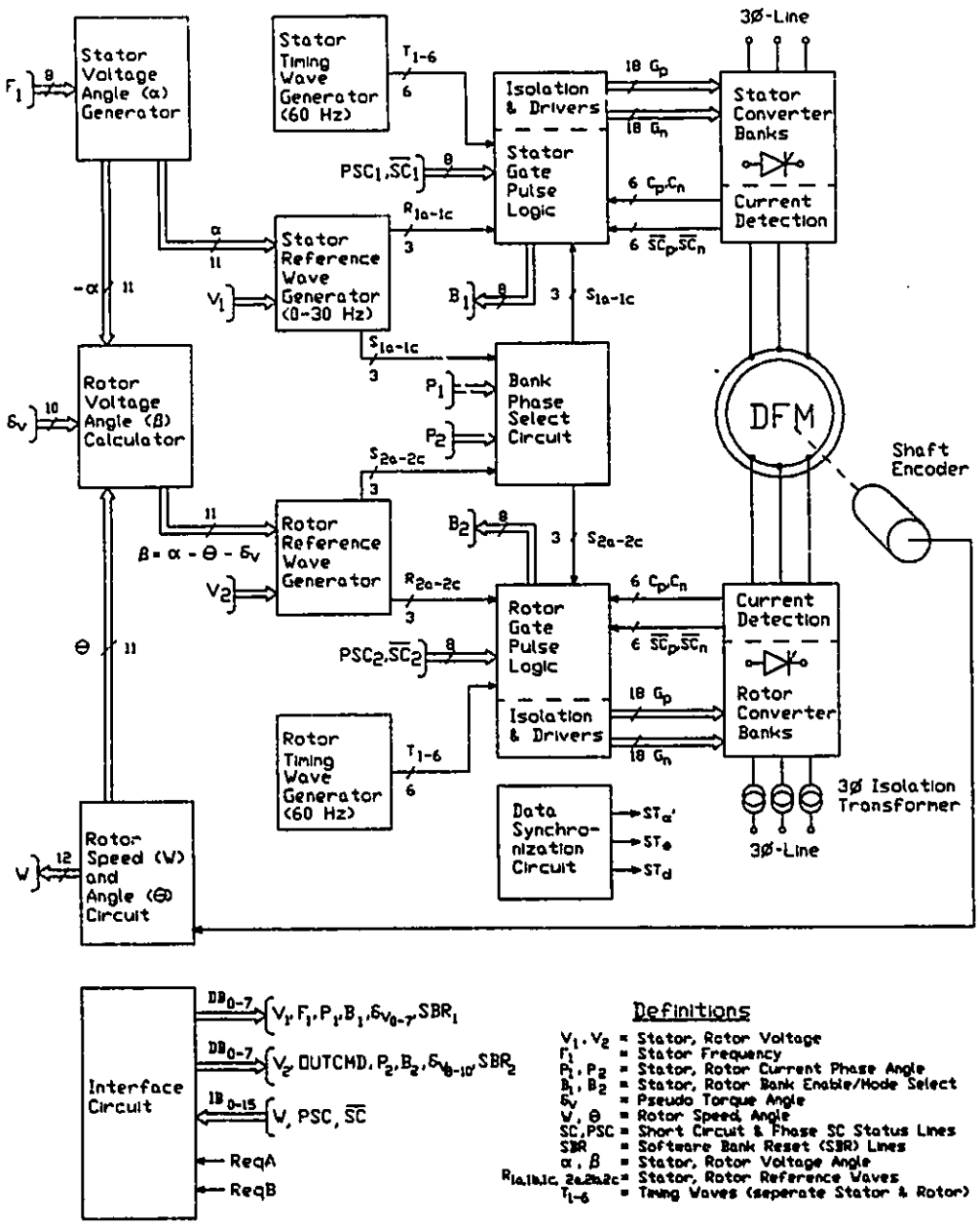

Figure 5.1 - DOUBLE FED MOTOR DRIVE WITH DUAL CYCLOCONVERTERS
The rotor voltage angle calculator ensures synchronization of the stator and rotor rotating mmfs. Dual cycloconverters provide smooth torque at high power from standstill to base speed (ie. 60 Hz operation).

using a digital shaft position encoder and the rotor mechanical angle (θ) and rotor speed (W) circuits of Figure 5.7. The desired speed is compared in software with the actual speed and appropriate values for the stator frequency F_1 and voltage V_1 are output to the hardware via a special interface board. F_1 controls a digital oscillator and counter to generate α, the stator voltage angle (Fig. 5.6), and V_1 determines the stator flux by controlling the amplitude of the stator reference wave generator (Fig. 5.5). The pseudo torque angle δ_v is combined with α and θ to determine the rotor voltage angle β (Fig. 5.7). Since the values for α, θ and δ_v are asynchronous, a special synchronization circuit ensures that all data values are strobed only when they are valid.

Two timing wave generators (one each for the stator and the rotor) each produce 6-phase sinewaves, T_{1-6}, synchronized with the stator and rotor 3-phase supply voltages, respectively (Fig. 5.4). The cosine wave control method is implemented in the gate pulse logic circuits of Figure 5.10 to compare the various timing and reference waves and generate the gate firing pulses. The gate trigger circuits fire the SCR's and provide isolation of the control circuits from the high working voltages present at the converter banks (Fig. 5.13). Phase information to correctly determine the switching instant from positive to negative converter banks is provided by the bank phase angle circuit of Figure 5.12 and the current 'off-detection' circuit of Figure 5.14. Short circuit protection is incorporated also in the current detection logic of Figure 5.13. B_1 and B_2 outputs provide selective enable/disable and reset control for each converter bank.

The hardware is a continuation of a prototype designed and built

for my Master's thesis [3]. The original design philosophy was to keep the circuitry as simple as possible, yet incorporate sufficient flexibility into the design that subsequent modifications, even those not anticipated, would not require any major rebuilding or redesign of working sections. This 'upward compatibility' has worked very well.

The choice of digital control circuits with analogue sections in the timing and reference wave generators [3] has proven to be very flexible and adaptable. In addition, digital sinewave generation (using a counter and a ROM look-up table) is inherently a phase-based approach, and is therefore ideally suited to the synchronization requirements of the double fed motor. CMOS components were used extensively throughout because of the higher noise margins they offer when run at 15 volts.

An important factor as well, was the requirement that the equipment be robust, and not easily damaged by misuse or while under development. Fuses are very expensive and were impractical for this purpose. Circuit breakers work well for relatively long duration overloads, which don't greatly exceed the SCR-ratings, but are too slow to prevent extensive thyristor damage during the very high surges present during line-to-line bank shorts. For this reason, it was necessary to design and implement a simple, effective method to detect bank shorts and immediately block all subsequent gate pulses. In addition, automatic reset circuitry is provided to reenable the power circuits as soon as the fault is cleared. This ensures that the motor will continue to run, even though there may be major errors in the software control parameters or in the hardware calibration. This novel provision was invaluable during the development of the DFM drive system (see Section 5.6.4).

Finally, in order to further simplify building and testing of the circuit, an effort was made to make circuit boards and component groupings as interchangeable as possible. As a result the comparator boards, gate trigger boards, converter banks and current detection elements of all 6 phases are identical. An intermittent or suspect circuit can be quickly replaced by another which is known to be good and problems can be isolated easily.

The hardware is logically organized, neatly constructed, and conveniently serviced. All circuit boards are polarized to prevent erroneous insertion and all cables and connections are clearly labelled. The hardware and software are well documented and are designed to function as a stand-alone unit. This facilitates the use of the equipment by other persons for further research beyond the scope of this thesis.

5.2 Computer Interface and Control Variables

Communication with the host computer (a PDP-11) is via an interface circuit and the DRV11, a general purpose parallel line driver for the PDP-11. Data and control bits are accessed from software via three 16-bit memory-mapped words; DROUTBUF, DRINBUF and DRCSR (output buffer, input buffer and control status register, respectively). Two other lines, New Data Ready (NDR) and Data Transmitted (DT) provide full handshake data transfer. Output data appear on the 16-bit data bus DB and are latched by the NDR pulse into various buffers according to bits

0 and 1 of DRCSR.

Likewise, on input to the host, the data to be strobed onto the input bus IB by the DT pulse are also determined by bits 0 and 1 of DRCSR. All inputs and outputs are buffered to CMOS or TTL voltage levels as required. In addition, two interrupt requests, ReqA and ReqB, are used for high speed servicing of the Phase Short Circuit (PSC) interrupts.

The DFM motor drive software DFMDRV (described in Chapter 6) outputs two types of data to the hardware. The first type pertain directly to the control variables of the motor, and are the same variables used by DFMPLT (Chapter 3). They are V_1, V_2, F_1, P_1, P_2 and δ_v. The second type of data control the operating mode and status of the cycloconverters. These are B_1, B_2, SBR, and OUTCMD. There is one motor related input, W, and the other inputs, $\overline{SC}$ and PSC, are for monitoring of the cycloconverters' current status.

Most of these data are 8 bits, and are paired to form 16-bit words such that the low order byte (bits 0-7) contains the stator quantity and the high order byte (bits 8-15) contains the rotor quantity. Figure 5.2 shows the various inputs and outputs that are possible, along with the DRCSR bit codes that access them. For example, when CSR1 and CSR0 both equal one, the stator and rotor phase angles P_1 and P_2 are output and latched by the strobe line ST_P into their respective buffers of the bank phase angle select circuit (Figure 5.12).

Since there is no specific control variable required for the rotor frequency F_2, an 8-bit control word OUTCMD is output in place of F_2 as the high order byte of data word #1. This provides 8 command bits

Data Word #	DRCSR bits CSR1	CSR0	SELBNK bit4	SELHBR bit 6	Strobe Line	Data Bus Contains high byte	low byte	Description
1	0	0	0	0	$ST_{F/CMD}$	OUTCMD	F_1	Command bits and stator frequency
2	0	1	0	0	ST_V	V_2	V_1	Rotor & stator voltage
3	0	1	0	1	ST_{HBR}	--- HBR lines ---		Strobe all stator and rotor HBR lines
4	0	1	1	0	ST_B	B_2	B_1	Rotor & stator bank enable bits
5	0	1	1	1	ST_{SBR}	--- SBR lines ---		Rotor & stator Soft Bank Reset bits
6	1	0	0	0	ST_δ	δ_{3-10}	δ_{0-2},EXTBTS	δ' (11 bits) plus 5 'extra' bits
7	1	1	0	0	ST_P	P_2	P_1	Rotor & stator phase angle

Data Word #	DRCSR bits CSR1	CSR0	Strobe Line	Input Bus Contains high byte	low byte	Description
8	0	0	ST_W	----- W -------		Rotor speed
9	0	1	ST_{SC}	-- SC lines ---		Rotor and stator bank Short Circuit & status lines
10	1	0	ST_{PSC}	-- PSC lines --		Rotor and stator Phase Short Circuit lines
11	1	1	ST_{CLR}	--- nothing ---		Clear ReqB interrupt request

Figure 5.2 - IO VARIABLES AND STROBE LINES - On output the DRCSR bits, SELBNK and SELHBR, determine which line is strobed and the destination of the data. On input the DRCSR bits determine which data is input.

OUTCMD Bit#	Bit Name	Description	Value	Meaning
0	P_0	Preset for W-counter	6	1 interval = 0 digits accuracy
1	P_1	determines the accuracy	5	2 intervals = 1 " "
2	P_2	of speed input	3	4 " = 2 " "
3	P_3		15	8 " = 3 " "

			Cleared	Set
4	* SELBNK	select voltage/bank latches	* voltage latches	* bank latches
5	SELRNG	select rotor voltage range	$-120 \le V_2 \le 120$	$0 \le V_2 \le 120$
6	* SELHBR	select hard & soft bank reset pulses (HBR & SBR)	*	*
7	SELDIR	select stator field direction	forward	reverse

* See Figure 5.2 for the exact function of these bits

Figure 5.3 - BIT MAP OF OUTPUT COMMAND BYTE 'OUTCMD'

for the DFMDRV hardware as shown in Figure 5.3. Bits 0 to 3 are preset bits used in the rotor speed measuring circuit (Figure 5.7) while the other 4 are independent, and control various functions.

Of special note here are bit 4, the 'select bank' bit SELBNK, and bit 6, the 'select HBR' bit SELHBR. These two bits are used to provide three additional strobe lines in place of the single ST_V line. The software sets up command bits SELBNK and SELHBR via the control byte OUTCMD, with both CSR0 and CSR1 bits cleared. Then with CSR0 set, the appropriate voltage, HBR command, bank enable, or SBR command data are output and will be latched according to the previously output values of SELBNK and SELHBR. The remaining combinations of CSR0 and CSR1 are used to output the phase and δ_V data.

The input data word #9 contains data from the $\overline{SC}$ (short circuit) lines. Twelve bits are used as bit flags to signal a short circuit has occurred in a particular converter bank. Bits 0 and 8 signify that the hardware short circuit protection has been disabled, on the stator or rotor respectively (ie. Manual Bank Enable, MBE), and bit 1 is a safety interlock bit. If any circuit board in the main rack is not inserted, bit 1 will go low and signal an LB (loose board) error. Bit 9 is unused at present.

Input data word #10 contains data from the PSC (Phase Short Circuit) lines. These are strobed when the software responds to a ReqA interrupt. Input data word #11 is a dummy read, but provides a strobe ST_{CLR} to clear the ReqB interrupt flag.

5.3 Timing and Reference Wave Generators

5.3.1 Hybrid Digital-Analogue Approach

The cosine wave method of cycloconverter control requires the generation of sinusoidal timing and reference waves that can be precisely controlled in terms of frequency and amplitude [17]. The stability and accuracy of the cycloconverter drive is determined by the control accuracy of these sinewaves. In addition, for the DFM system, precise phase control of the reference waves is also necessary.

These requirements are readily met by using hybrid digital-analogue sinewave generators [3]. The basic idea is to use the outputs of a digital counter as address lines to access EPROM (or other memory) in which the desired timing or reference wave is stored. As the counter repeatedly cycles through the appropriate memory address range, the memory data values are output and strobed into a D/A converter to provide an analogue signal. Precise frequency control is determined by the count rate, phase control is directly related to the EPROM address, and voltage control is achieved by an additional D/A converter connected to provide a programmable reference voltage V_{prog} for the other D/A converters. This form of digital amplitude control is very elegant because it provides the real-time scaling (multiplication) of the sinewaves that are necessary for voltage control of the cycloconverter output.

5.3.2 Timing Wave Generation

The stator and rotor cycloconverters are each composed of three 6-pulse bridge-configured dual converters, one for each phase. The particular wound rotor motor used in this research however has a wye-connected rotor, and so the rotor converters must be isolated from each other at their inputs (or outputs). Considering the wide frequency range of the output, input isolation was chosen and a 3-phase Δ-Y, 1:1 isolation transformer was built. This transformer introduces a 30^{o} phase shift in the rotor supply and so separate timing wave generators (T1 and T2) are required for the stator and rotor cycloconverters. Each timing wave generator produces a symmetrical 6-phase sinewave set which is synchronized with the stator or rotor supply lines.

Figure 5.4 shows the timing wave generator circuit. A 60 Hz signal, synchronized with the AC supply, is derived through the low voltage transformer, adjustable phase delay filter, and zero-crossing detector (ZCD). The phase comparator (PC) and voltage controlled oscillator (VCO), both in the same chip (CMOS 4046), in conjunction with the timing wave address counter (T-Counter) and low pass filter LP, form a phase locked loop (PLL). When the 11-bit T-counter reaches zero, it generates a pulse which is fed back to the phase comparator, along with the ZCD output. The filtered output of the phase comparator therefore provides a control voltage for the VCO which produces a 122,880 Hz (2048 x 60) clock signal and causes the counter output to cycle through the EPROM address range at exactly 60 Hz. A trim pot in the ZCD and the selectable ZCD filter parameters provide approximately 75^{o} of phase

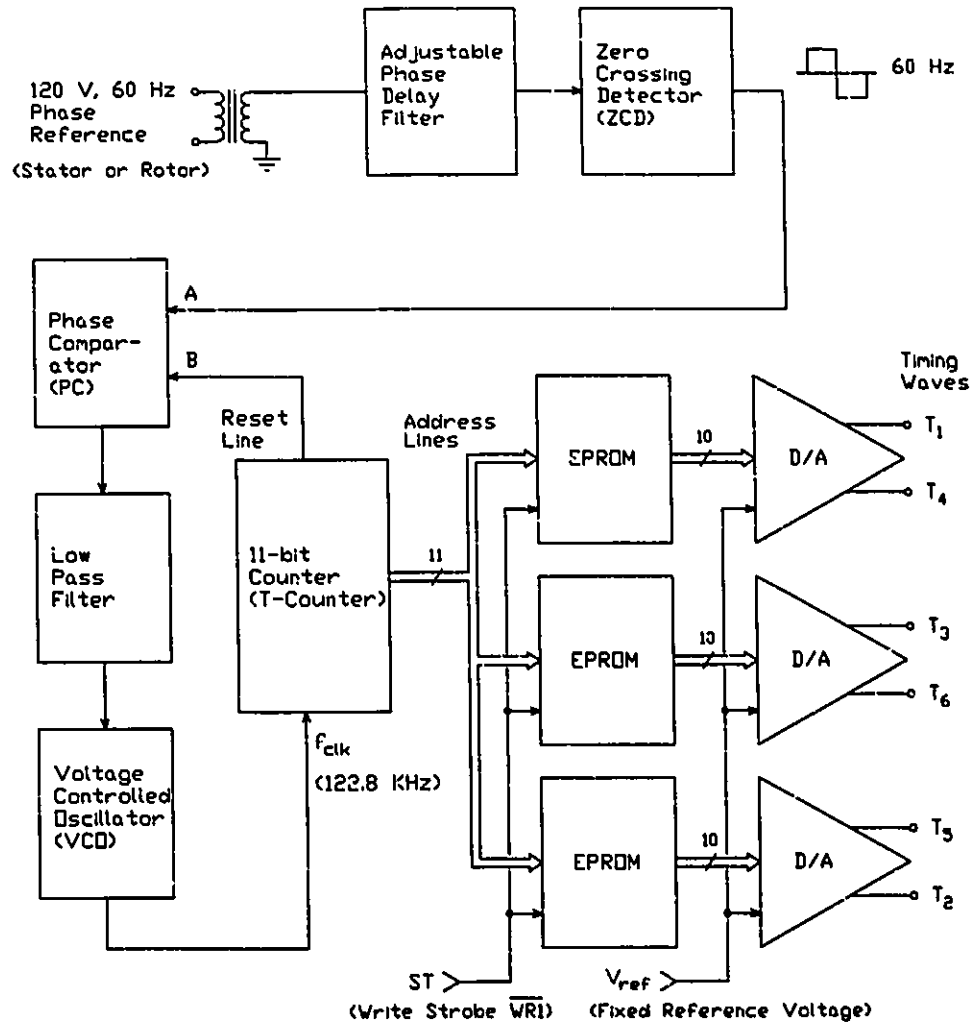

Figure 5.4 - TIMING WAVE GENERATION (T_1 to T_6)
A ZCD and PLL produce a 122.8 KHz clock which cycles through the EPROM address range at exactly 60 Hz, generating the 6-phase sinusoidal timing waves.

adjustment so that the resulting timing waves can be set to lead the line-line AC supply voltages by 60^{o}.

For both the timing and reference wave generators, four 8-bit 2732 EPROM's have been partitioned to provide three 10-bit sinewaves, each with 2048 increments. The sinewaves are stored with a 120^{o} phase shift between each of them. The 3 additional phases required by the timing wave generators are derived by inverting these signals.

5.3.3 Reference Wave Generation

The reference wave generators, Ref_1 and Ref_2 provide symmetrical 3-phase sinewaves (R_{1a}, R_{1b}, R_{1c}, R_{2a}, R_{2b}, R_{2c}) of the desired voltage, frequency and phase for the stator and rotor cycloconverters (Fig. 5.5). The EPROM and D/A sections are similar to those of the timing wave generators, but the source of the EPROM addresses are different, and the output amplitude is controllable instead of fixed.

The stator voltage angle α comes from the stator voltage angle generator circuit (Section 5.4.2), and the rotor voltage angle β comes from the rotor voltage angle calculator circuit (Section 5.4.4). The inverted values of α and β (α' and β' respectively) are input to the appropriate reference wave generators Ref_1 and Ref_2. Inverting level shifters (CMOS 4049) provide the correct count direction and voltage levels for the EPROM's.

Data bus lines DB_{0-7} and DB_{8-15} provide the scaled 8-bit stator and rotor voltage control values, V_1 and V_2, for the 10-bit D/A input

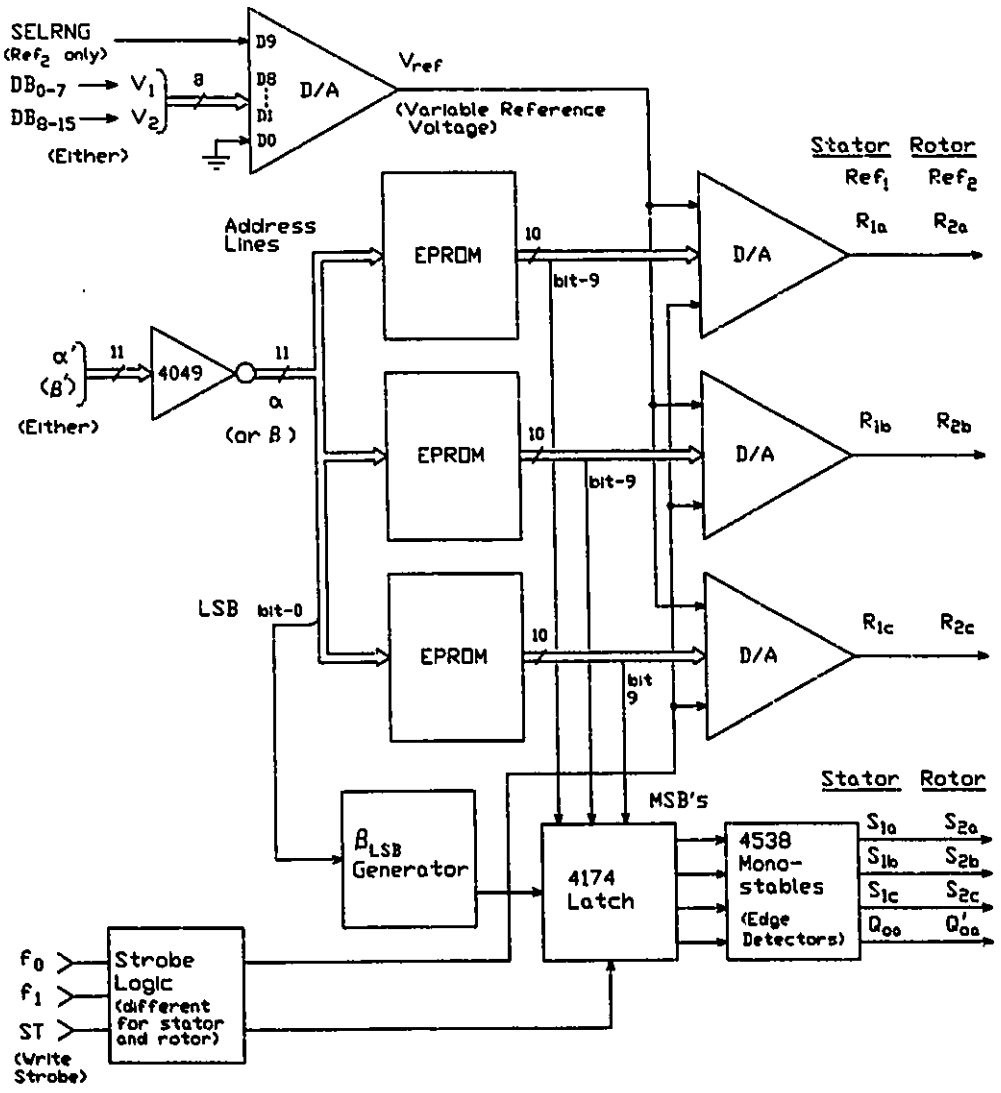

Figure 5.5 - REFERENCE WAVE GENERATION (Ref_1 and Ref_2)
The input α' (or β') forms the address of the sinewave look-up tables to generate the reference waves R_{1a}-R_{1c} (or R_{2a}-R_{2c} for the Rotor). Edge detectors produce sync pulses for the bank phase select logic.

pins, D1-D8. D0 is grounded and D9, the most significant bit (MSB), is connected high (for Ref_1) or to the SELRNG bit of OUTCMD (for Ref_2), as in Figure 5.3. This provides an 8-bit unipolar output reference voltage for Ref_1 and a 9-bit bi-polar output reference voltage for Ref_2 (Figure 5.3). The additional flexibility provided by the bi-polar reference voltage is very useful for testing purposes, when operating the converter bank in MANUAL mode (Section 6.3.3).

For example, by setting F_1 to 0.1 Hz, and observing V_2 on the oscilloscope, F_1 can be set to 0 Hz when V_2 is precisely at it's maximum value. This corresponds to the EPROM address being fixed at $\beta = 90^{o}$. Then by controlling V_2 in MANUAL mode from the keyboard, the Ref_2 voltage can be smoothly varied between -120 and +120 volts, with the MANUAL mode software controlling the SELRNG line, and thus the MSB D9. This allows the converter to be run as a 6-pulse bridge rectifier with manual control of the firing angle.

The bank phase angle select circuit of Figure 5.12 requires a synchronizing pulse at the 180^{o} mark of each reference wave. These are derived from the MSB of the D/A converter input of each phase of the Ref_1 and Ref_2 reference wave generators, using a level shifter and 4538 dual monostable to give a short pulse. A 4174 hex D flip-flop is required to ensure that the resulting sync pulses ($S_{1a\text{-}1c}$, $S_{2a\text{-}2c}$) and their associated clock signals (Q_{oa} and Q'_{oa}) are correctly synchronized with the D/A write strobes. Otherwise transition noise on the MSB line can cause spurious sync pulses to be generated.

There are two additional synchronization problems with the rotor address β' that are not obvious at first. The MSB of the rotor D/A

converter input (bit 10 of β') should be a square wave at the rotor frequency Ω. However, for reasons to be explained in Section 5.4.4, there are multiple edge transitions at both the rising and falling edges under certain operating conditions. These must be ignored for proper operation.

The solution is to use two retriggerable edge detectors to generate pulses which are mutually exclusive. One detector triggers on the rising edge of bit 10, and the other on the falling-edge. For example, when a falling-edge is detected, a relatively long pulse is generated by the falling edge detector (a monostable) which then generates the desired sync pulse via a second monostable. The first pulse also prevents the rising-edge detector (a third monostable) from triggering on any spurious transitions that may occur in the same vicinity. However, once the output pulse of the first monostable clears, the next rising edge will trigger another pulse which blocks the detection of an undesired falling edge. This effectively debounces the MSB line so that only one distinct sync pulse is passed on to the bank select logic.

Synchronized strobe signals are provided for both the Ref_1 and Ref_2 sinewave generator circuits, to latch the EPROM data into the D/A's after it has stabilized. The strobe circuits are slightly different for the stator and rotor, but the details have been omitted here for clarity.

5.4 Stator and Rotor Voltage Angle Calculation and Synchronization

5.4.1 Double Fed Motor Synchronization

Control of the double fed motor requires:

i) Control of the flux level via the stator and rotor voltages V_1 and V_2.

ii) Control of the stator frequency F_1, and the resultant stator voltage angle α.

iii) Determination of the rotor shaft angle θ (in electrical degrees), and the rotor speed W ($\omega = 2\pi W$).

iv) Calculation and control of the rotor voltage angle β via the pseudo torque angle δ_V.

Control of the flux level is through the stator and rotor reference voltage levels as outlined in the previous section. F_1 is a controlled variable and is chosen on the basis of the software control algorithm to minimize torque harmonics and otherwise optimize the system performance. Section 5.4.2 describes how F_1 is used to generate the stator voltage angle α. The rotor angle θ is determined using a shaft position encoder connected to a counter. This circuit and the speed measurement circuit are explained in Section 5.4.3. Finally, the calculation of the rotor voltage angle β is described in Section 5.4.4. Two 12-bit binary adders perform the real time calculation of β from θ, α and δ_V (the pseudo torque angle), and thus provide a stable drive system by ensuring the continuous synchronization of the stator and

rotor mmfs. Section 5.4.5 covers the data synchronizing circuit and the OUTCMD register.

5.4.2 Stator Voltage Angle Generator (α)

As shown in Figure 5.6, the stator voltage generator consists of two sections. The first is a wide-range digitally-controlled variable frequency oscillator, controlled by the stator frequency variable F_1. It has a range of 0 to 61,200 Hz, in steps of 240 Hz, and is used as a clock for the second section, an 11-bit address counter (the α-Counter). The α-counter output cycle will therefore have a frequency range of 0 to 29.883 Hz. The precise phase angle α of the stator voltage is determined by the value of the count. The counter output is actually α', the inverted value of α. That is $\alpha' = \bar{\alpha} = -\alpha - 1$. The input to the Ref_1 circuit of Figure 5.5 inverts α' to get α again, but this arrangement simplifies the later calculation of the rotor voltage angle β.

The digitally controlled oscillator consists of two VCO's configured with separate binary counters to yield two independent phase locked loops (PLL's). Since each VCO has a maximum frequency variation of about 10 to 1 (for a given RC oscillator network), this arrangement allows one PLL to be set up to cover the required low frequency range and the other to cover the necessary high frequency range. The preset logic ensures a smooth crossover between the two frequency ranges by producing an appropriate Range Select signal, and simultaneously setting the other PLL to its crossover frequency (15 or 16 times 240 Hz).

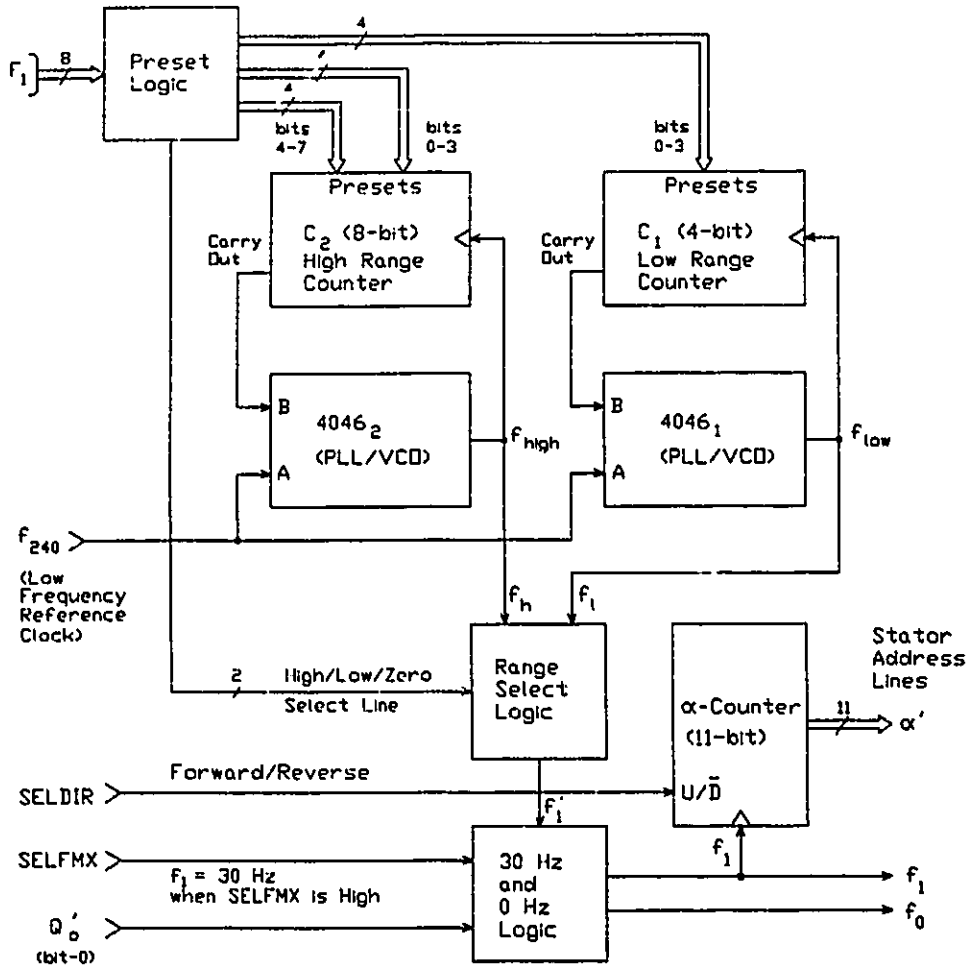

Figure 5.6 - STATOR VOLTAGE ANGLE GENERATOR (α)
The two PLL's form a wide range digitally-controlled oscillator. The output f_1 has the frequency range 0 to 61,200 Hz (in increments of 240 Hz) so that α' cycles over the range 0 to 30 Hz (in steps of .117 Hz).

For example, when the value of F_1 is between 0 and 15 Hz (inclusive), the 4 low order bits of F_1 determine the preset inputs of the 4-bit counter C_1, and the low range PLL composed of C_1 and 4046_1 will have an output frequency of $f_\ell = 240 \times F_1$ Hz. Simultaneously, the 4 low-order presets to the 8-bit counter C_2 are all clamped to 1 (binary 15) and the high range PLL composed of C_2, and 4046_2 will have an output frequency of $f_h = 240 \times 16$ Hz, near it's lowest possible frequency.

On the other hand, when F_1 is between 16 and 255 (inclusive), the low range PLL is clamped to it's highest frequency of $f_\ell = 240 \times 15$ Hz and all 8 bits of F_1 determine the presets of the high order PLL. f_h will therefore be $240 \times F_1$ Hz with a full 8 bits of accuracy. The output frequency f_1 is either f_ℓ or f_h, according to the Range Select logic.

In the case where $F_1 = 0$, and α is constant, it is still necessary to strobe the D/A $\overline{WR1}$ line so that changes in the stator voltage level V_1 can be made. This is provided for by the f_o output.

In order to reverse the direction of the stator voltage α, and the resulting mmf, the SELDIR bit of OUTCMD is used to control the up/down direction of the α-counter via the F/R line (Figs. 5.3 and 5.6).

Since the output frequency F_1 only goes to 29.883 Hz, it is not possible to have a periodic output from the cycloconverter at 30 Hz which will remain stationary on the oscilloscope. This limitation is conveniently overcome by means of one extra bit, SELFMX (select frequency maximum), which is output with the pseudo torque angle δ_v as part of the variable EXTBTS (extra bits). In Figure 5.6 the SELFMX line fixes the output frequency f_1 to exactly 30 Hz (when SELFMX = 1) or to the present value of f_1' (when SELFMX = 0) according to the output

variable F_1. There are 4 unused bits in δ_V' which are available for future use.

5.4.3 Rotor Angle (θ) and Speed Circuits (W)

Determination of the rotor angle θ is accomplished by means of a shaft position encoder and an up/down counter (θ-counter) as shown in Figure 5.7. The encoder is an Ono Sokki model RP-432Z which produces two pulse trains (Sig1 and Sig2, in quadrature) of 1024 pulses per revolution (ppr). An XOR gate (CMOS 4070) and dual monostable 4538_2 effectively quadruple this signal to 4096 ppr which are counted by the 11-bit θ-counter. Only the lower 10 bits are used, but they are shifted to correspond with the 11-bit stator address α in the rotor voltage angle calculator (sections 5.4.4). This effectively scales θ to electrical degrees, since for a 4-pole motor $\theta_e = 2\theta_m$. A third input from the encoder is a synchronizing pulse (SigZ) which occurs once for each mechanical revolution of the shaft. All inputs are buffered with Schmidt inverters for greater noise immunity, followed by 4584 TTL to 15V CMOS level shifters (not shown).

The relative phase of the Sig1 and Sig2 pulse trains are used to determine the direction of rotation and control the up/down line $U/\overline{D}$ for the θ-Counter. A dual monostable, is used as an edge detector for the sync pulse SigZ to provide a reset pulse to keep the θ-counter from drifting if spurious pulses are detected. Therefore, the value in the θ-counter is always a precise measure of the rotor angle, regardless of

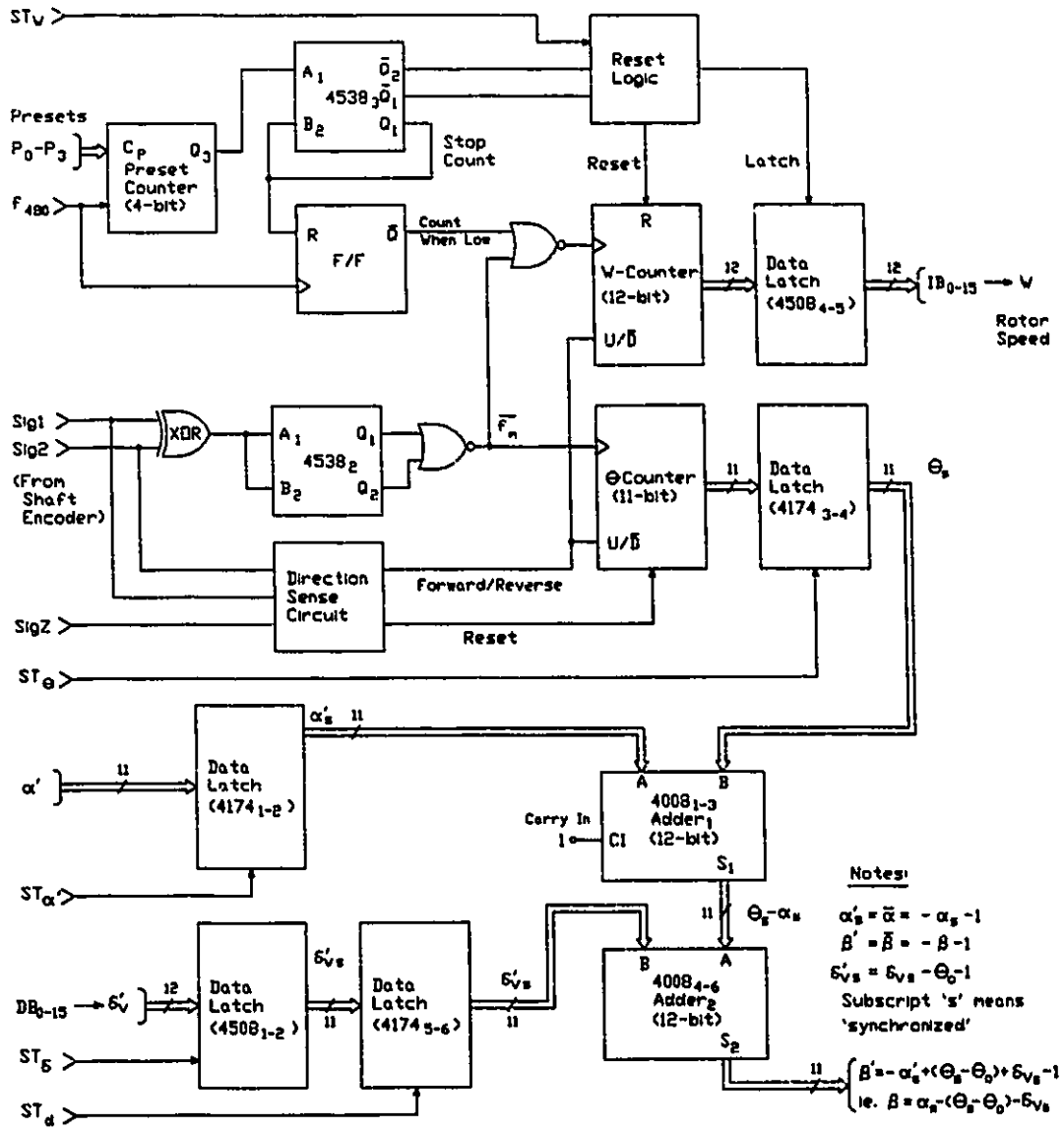

Figure 5.7 - ROTOR ANGLE, SPEED AND VOLTAGE ANGLE CALCULATOR (θ,W,β) From the shaft encoder, the rotor angle θ and speed W are determined. The adders then produce the correct rotor voltage angle β for synchronized operation.

it's speed or direction, to within 1/2048 of a cycle. The accuracy of the speed measuring circuit is determined by the ppr of the shaft encoder and the length of time over which the pulses are counted. During the initial design stages however, it was not known what accuracy would be required, and so the circuit was built with a software programmable accuracy level. Figure 5.7 shows how this is accomplished using the 4 LSB's of OUTCMD as presets to a 4-bit up-counter, Cp. The preset value P_0-P_3 determines the time base over which pulses $\overline{f_m}$ will be counted. The upward transition of Q_3 triggers the monostable 4538_3 to stop the speed counter (W-counter) via Q_1, and to reset both counters via $\overline{Q}$. The number of 480 Hz periods that elapse before Q_3 goes high is determined by the presets P_0-P_3 and can be 1, 2, 4, or 8 to yield 0, 1, 2, or 3, binary digits of accuracy.

The 12-bit W-counter counts the pulses $\overline{f_m}$ from the frequency quadrupler. When Q_1 stops the count, $\overline{Q_1}$ also strobes the W-count into the $4508_{4\text{-}5}$ data latches via the reset logic. The ST_W line causes the most recent value of W-count that was latched in the 4508's to appear on the input bus IB. Simultaneously, the ST_W line prevents new data from being strobed into the latches while the present data is being strobed out. This ensures the integrity of the speed data W at all times. ST_W is normally high, disabling the 4508 output, so that other latches can also drive the input bus IB.

5.4.4 Rotor Voltage Angle Calculator (β)

From Chapter 4, stable operation of the double fed motor requires that the rotor voltage β be controlled such that

$$\beta = \alpha - \theta - \delta_V + \theta_O \tag{5.1}$$

at all times. An appropriate value for δ_V is determined by the control software in response to the rotor speed W and the desired torque. δ_V is then combined with θ_O (a constant) and output to the rotor voltage angle calculator (Fig. 5.7).

The real-time values of α and θ are available as the outputs of the α-Counter and θ-Counter respectively, and are added with two binary adders to give β. For a given δ_V and θ_O therefore, the continually varying values of α and θ are combined to give the correct angle β for the rotor reference voltage. Any change in F_1 (or rotor speed W) merely alters the rate of change of α (or θ), and no further compensation is necessary to maintain synchronization.

The implementation of equation (5.1) is done as follows. As shown in Figure 5.7, the inputs to the first adder A_1 (composed of $4008_{1\text{-}3}$) are α' and θ. α' is the inverted value (or 1's complement) of α such that

$$\alpha' = \bar{\alpha} = -\alpha - 1 \tag{5.2}$$

When added to θ, with the carry bit of $4008_{1\text{-}3}$ set, the sum S_1, is therefore

$$S_1 = \theta + \bar{\alpha} + 1 = \theta - \alpha \tag{5.3}$$

The output of the second adder, A_2 (composed of $4008_{4\text{-}6}$), is

$$S_2 = \delta_V' + \theta - \alpha \tag{5.4}$$

Examination of the Ref_2 circuit of Figure 5.5 shows that the input data β' is inverted to form the EPROM address. Thus, the actual rotor voltage address will be

$$\beta = \overline{S}_2 = - S_2 - 1 = \alpha - \theta - \delta_v' - 1 \qquad (5.5)$$

The DFMDRV software takes into consideration the -1 term, as well as the rotor offset θ_o, so that δ_v', the value output by the computer, is

$$\delta_v' = \delta_v - \theta_o - 1 \qquad (5.6)$$

giving

$$\beta = \alpha - \theta - \delta_v + \theta_o \qquad (5.7)$$

which is the rotor voltage angle (and EPROM address).

Comparison of these equations with Figure 5.7 requires a couple of additional comments. Firstly, the data presented to the adders must be synchronized to ensure that the output sums will always be valid and be free from any transition glitches. This is done by using additional latches and synchronized strobes, as described in the next Section. Two of these latches will be described here though.

Data latches 4508_{1-2} receive the δ_v' value from the data bus DB_{0-15} in response to the ST_δ strobe. The lowest 5 bits are not required for δ_v and are thus 'extra'. These are set by the software variable EXTBTS and are available for future use. 4174_{5-6} provide the additional buffering required for the δ_v' data and the ST_d strobe latches it to give the synchronized data δ_{vs}'. Likewise, the θ data is synchronized by ST_θ to give θ_s and the α' data is synchronized with ST_α to give α_s'.

As mentioned in Section 5.3.3, there is a subtle synchronization problem with the rotor address β' that is not caused merely by the settling time after transitions in the data bus. The problem occurs when

the values of θ_s and α'_s are moving in opposite directions (ie. one is increasing and the other is decreasing). In this case the sum of θ_s and α'_s (which are both discrete quantized numbers) will not always be monotonic, because the two inputs are changing asynchronously. This leads to an asynchronous quantization error (AQE) in the binary sum S_1 from the first adder, and the output is no longer monotonic as shown in Figure 5.8a.

This does not present a problem, as far as the analogue Ref_2 outputs (R_{2a-2c}) are concerned, because the absolute error is within one LSB. But for the bank phase angle select circuit, the additional edge transitions in Q'_{oa} and the sync lines S_{2a}, S_{2b}, S_{2c} create havoc. This was remedied quite easily by the addition of the debounce logic on the MSB's of R_{2a-2c}, as outlined in Section 5.3.3.

The extra transitions in the LSB of β', on the other hand, can not be 'debounced' and have the same effect on the bank select circuit as would raising the frequency of Q'_{oa}. In actual fact, all 11 bits of β' do not need to behave monotonically, but only the LSB of β', which is used to derive Q'_{oa}. The concept of a monotonic pattern on a one bit signal is meaningless, but when associated with the other bits of β', the concept of 'monotonic behavior' is straightforward.

The algorithm to derive the correct Q'_{oa} signal basically involves ignoring any change in β' if it is in the opposite sense as a previous change. Thus, if β' was increasing and it increases again, then this progression is monotonic and valid, so change Q'_{oa}. But if β' increases and then decreases, don't do anything unless it decreases again. In this way, pairs of increase-decrease transitions cancel out

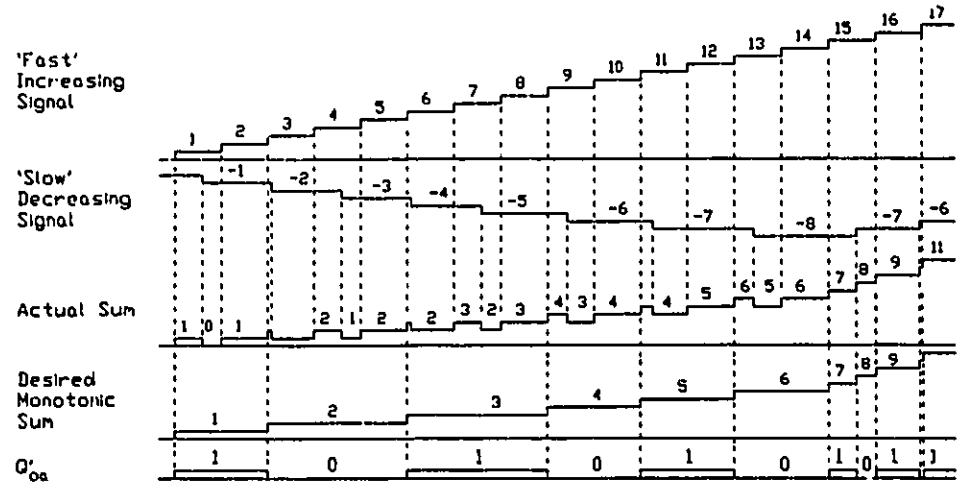

(a)

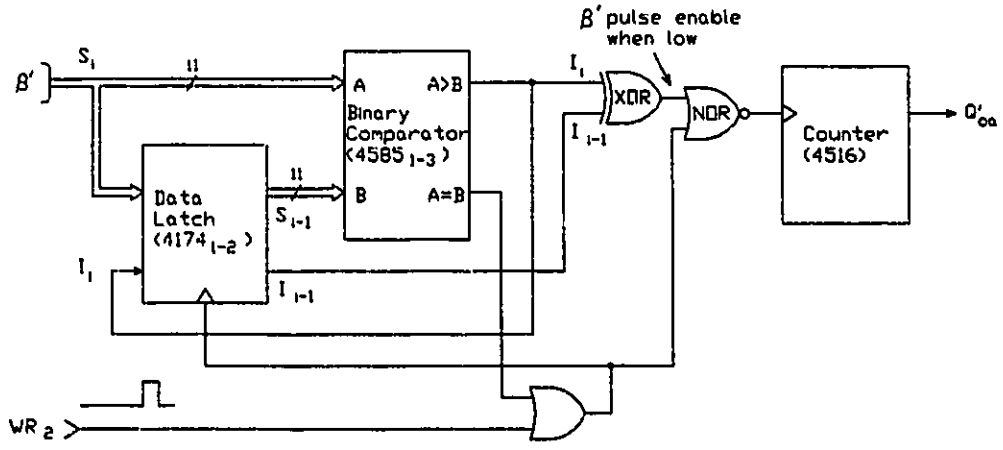

(b)

Figure 5.8 - ASYNCHRONOUS QUANTIZATION ERROR AND MONOTONIC β_{LSB} CIRCUIT - Asynchronous changes in α and θ can lead to extra transitions in the LSB of β. The circuit of 5.8b eliminates them to give Q'_{oa}, which appears monotonic.

and the resulting Q'_{oa} signal simulates the LSB of a monotonically changing β' (Fig.5.8). Errors occurring at the modulo point of the comparator can be ignored. (If a completely monotonic β' was required, this 'monotonically behaving' Q'_{oa} signal could be used as the clock input for a separate 11-bit β-Counter.)

The circuit is implemented using a binary comparator 4585_{1-3} in conjunction with a latch 4174_{1-2} to keep track of the previous state. The 4070 XOR gate yields the desired low-true signal for a valid transition. The WR_2 line, from the data sync circuit, and 4001 NOR gate combine to give a synchronized pulse for each valid transition. Counter 4516 divides by two to give a square wave corresponding to the LSB of a monotonically changing β', as required.

5.4.5 Data Synchronization

The stator voltage angle α is used directly to generate the stator reference waves (R_{1a}, R_{1b}, R_{1c}), and strobes for the D/A converters are supplied by f_o and f_1 (Figures 5.5 and 5.6). The situation is different for the rotor voltage angle β though, because output from the shaft encoder (θ) and the torque angle (δ'_v) from the host computer are asynchronous and can occur at any time. Therefore, intermediate latches are provided before the adders of the rotor voltage angle calculator, to synchronize the transfer of data through the adders and into the rotor reference wave generator Ref_2. By doing so, the D/A strobe for Ref_2 will always occur when the rotor voltage address β is

valid, and any asynchronous transition noise in β will have no effect.

Note: The term synchronization used in this section is in the sense of synchronous versus asynchronous data transfer. It is not referring to, or related to, the inherent stability of the double fed motor provided by synchronization of the phase angle between the stator and rotor voltages (although it deals with the same sections of the hardware).

The data synchronization circuit is shown in Figure 5.9 and consists of three sections; data buffers, strobe latching, and circuits to generate synchronized strobes to transfer the data. The data to be synchronized are the stator voltage angle α', the rotor electrical angle θ, and the pseudo torque angle δ_v'. These are buffered respectively by the data latches 4174_{1-2}, 4174_{3-4}, and 4174_{5-6} of Figure 5.7 with strobes $ST_{\alpha'}$, ST_{θ} and ST_d. When valid data is present at the inputs to these latches, the corresponding strobe line f_1, f_m or ST_δ will transition from high to low. Each monostable and flip-flop pair functions as a 1-bit memory element and 'remembers' if a transition has occurred. Proper synchronization is achieved by using this information to transfer α', θ or δ_v' into the 4174 latches while it is still valid, but not while the Ref_2 D/A $\overline{WRI}$ line is being strobed.

The synchronized strobes are generated by a free running 3-phase clock composed of the lower two monostables in the Figure, and their associated RC timing elements (not shown). The clock generates 3 consecutive non-overlapping pulses T_L, T_R and T_W. T_L strobes the α', θ, or δ_v' data into the appropriate 4174 latch if the corresponding f_1, f_m or ST_δ strobe was previously latched in the 4538-4027 memory element.

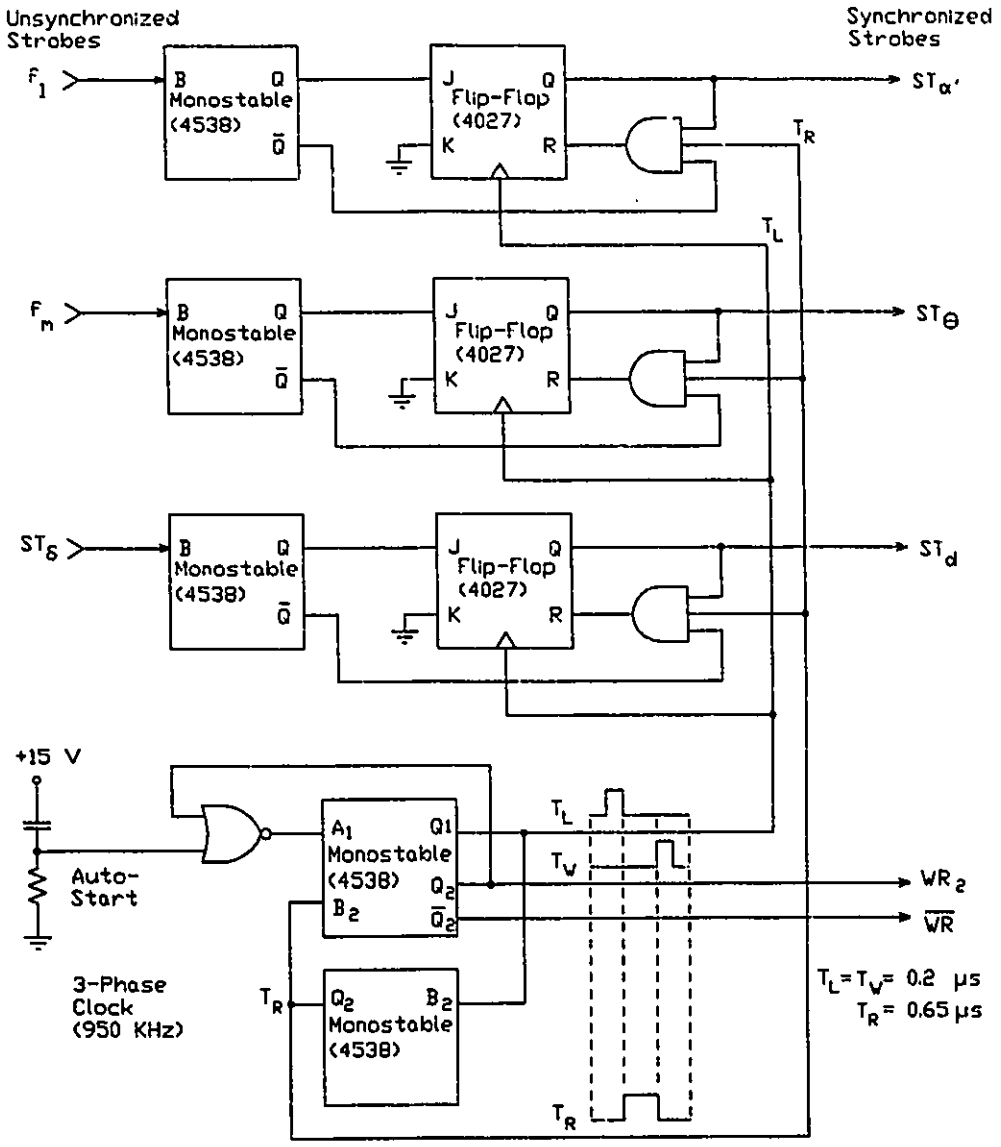

Figure 5.9 - DATA SYNCHRONIZATION CIRCUIT
T_L strobes the asynchronous signals (f_l, f_m, ST_δ) into the 4538-4027 memory cell. T_R resets the flip-flops and allows the data to propagate through the adders of Fig. 5.7. At T_W the β data is valid and is strobed into the Ref_2 D/A converters.

The data rapidly propagates through the adders of Figure 5.7 to give β, the desired rotor EPROM address. T_R resets the memory elements and then T_W strobes the EPROM output into the D/A converters of Ref_2.

The 3-phase clock frequency is high enough that any input data will be latched within approximately 1 μs (much less than half of 1/(2048 x 60)). If no strobe (f_1, f_m or ST_δ) is present, the AND gates do not pass on the reset pulse T_R, and any incoming strobe is not lost during T_R. The duration of T_R is long enough so that the data will have time to propagate and settle through the latches, adders, inverters and EPROMS before T_W strobes the D/A converter. Actually $\overline{T}_W$ (the $\overline{WR}$ line), is used to strobe the Ref_2 D/A's, while T_W (the WR2 line), is used to strobe the rotor sync pulses S_{2a}, S_{2b}, S_{2c} and Q'_{oa} of Figure 5.5.

5.5 Gate Pulse Logic and Bank Select Circuit

5.5.1 Overview

The frequency, voltage and phase information of the reference waves is transformed into time varying gate pulses for controlling the converter phases by the comparator circuits and gate pulse logic of Figure 5.10. The comparator matrix generates 12 basic gate pulse envelopes for the 12 SCR's that comprise the 2 banks of each phase. Positive and negative gate pulse logic sections then route these pulses to the appropriate SCR's, with provision for bank switching and enable/disable functions (see Fig. 5.11). The bank switching circuit

contains software enable lines (EP and EN), and uses the K_N and K_P clear signals from the off-detection circuits to direct the gate pulse trains to either the positive or negative gate pulse logic circuits, depending on the load current polarity. In the event of a short circuit, the hardware bank enable circuit will disable both banks and set flags for the software. It also provides reset and manual enable/disable features for each SCR in the bank.

5.5.2 Comparators and Gate Pulse Logic

Implementation of the cosine wave control method [17] is performed by six comparators and their associated debounce logic (Fig. 5.10). When a reference wave crosses a timing wave from below, the comparator output will swing high and generate a fairly long pulse (0.4 ms), or gate pulse envelope (P_1-P_6), for one SCR in the positive bank. When the reference wave again crosses the timing wave, this time from above, the comparator output swings low and a second gate pulse envelope is generated for one SCR in the negative bank (P_7-P_{12}). The dual monostables (4538) associated with each comparator provide an anti-bounce function via the clear inputs so that the relatively slow reference wave crossings will only generate one gate pulse envelope for each crossing point. With six comparators then, each timing wave is compared with one reference wave (R_{1a}, R_{1b}, R_{1c}, R_{2a}, R_{2b} or R_{2c}) to produce 12 firing pulse envelopes ($P_{1\text{-}12}$) for 2 banks (ie. 1 phase) of the cycloconverter.

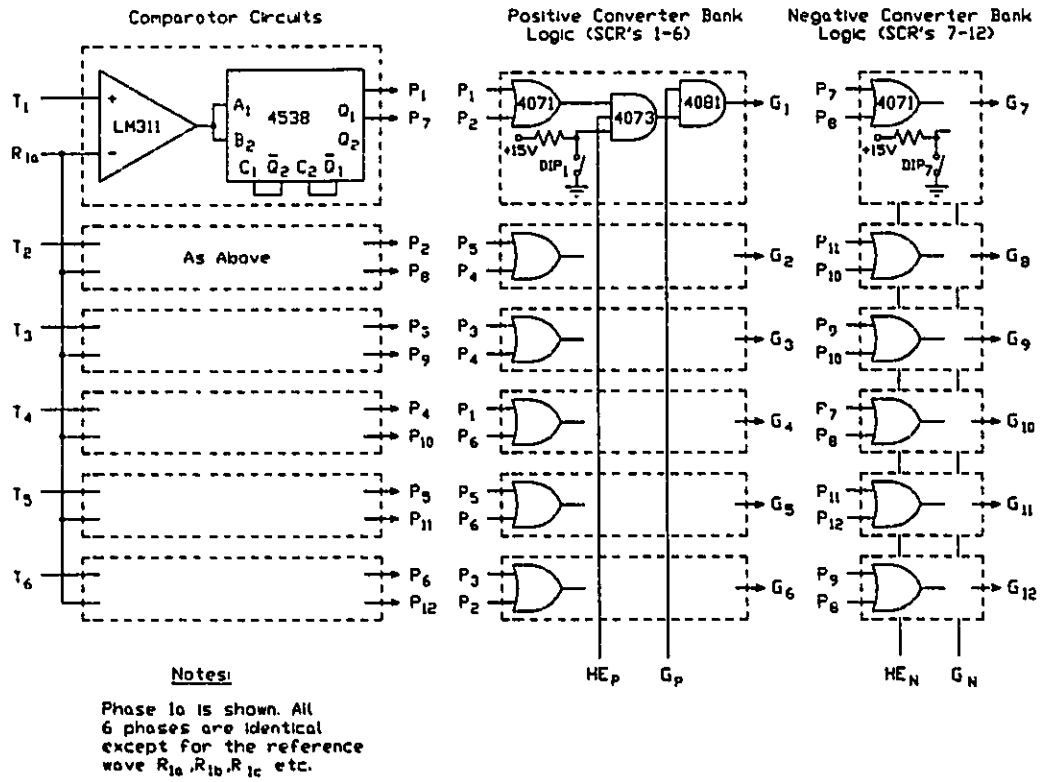

Figure 5.10 - COMPARATOR BOARD AND GATE PULSE LOGIC CIRCUIT
A reference wave is compared to each timing wave to produce 12 gate pulses P_{1-12}. These are combined with hardware enable signals HE_P and HE_N, and the gate pulse streams G_P or G_N, to fire either the positive or negative converter bank.

With a bridge configured converter, it is necessary to fire the SCR's in pairs to achieve conduction through the load. The 4071 OR gates of the pulse routing circuits perform this function. The 4073 AND gates allow each SCR to be individually disabled using a DIP switch, or as a bank, using the Hard (bank) Enable HE_P and HE_N lines. The 4081 AND gates combine the gate pulse envelopes P_{1-12} with the gate pulse streams G_P or G_N to produce the gate signals G_{1-12}. G_P and G_N are mutually exclusive and therefore ensure that only one bank will be fired at a time. Output transistors then drive the pulse transformer circuits of Figure 5.13 to fire the SCR's.

5.5.3 Hardware Bank Enable and Short Circuit Detection Logic

Referring to Figure 5.11, the presence of a negative pulse, $\overline{SC}_P$ or $\overline{SC}_N$, from the short circuit detection hardware (Fig. 5.14) indicates a transient overcurrent condition in the positive or negative converter bank respectively. This condition is latched by a flip-flop which in turn sets the short circuit lines SCP and/or SCN high for the software to detect. Simultaneously, the appropriate Phase Short Circuit (PSC) line goes high and both HE_P and HE_N lines go low, disabling all SCR's in the two banks. When the fault has been cleared, reset is provided from software via the Soft Bank Reset (SBR) line.

For testing and development purposes, it is necessary to be able to disable the SC detection logic. This can be done separately for each bank by closing the appropriate DIP switch MBE_P or MBE_N (Manual Bank

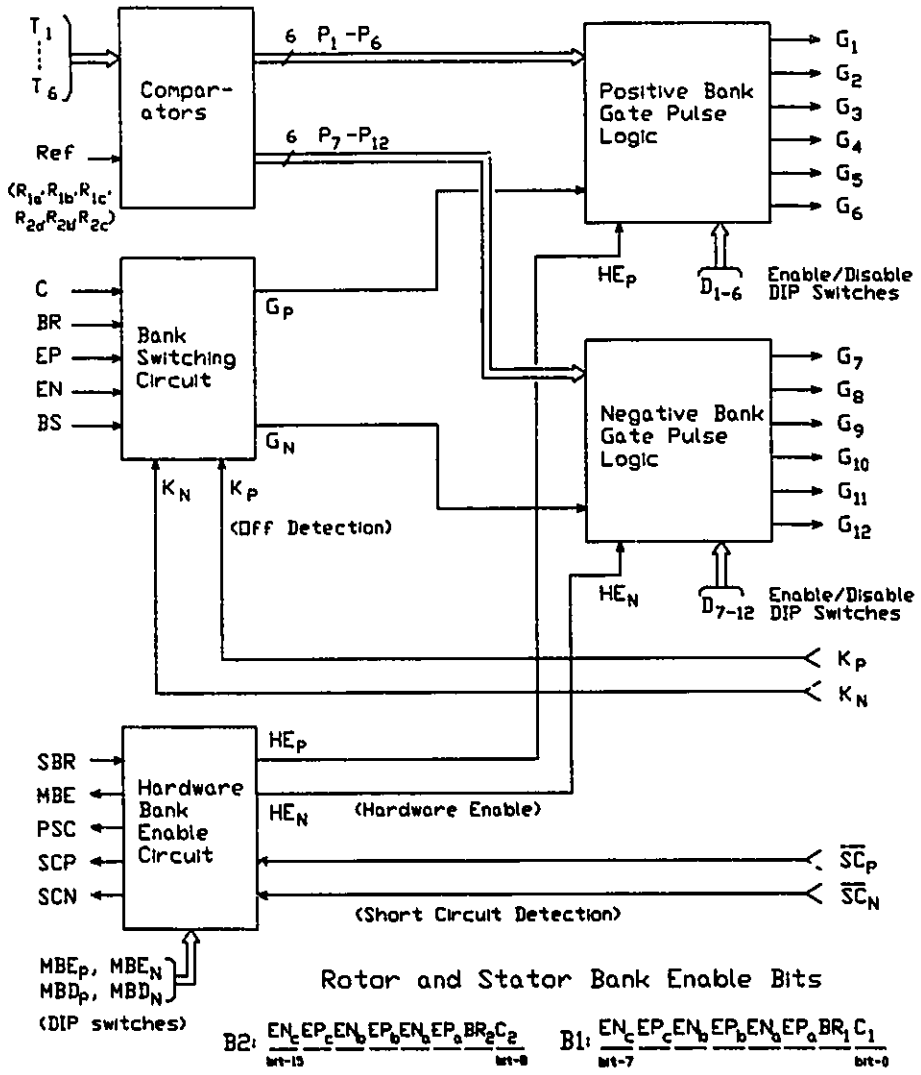

Figure 5.11 - BANK ENABLE AND CURRENT DETECTION LOGIC
Bank switching is initiated in response to K_P or K_N clear pulses. The hardware bank enable circuit determines the response to short circuits ($\overline{SC_P}$ and $\overline{SC_N}$) and provides software and hardware reset and enable/disable functions.

Enable). To indicate this potentially unsafe state of operation, the MBE line is raised and the software will indicate on the screen that the short circuit protection has been disabled for at least one of the stator or rotor banks.

DIP switches MBD_P and MBD_N allow all 6 SCR's of each bank to be disabled simultaneously. Note however, that MBE_P or MBE_N override this setting and so it does not provide an absolute disable function like DIP switches D_{1-6} and D_{7-12} of Figure 5.10 do.

5.5.4 Software Bank Enable and Bank Switching

5.5.4.1 Basic Operation

Each bank of the 2 cycloconverters, 12 banks in all, can be enabled or disabled by the software via the B_1 and B_2 bank enable outputs. Each output contains 6 enable bits, as shown in Figure 5.11, one bank reset line BR, and one current mode control bit C. These enable bits do not override the hardware disable features, but they do override the hardware enable features. That is, if the hardware is disabled, the B_1 and B_2 software codes cannot cause the respective bank to fire, but if B_1 and B_2 are cleared (disabled), then the hardware enable features cannot cause the circuits to fire.

The SCR's are fired using a stream of gate pulses, to ensure that each SCR will turn on, even if it was reverse biased at the beginning of the gate pulse envelope. A 555 timer circuit in the bank

switching circuit of Fig 5.11 generates a 40 KHz stream of pulses for this purpose. The essential function of the bank switching circuit then, is to direct these pulses to only one bank at any given time, and this on the basis of the load current polarity (for natural commutation).

For example, when the load current is positive, the positive bank, SCR's$_{1-6}$, are to be fired via G_P and G_{1-6}. When the off-detection circuit (Fig. 5.14) detects the end of the positive current half-cycle, the clear pulse K_P is generated which will initiate gate pulse transfer over to the negative converter bank. From this point G_N and G_{7-12} fire the negative converter. When the negative load current reaches zero, the clear pulse K_N is generated, indicating the end of the negative current half cycle, and initiates transferring the gate pulses back to the positive bank.

5.5.4.2 Bank Select with Discontinuous or Continuous Load Current

The bank select line BS and current mode line C provide additional control of the bank switching function. When C = 0, the discontinuous current mode, the BS line has the ability to prevent the clear pulses (K_P and K_N) from initiating bank switching. The BS line comes from Figure 5.12 and is a square wave signal, at the converter output frequency, with a phase relationship determined by the current phase variables P_1 or P_2. In this way, if P_1 (or P_2) = 20^o, for instance, then bank switching is blocked until 20^o after the reference wave Ref_1 (or Ref_2) crosses zero. Because the cycloconverters used here

are naturally commutated, the bank select line cannot initiate or force bank switching, but it can delay or prevent bank switching by blocking the clear pulses for a desired interval.

This feature is designed to facilitate reliable bank switching in the presence of a discontinuous load current and its resulting multiple zero crossings and premature clear pulses. It also provides a more reliable method of bank switching since only 2 bank switches are permitted per cycle.

When C = 1, the circuit is in continuous current mode and it is assumed that the load current zero crossing will provide one, and only one, clear pulse (K_P or K_N). Therefore, when C = 1, any clear pulse from the operating bank initiates gate pulse transfer to the other bank. A short dead time of about 100 μs is provided between G_P and G_N as a safety margin to ensure that the outgoing SCR bank is definitely off.

There is a potential difficulty with the continuous current mode of operation though. Any spurious pulse on the clear line of the operating bank will initiate a transfer to the other bank, and the 100 μs safety margin will not likely provide enough time for the load current to decay to zero. For this reason a 'multiple bank switch lockout' feature is provided by a simple monostable circuit so that after a valid end-of-cycle (EOC) signal is detected, and the banks have been switched, any spurious EOC signal will be blocked for approximately 12 ms and thus prevent premature bank switching. None-the-less, it is still possible to have occasional false clear pulses initiate a bank switch after 12 ms, but before the load current goes to zero. Then the short circuit protection circuit is really appreciated!

5.5.5 Bank Phase Angle Select Circuit

Whereas the bank switching process is performed by the off-detection and bank switching circuits of Figure 5.11, the selection of the desired bank, and to some degree the phase of the load current, is controlled by the bank phase angle select circuit of Figure 5.12. This circuit contains 6 identical sections; 3 for the stator phases and 3 for the rotor phases.

The desired stator and rotor current phase angles P_1 and P_2 are latched by ST_P into 4508_{1-2}. Double buffering is provided by latches 4174_{1-2} and strobe logic to ensure synchronized transfer of the phase data into the presets of counters 4516_{1-6} without any glitches.

Examination of Figure 5.12 shows that the 12-bit up-counters (4040_{1-6}) provide a square wave synchronized with each phase of the reference waves. The 3 counter outputs Q_{10}, Q_9 and Q_1 are decoded and used to provide set and reset commands for the output flip-flop 4027.

Referring to the timing diagram in the upper half of the Figure, each transition of Q_9 generates a pulse, either P_{lag} or P_{lead}, every 90^o (of the output cycle). Bit 7 of the phase variable P_1 or P_2 determines if the phase angle is lagging or leading, and thus puts the flip-flop 4027 into set or reset mode, and selects either P_{lag} or P_{lead} to provide the PE pulse accordingly. Every 180^o thereafter, Q_{10} toggles the set/reset mode of the flip-flop and the P_{lag} (or P_{lead}) pulse resets the counter. The counter carry out $\overline{CO}$ serves as the clock for the flip-flop and thus provides a programmable phase delay for the bank select line BS. The current phase angles can therefore control the angle of the bank

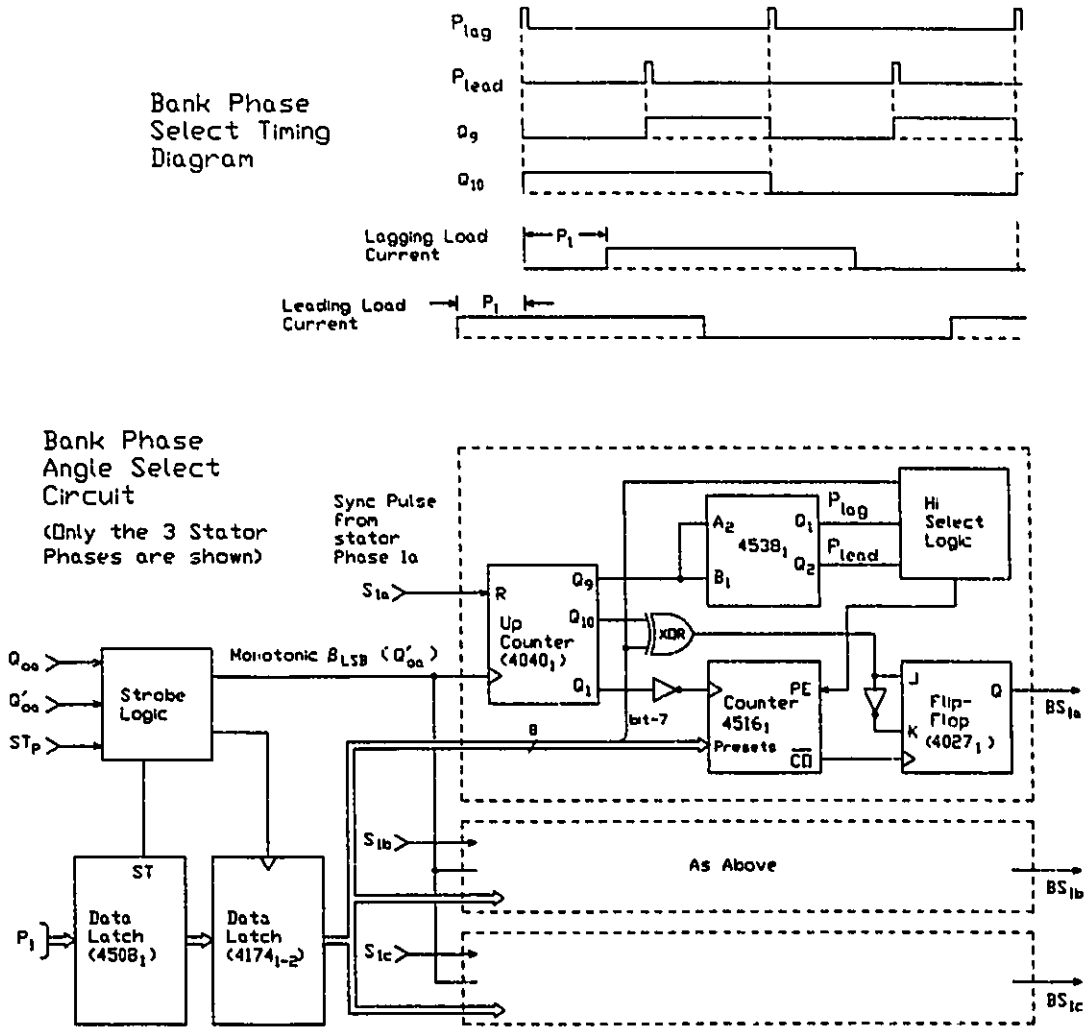

Figure 5.12 - BANK PHASE ANGLE SELECT CIRCUIT
The sync pulses $S_{1a\text{-}1c}$ and clock Q'_{0a} cause the 4040 counter to cycle at the output frequency. P_1 controls the preset lines of counter 4516 to give BS with a programmable phase delay, with respect to the sync pulse.

select signal over the range of $\pm 90^{o}$.

5.6 Cycloconverter Output Section

5.6.1 Converter Banks

Each phase of each cycloconverter contains 2 converter banks, as shown in Figure 5.13, with the SCR's being grouped into 3's and mounted on 4 heatsinks. Every SCR has an individual gate trigger circuit providing isolation and amplification of the gate pulse. Each SCR also contains an RC snubber circuit for dv/dt suppression and a 0.01 μF capacitor between the gate and cathode to minimize spurious triggering. These elements are mounted directly on the SCR's.

Each major section of the drive is modular and can be easily accessed for servicing. All 6 output phases and their associated trigger circuits, current detection circuits, and gate circuits are identical and can therefore be interchanged to pinpoint the location of faulty elements.

5.6.2 Current Off-Detection

Reliable bank switching is dependent upon accurate detection of the load current zero, and subsequent transferring of the gate pulses to the other converter bank. When a cycloconverter is operating under

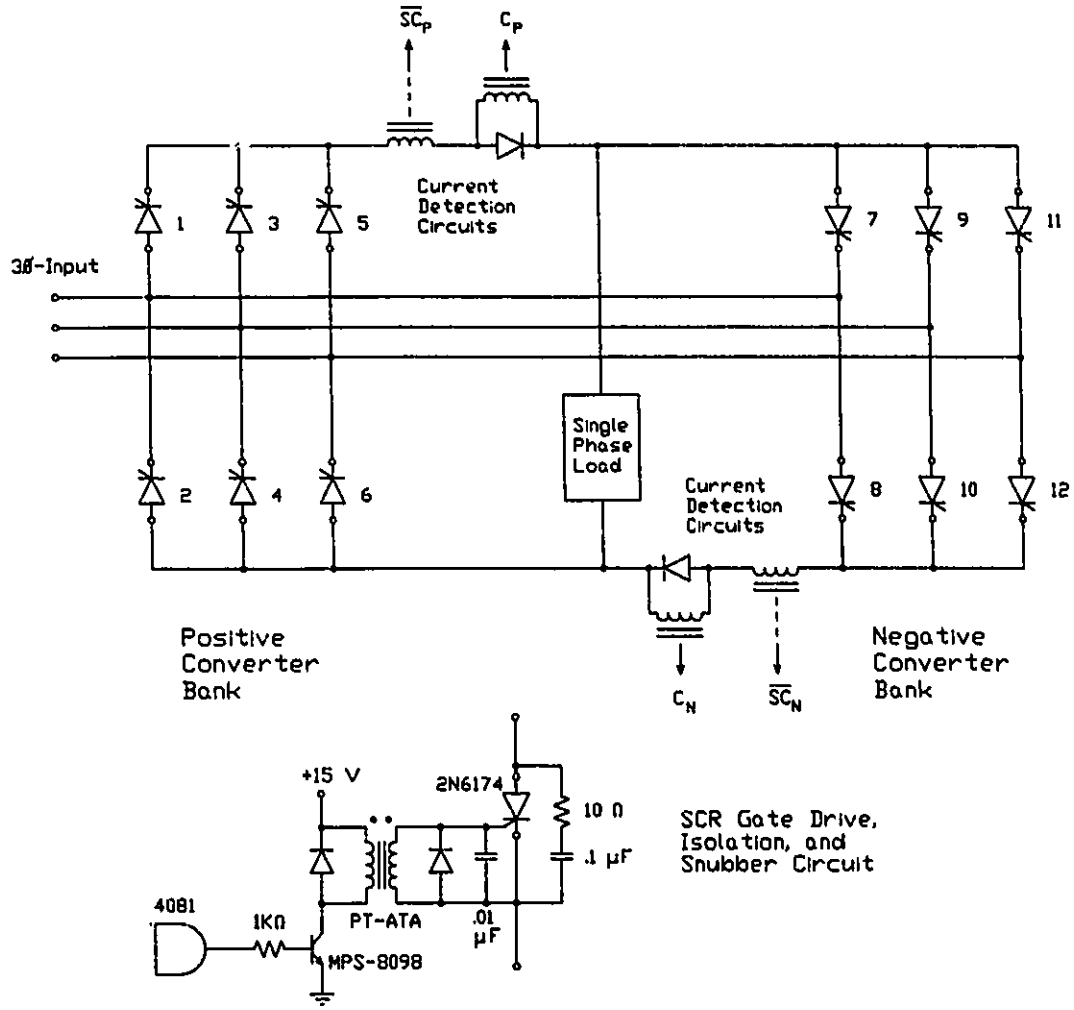

Figure 5.13 - CYCLOCONVERTER OUTPUT CIRCUIT (Single phase shown) Each phase is composed of two phase-controlled 6-pulse bridges. Each bank has its own off-detection and short detection circuits.

natural commutation, then as each SCR turns on, it reverse biases the outgoing SCR. Likewise, when the load is inductive and the load current goes to zero, the last SCR to conduct will be reverse biased when it shuts off.

In my Master's research I developed a circuit, using opto-couplers, to detect this reverse bias condition and use it to determine the conduction state of each SCR [3]. The circuit worked well as designed, but would require a total of 72 detectors for the 2 cycloconverters. Ueda et. al. [28] developed another method employing the same principle of reverse bias detection but which has several advantages.

If one connects an SCR and diode in series and then reverse biases the combination, the total reverse voltage first appears across the diode, because of the larger junction capacitance of the SCR. It then decays to distribute evenly between the two junctions. A reverse bias detector across the diode can therefore provide a reliable detection of the turn-off, or reverse bias, of the SCR.

The major advantage of this system over the method developed in my earlier work, is that the diode can be used to detect the current zero for a whole bank of SCR's, thus reducing the required number of detectors from 72 to 12. Also, the use of a pulse transformer instead of an opto-coupler greatly increases the sensitivity of the detector. This method introduces another PN junction in the load current path, with its associated losses and cost, but it also reduces the reverse voltage blocking requirement of the SCR's, if high voltage diodes are used.

Figure 5.14 shows the bank current off-detector circuit used.

The trim pot is adjusted to approximately 10 Ω and provides a low impedance input to reduce noise pick-up. V_{BSth} is a bipolar adjustable reference voltage that determines the amplitude threshold for the LM311 comparator.

Because of the large voltage and current transients in the converter banks when any SCR turns on or off, the pulse transformer picks up numerous 'false' off signals. These typically have very high amplitude but are very short in duration and therefore contain little energy. The 'true' off pulses have both a fairly high amplitude and a long duration. The 4538 monostable is used to block any C_P or C_N pulses that are shorter than the associated RC time constant of the 4538. This delay time is adjustable and is the key to deriving valid pulses K_P and K_N for reliable bank switching.

Of note, also, is the fact that if the SCR bank is fired when it is reverse biased, the SCR's operate in the reverse conducting mode and a large reverse voltage will appear across the off-detection diode for the duration of the gate pulse. This is ideal because, if there is only a small reverse bias across the SCR-diode combination when the current goes to zero (due to motor back EMF for instance), then the next gate trigger pulse will create a large off-detection signal and initiate the desired bank switching function.

5.6.3 Short Circuit Detection

If the cycloconverter output is shorted, or if both banks are

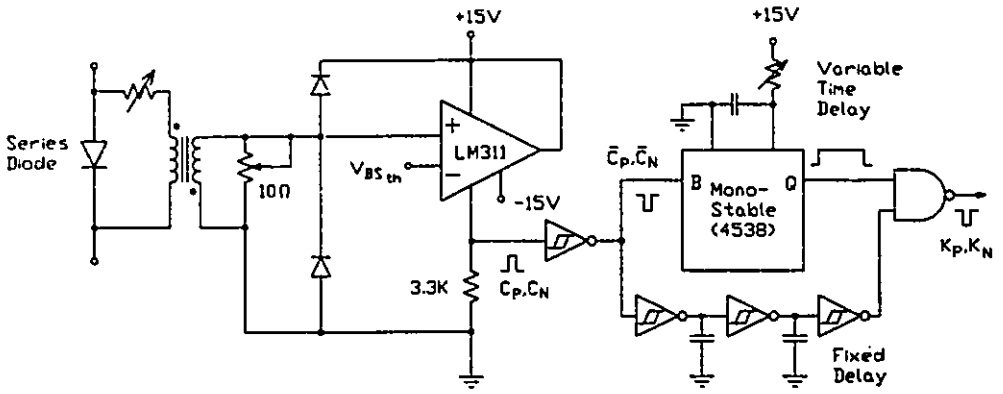

Current Off-Detection Circuit

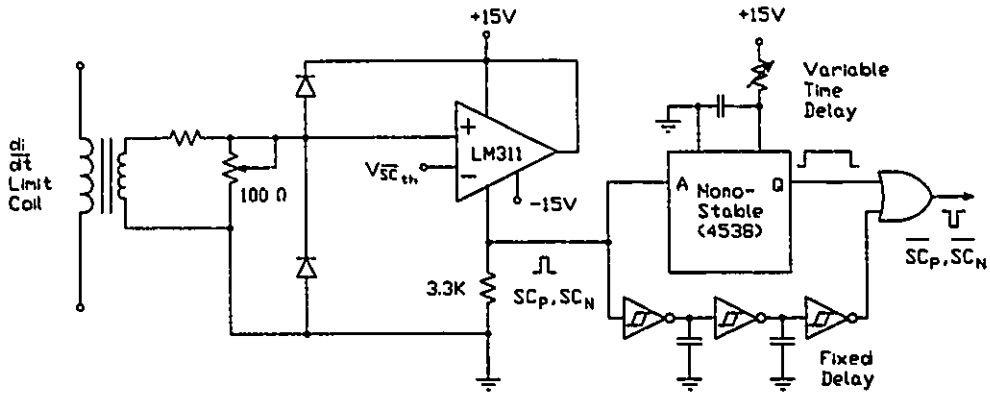

Short Circuit Detection Circuit

Figure 5.14 - CURRENT DETECTION CIRCUITS
The comparator threshold sets the amplitude cutoff and the monostable time delay determines the minimum pulse width required to produce a valid current off-detection or short circuit signal.

fired simultaneously, a very large surge current will flow, limited only by the AC supply inductance. Proper fuse selection could be used to protect the SCR's, but less expensive and more convenient is the use of surge detection circuits, with provision to block all gate pulses immediately after a short occurs.

The SCR's used in this equipment are rated at 35 A continuous, but have a half-cycle surge rating of 350 A. This is a very significant overcurrent margin, and provided that it is not exceeded, or that the SCR is not retriggered into the same fault condition, the SCR will recover its blocking ability before the next cycle and will not be damaged. The variac used for input voltage reduction provides sufficient current limiting for this purpose. In addition, 30 μH inductors are included in each bank to limit the di/dt in each SCR, and ensure effective spreading of the conduction area across the pellet during a short.

Figure 5.14 shows the short circuit detection circuit. The inductive pickup is located inside the di/dt limiting choke and the trimpots are adjusted to give a low impedance input. As with the off-detection circuits $V_{\overline{SC}th}$ sets the amplitude threshold and the 4538 monostable time constant determines the minimum pulse width that will cause a $\overline{SC}$ signal to appear at the output.

Since the pickup is inductive, the circuit is detecting the rate of increase (di/dt) of the current, and not its actual magnitude. This combination of amplitude and pulse-width thresholds though, acts as an integrator and provides an accurate measure of the energy in the detected pulse. In conjunction with the SC detection logic of Section

5.5.3, this allows the converter banks to be disabled immediately in the event of a large overcurrent without damage.

5.6.4 Automatic Short Circuit Reset (ASCR)

A very difficult problem in the development of the cycloconverters, was the calibration of the current off-detection and short circuit (SC) detection circuits. Initially, static resistive and inductive loads were used and each phase was calibrated individually. The phases were then operated together on isolated loads and the calibration was readjusted accordingly. This was fairly straightforward.

When connected to the motor, all three phases are mutually coupled by the magnetic paths and the electrical connections of the windings. This gives rise to many false bank switch attempts, SC's, and apparent SC's, unless the circuits are correctly calibrated. In general, the short circuit detection circuits can be set over sensitive to prevent damage, but with the result that one or two phases are always being disabled due to calibration errors. As soon as they are reset (via an HBR pulse), one or more of the other phases detects a short (real or false) and is immediately disabled. The circuit cannot be calibrated unless all three phases (or six for DFM operation) are running simultaneously.

Cycloconverter firing pulses almost always form a non-periodic pattern, and so the mutually coupled transients that produce the false detection signals are also non-periodic. If the disabled banks were

immediately enabled again, the exact fault condition would not likely repeat itself and the circuit would run until some other fault was detected and disabled the output.

Since the SCR's can ride through a one cycle short with no damage, it was decided to reenable any disabled bank automatically via an SBR (Software Bank Reset) pulse instead of in response to a manual HBR (Hardware Bank Reset) command from the computer keyboard. In this way the circuit can run on all three phases in the presence of many faults or possible short circuits, with only single-cycle dropouts at each occurrence.

The automatic short circuit reset feature consists of two interrupt clocks, six software counters (Section 6.4.2), one input latch and one output latch (Figure 5.15).

In Figure 5.15, the 4072_{1a} OR gate, DIP switches 1 to 4, 4040 counter and 4538_{1a} monostable generate the ReqA interrupt. ReqA is programmable from approximately 1 ms to 8 ms and provides the time base for the software counters which determine when to reset the disabled banks. The PSC interrupt service routine PSCISR is fast enough to allow a 1 ms interrupt rate without affecting the overall system performance.

4072_{1b}, DIP switches 5 to 8, and 4538_{1b} generate a second interrupt, ReqB, which causes the software to reset all the SCCNT variables to zero at a much slower rate. It is programmable from 1/4 to 16 seconds using DIP_{1-4} and DIP_{5-8}.

In the hardware bank enable circuit of Figure 5.11, the SCP and SCN lines are OR'd to give one PCS (Phase Short Circuit) signal. These are input to the host computer with the ST_{PSC} strobe and a latch on the

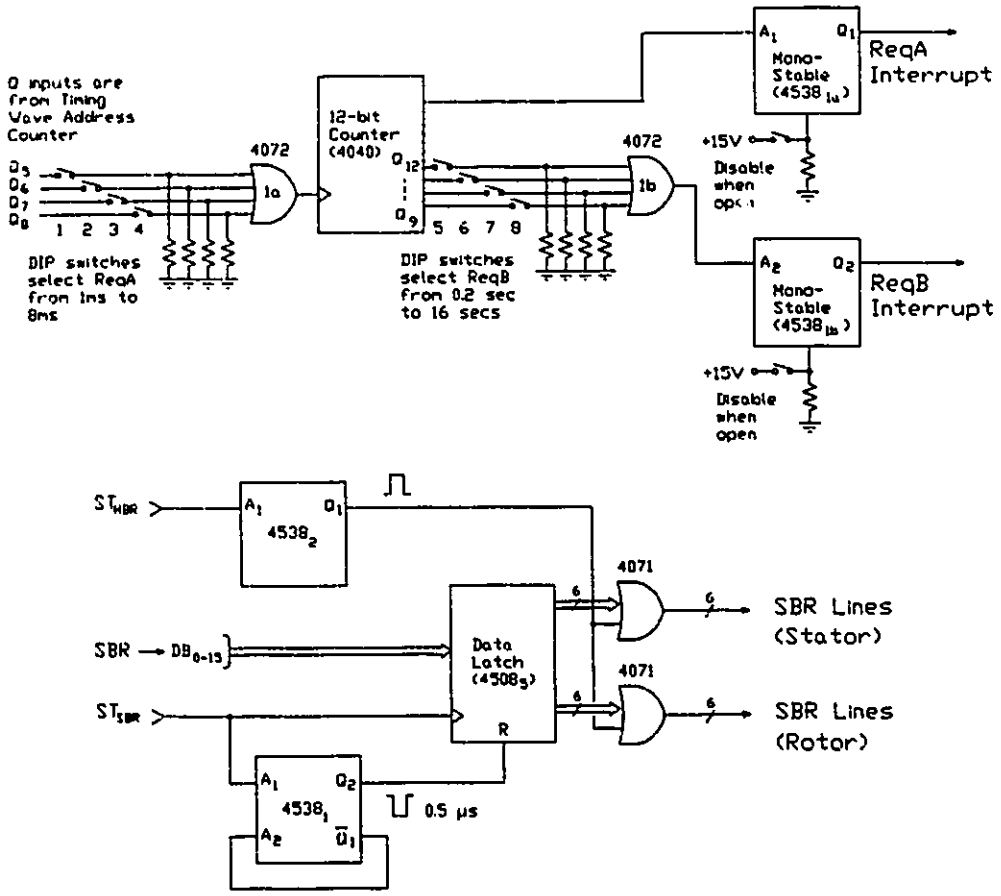

Figure 5.15 - AUTOMATIC SHORT CIRCUIT RESET (ASCR) CIRCUIT
DIP switches set the ReqA interrupt frequency in the range 1-8 ms and ReqB in the range 1/4 to 16 secs. After a programmable delay, the software resets the disabled bank via the Soft Bank Reset (SBR) output.

interface board. When any PSC is detected, the appropriate software counter is initialized. When this counter reaches zero, the ST_{SBR} pulse resets only the disabled bank(s), via the data latch 4508_5. This ensures that other disabled phases are not prematurely reset, as would be the case if an HBR command was sent. The monostable 4538_1 clears the latch to provide a short 0.5 μs SBR pulse. (ST_{HBR} strobe actually causes all 6 SBR lines to pulse simultaneously via 4538_2 and the 4071 OR gates.)

5.6.5 Motor Connections

The motor connections are all made at the front panel of the current detection unit. It is VERY IMPORTANT that the stator cycloconverter outputs be connected to isolated loads, and NOT in wye or delta, because their inputs are not isolated and line-to-line shorts will occur as soon as the SCR's are fired. The rotor inputs are isolated via the isolation transformer and so the rotor cycloconverter outputs can be connected in wye, as required for the motor used in this research.

No voltage or current sensors have been used for the purposes of torque, or speed control. The only feedback information is that of the rotor angular position, as determined by the shaft encoder. This has been sufficient for the requirements of this work to date.

CHAPTER 6

DOUBLE FED MOTOR DRIVE SOFTWARE

6.1 Introduction

This Chapter outlines the basic features of the DFMDRV software for the double fed motor cycloconverter drive system shown in Figure 5.1. Particular emphasis will be given to describe those features which are novel or which were most helpful in the development process. The remaining features will only be described briefly, since they are quite straightforward and are of a more general nature.

The DFMDRV software is interactive, flexible, and extensively documented. Since the software was designed as part of a development system, many of the parameter values, and the exact control requirements of the hardware were not initially known. Therefore, the software has provision for modifying most of the parameters and operating points, and has several modes of manual and automatic operation. During automatic operation, different control algorithms can be selected to control the output variables, and all the parameters are adjustable on-line.

To further facilitate development and testing of the DFM hardware, the software also allows complete control over which converter banks are to be fired and what action is to be taken when faults are

detected in the hardware. Short circuits are displayed on the screen along with status information, warning messages, and the present operating mode of the system. The rotor speed is continually updated on the screen and brief help screens are available in each mode of operation.

In brief, the software performs the following major functions:

i) Retrieve (or store) the operating set points and parameters from (or to) a data file.

ii) Display the set points, parameters, operating status and error conditions on the screen.

iii) Accept changes to all set points and parameters from the operator on-line, while running the double fed motor.

iv) Read rotor speed, short circuit current status, and any error conditions from the DFM hardware.

v) Determine appropriate values for the output variables, either manually or automatically, according to various internal control algorithms and/or operating modes.

vi) Output commands to the hardware for the stator and rotor voltage magnitudes (V_1 and V_2), the current phase angles (P_1 and P_2), the stator frequency (F_1) and the pseudo torque angle (δ_v).

vii) Enable or disable individual banks of the cycloconverters under either manual or automatic control. Automatic control provides various degrees of response when short circuits are detected and can include the very useful feature of automatic reset of the disabled bank(s) (ASCR).

viii) Allow the operator to enable or disable various operating modes, to prevent the possibility of unsafe operation (unless specifically required for testing purposes).

ix) Facilitate DFM drive system development by providing access to internal data values and unscaled output values as required.

6.2 Program Structure, Data Display, and Command Summary

The code is written in FORTRAN and MACRO. FORTRAN is used for real data scaling, control algorithms and file handling, while MACRO routines perform all the hardware I/O, keyboard input, screen display and special fixed-point arithmetic routines. A FORTRAN scheduling routine (ITIMER) calls the control algorithm CONTRL every 100 ms, with keyboard and screen I/O occuring in the foreground.

All data and flags are located in common areas, providing a convenient interface between the FORTRAN and MACRO code segments. Data types include the following:

set point values - A limited range of real values, input by the operator (in user units), to specify the motor operating points (eg. V1S).

scale factors - Real values for conversion from set point values to scaled set point values.

scaled set point values - Scaled to internal fixed-point format for the control algorithms (eg. V1K).

incremental values - Used in MANUAL mode to modify the actual values (eg. V1I).

actual values - Computed values (eg. V1A) derived from either:
i) the scaled set point values and time
ii) the incremental values
iii) a control algorithm according to the current operating mode

output values - Actual values which are packed for convenient output to the DFM hardware (eg. V1O).

ASCII strings - Used for input prompts, screen displays, error messages, and help screens.

In choosing the form of data representation, real values were avoided because of the longer time required for real arithmetic. On the other hand, straight integer arithmetic would not provide the necessary accuracy. A good compromise was to use fixed-point arithmetic based upon 16-bit numbers, with the binary point located between the high and low order bytes. The integer portion (the high order 8 bits) therefore yields a range of 0 to 255, or -128 to +127, and is directly compatible with the external DFM hardware. At the same time, the 8 bits to the right of the binary point maintain the accuracy of internal calculations to ± 1/127.

Special fixed-point addition and multiplication routines (ADDOVF and KMUL), written in MACRO (and FORTRAN callable), provide for integer-speed arithmetic with automatic overflow and underflow protection. Therefore, no error checking is required on the magnitudes of any of the control variables in the FORTRAN code. All values are automatically clamped to a value specified in the call to ADDOVF (for addition and subtractions) or to KMUL (for multiplication).

Special code was written, as well, to accept and display set point values and parameter values from the keyboard. These values are

first converted to the internal fixed-point format and then scaled with real scale factors to convert from user units (volts, rpm, etc.) to binary values that utilize the full 16-bit range of the internal variables. Speed input from the hardware is scaled into internal fixed-point format, as well as to an integer representing rpm, which is in turn converted to ASCII for display on the screen as the 'actual speed'. The accuracy of the speed input is determined by the sample time of the hardware (Section 5.4.3) and is programmable via the DIGITS command.

The current value of the set points are displayed continually in the upper half of the screen (see Figure 6.1). All prompts and command responses appear in the lower half of the screen, which scrolls as neccessary. Range and type checking is done on all keyboard inputs with appropriate messages in the event of an error. Most commands require only a single key stroke (with no carriage return), providing a very convenient and quick operator interface. In addition, the question mark key invokes the HELP command to display a summary of the currently available commands. Figure 6.2 summarizes the main system commands.

The total DFMDRV system has a large number of features which can be enabled or disabled for development purposes. Numerous settings, if incorrectly set, can result in a 'dead' or malfunctioning system. It is useful to have this great degree of flexibility, but it is easy to overlook something and then the system won't perform as expected. Therefore, every change in operating mode, whether due to a command from the operator, or in response to changing conditions or settings in the hardware, is represented on the screen. This combination of data display, mode display, prompt messages, and help screens make the

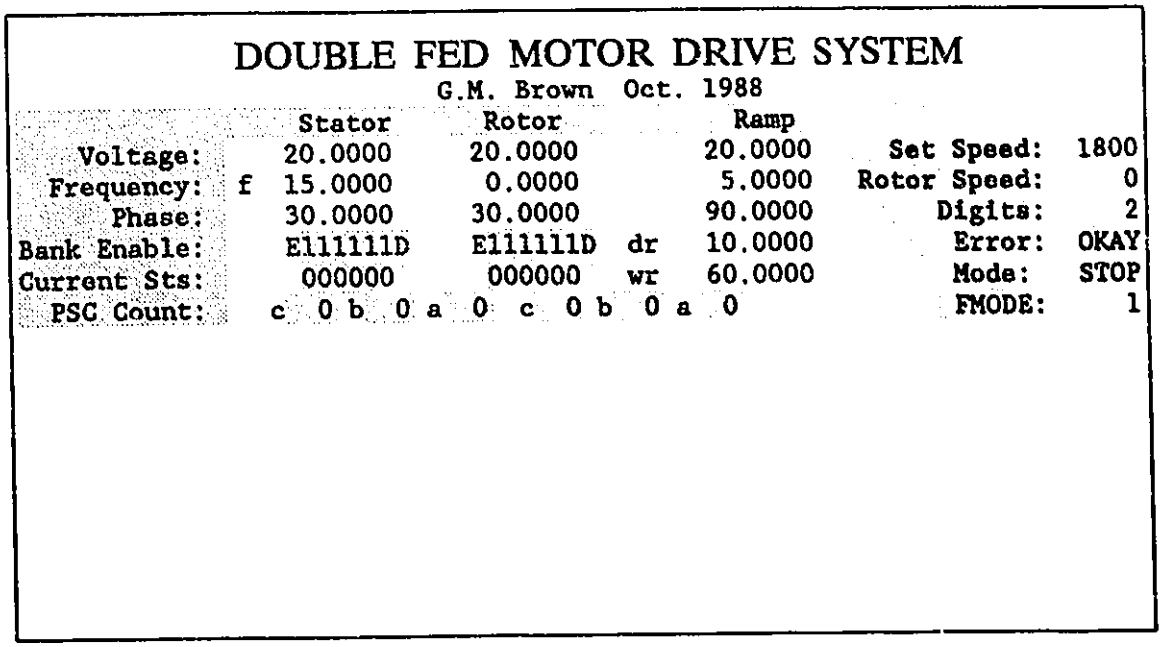

Figure 6.1 - SCREEN DATA DISPLAY

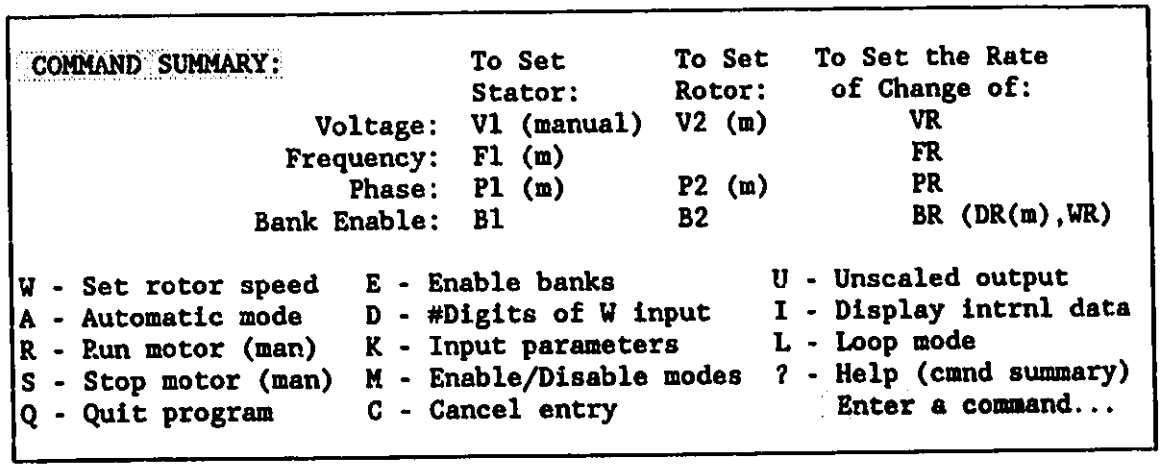

Figure 6.2 - MAIN COMMAND SUMMARY

program easy to use and provides the maximum amount of information about the system status to the user.

For testing purposes, unscaled data can be output directly to the hardware and most internal data values can also be displayed on the screen (using the UNSCALED and INTERNAL commands respectively). Data which are settable by the user, including all parameters, can be saved conveniently in a data file for future runs of the program.

6.3 Modes of Operation

6.3.1 Introduction

There are basically two modes of operation for the DFM system, manual and automatic. Manual operation implies that the operator has direct control over all control variables via their set points and can change them individually using the keyboard commands. Automatic operation implies that some (or most) of the control variables are determined by the control algorithm, as a function of other control variables (such as the stator frequency F_1) or the system state (such as the rotor speed W). The remaining variables, such as the desired torque, are input from the keyboard. Several automatic modes are available (Section 6.3.4).

In both manual and automatic modes, operator input can be discrete, in terms of specific set point values, or continuous, via a special MANUAL feature. The term MANUAL refers to 'manually variable set point' as opposed to a 'discrete set point'. This feature, described

further in Section 6.3.3, enables the operator to use the keyboard to simulate a continuously variable analogue input for the specified value. This is much quicker than typing a consecutive set of specific values and is very helpful during certain calibration and test procedures.

6.3.2 Mode Setup and Display

In addition to the general case of manual versus automatic operation, there are also numerous other modes, or configurations, of the hardware and software that determine the system operation. In terms of the hardware, for example; individual converter banks can be enabled or disabled, bank switching can be based on the assumption of continuous or discontinuous conduction, and manual reset commands can be sent to disabled banks (with HBR and RESET commands). These hardware features are all under software control.

It is also possible to alter the software's response to various errors or commands by enabling or disabling specific status bits. For example; most commands can be disabled to prevent their accidental use when not required (such as outputting unscaled output values), short circuits can be ignored or responded to, and single fed or double fed operation may be specified.

For the most part, the operating modes are controlled using the MODE command. A 16-bit mode status word MDESTS, and several other flags, are used to control the program flow. Figure 6.3 shows the bit assignments of MDESTS and their function. When the MODE command is

invoked, the current bit values of MDESTS are displayed on the screen and the arrow keys can be used to move the cursor to any particular bit. A '1' (or '0') then sets (clears) the bit and enables (disables) the corresponding mode. Other commands are also available as outlined in the help screen of Figure 6.4. Each command prompts the user for the necessary value and updates the screen display to reflect the new status. This includes the C, D, and F commands (Current mode, stator field Direction, and stator Frequency selection algorithm respectively).

If a command refers to stator or rotor banks individually, such as the C, D, or E (Enable banks) commands, then a value of 0, 1, 2 or 3 is entered and refers to; neither, stator only, rotor only, or both stator and rotor banks, respectively.

6.3.3 Manual Operation

As mentioned in Section 6.3.1, manual operation implies that all control variables are set on the basis of their set points only, and not as a function of other control variables. Set commands are available for the desired rotor speed, the stator frequency, the stator and rotor voltages, and the stator and rotor current phase angles. During manual operation, the control routine CONTRL adjusts the control variables from their present state to the new scaled set point value at a rate determined by a corresponding 'ramp' value. The magnitude of the ramp value determines how fast the transition occurs, ranging from no change (if the ramp value = 0) to instantaneous (if the ramp value equals the

```
Enable/Disable Modes:   DABKasml BrILUESR  (press'?' or 'L' for help)
                MODE                          1          0
  D - DFM/SFM mode of operation               enable     disable
  A - Interrupt Reg A (PSCISR)                enable     disable
  B - Interrupt Reg B (CLRISR)                enable     disable
  K - KPARAMeter mode command                 enable     disable
  a - AUTOmatic mode command                  enable     disable
  s - SC (BANK SHORT) protection              stop motor ignore
  m - MBE disable SC protection               stop motor ignore
  l - Loose circuit board                     stop motor ignore
      Press any key to continue
  B - set BANK enable bits command            enable     disable
  r - set RAMP values                         enable     disable
  I - Display INTERNAL data values            enable     disable
  L - LOOP mode command                       enable     disable
  U - Output UNSCALED data values             enable     disable
  E - ENABLE output banks comand              enable     disable
  S - STOP command (disable all banks)        enable     disable
  R - RUN command (manual setpoints)          enable     disable
      Press any key to continue
Enable/Disable Modes:   DABKasml BrILUESR  (press'?' or 'L' for help)
   Mode Status word:    11111011 11000111
```

Figure 6.3 - MODE STATUS WORD BIT DEFINITIONS

```
Enable/Disable Modes:   DABKasml BrILUESR  (press'?' or 'L' for help)
   Mode Status word:    11111011 11000111
                              press - arrows to move cursor
                                    - '1' to enable mode
                                    - '0' to disable mode
                                    - 'H' to send HBR pulse
                                    - 'R' to RESET all PSC counters
                                    - 'B' to toggle SC bell on/off
                                    - 'C' to change Current mode
                                    - 'D' to change F1 direction
                                    - 'F' to change F1 algorithm
                                    - 'N' to return to Next command
    Mode Status word:   11111011 11000111
```

Figure 6.4 - MODE STATUS WORD COMMAND SUMMARY

maximum value of the variable). Ramp values exist for all the set points as well as for the pseudo torque angle δ_v.

Manual operation is in effect when the operating mode is RUN, and the corresponding mode display will be RUN. During RUN, the control algorithm uses the special FORTRAN routine RAMP, to bring the actual value of the variable to the new set point (to the scaled set point value in fact) at the desired ramp rate. RAMP in turn calls the MACRO routine ADDOVF to add (or subtract) the ramp value to (or from) the control variable to get the new actual operating point. In this way, the actual value is clamped to within the maximum and minimum range of the specific variable. While in RUN mode, any parameter can be changed by typing 'K'. The mode display will change to PARAM and the screen will prompt for new parameter values. Any changes are immediately taken into consideration. Typing 'N' returns to NOTHING mode.

Whenever the operator is prompted for a set point value, he/she can enter a specific value in the appropriate physical units such as volts, degrees, hertz or rpm. Sometimes though, it is more convenient to simply increase or decrease the variable slightly from its present value. By entering 'M' in response to a set point prompt, the system enters the MANUAL mode of set point variation (Fig. 6.5). This may occur during manual or automatic operation, and refers to how the specific variable in question is to be specified, and not to how all the control variables are determined (Section 6.3.1).

MANUAL control simulates an analogue control input by giving the operator continuously variable adjustment over the specified control variable. This is done by invoking the MACRO routine ADDOVF with the

```
V1 - MANUAL mode          (press '?' fo help)
                press - a digit to increase a value
                      - 'shift & digit' to decrease a value
                      - 'space' to freeze a value
                      - 'H' to output HBR command
                      - 'S' to stop motor
                      - 'R' to reset all PSC counters
                      - 'N' to return to Next command (NOTHING mode)
```

Figure 6.5 - MANUAL MODE COMMAND SUMMARY

```
PARAMETER INPUT          (press '?' for help)
  Shaft encoder offset    THE0 = -412  :
        Extra bit code  EXTBTS = 0     :
          Torque angle    DEL = 0      :
   Freq/W range offset     FW = 2      :                (must = 2)
 Stator Voltage offset    V01 = 20     :
      Stator V/Hz gain    V1F1 = 3     :
   Stator Phase offset     P01 = 5     :
Stator Phase/Freq gain    P1F1 = 1.5   :
  Rotor Voltage offset    V02 = 20     :
       Rotor V/Hz gain    V2F2 = 3     :
    Rotor Phase offset     P02 = 5     :
 Rotor Phase/Freq gain    P2F2 = 1.5   :
       ASCR time delay   DELAY = 8     :      WARNING: use 8msec min.
   Max # PSC's allowed  SCCMAX = 2     :
   Torque angle offset      D0 = 40    :
    Torque/speed gain       DW = 0     :
DFM Stator freq offset   DFMF0 = 15    :
  DFM Stator f/W ratio   DFMFW =  0    :


                press - 'P' to go back to Previous value
                      - 'CR' to skip to the following value
                      - 'J' to jump to the delta & torque parmeters
                      - 'H' to issue HBR command
                      - 'R' to Reset all PSC counters
                      - 'S' to disable all banks (emergency STOP)
                      - 'N' to skip all values, go to 'Next' command
                      - 'C' same as 'N'
```

Figure 6.6 - PARAMETER MODE COMMAND SUMMARY

actual and incremental values as arguments. The incremental value (Section 6.2) is determined by pressing a number key on the keyboard. The number indexes a look-up table to get a value for the incremental variable. This value is added to the actual value each time CONTRL is called. The larger the number, the more the actual value will be increased. The increase continues every 100 ms until the number key is released, or until the maximum value is reached. By simultaneously pressing 'shift' and a number, the value will decrease in a similar manner.

MANUAL control is very useful for sweeping a control variable smoothly through its entire range (to check for glitches in the hardware), and for making very small adjustments to phase, frequency or voltage variables when calibrating the hardware. This feature was a great benefit in the overall development of the DFM system.

When MANUAL variable control is entered from RUN mode, the mode display will change from RUN to MANUAL. To exit from MANUAL variable entry mode, the operator presses 'N' for Next (or Nothing). The system then goes into an intermediate state (with the mode display indicating NOTHING) so that another set point can also be set manually if desired. No changes occur in any of the other actual values until RUN (or AUTO) is entered again. During this period, the set points displayed on the screen do not necessarily reflect the actual values of the control variables. When RUN is entered, for example, all values are ramped back to their previous set point values and the mode display goes from NOTHING to RUN to indicate this.

6.3.4 Automatic Operation

Chapter 4 outlined some of the control requirements for the double fed motor drive system. The stator and rotor voltages (V_1 and V_2), when controlled as functions of their respective frequency, determine the air gap flux. The stator frequency F_1 must be chosen according to; the frequency limitations of the cycloconverter, the actual rotor speed W, and an appropriate harmonic reduction scheme (if in effect). The rotor voltage V_2 and the torque angle δ_v can then be used to control the torque and thereby the rotor speed. Although manual operation is useful and necessary for testing and development purposes, dynamic control of these interrelated variables requires that some form of automatic control be implemented.

The DFMDRV software developed here automatically adjusts the control variables in real time. It is possible to modify most of the equation parameters on-line, as well as to select different control algorithms for specifying the stator frequency, making the automatic control scheme very flexible.

The double fed motor can be run as a single fed motor by shorting together the rotor windings and using only the stator cycloconverter to provide power. This SFM/DFM option is determined by clearing/setting bit-15 of MDESTS (as in Fig. 6.3) to select the appropriate control algorithm.

When running in single fed mode, the SFM operates as an induction machine and the mode display will be SFM_AUTO. Single fed control can be implemented on the basis of; controlled slip, with speed

feedback to determine the stator frequency F_1, or open loop. In each case, the control variables are the stator frequency F_1, the stator voltage V_1 and current phase angle P_1.

Since the cycloconverters used in this research are naturally commutated, P_1 can not control the exact phase of the load current. That is, if P_1 is larger than the naturally occuring load current angle ϕ_1, then the bank switching time (or angle) can be delayed. On the other hand, when P_1 is less than ϕ_1, P_1 will have no effect on the bank switching time (Sections 4.1 and 5.5.4.2).

At present, only open loop control has been implemented for single fed operation. The control algorithm is:

$$WAD = WS' \quad \text{(with RAMP)} \tag{6.1a}$$
$$F1A = F1W \times WAD \tag{6.1b}$$
$$V1A = V01 + V1F1 \times |F1A| \tag{6.1c}$$
$$P1A = P01 + P1F1 \times |F1A| \tag{6.1d}$$

where

WS = rotor set speed
WS' = scaled rotor set speed (after ramping)
WAD = actual desired rotor speed
F1W = constant to convert actual rotor speed to elec. hertz
F1A = actual stator frequency
F2A = implied actual rotor frequency
V1A, V2A = actual stator, rotor voltage
P1A, P2A = actual stator, rotor current phase angle
V01, V02 = stator, rotor voltage offsets
P01, P02 = stator, rotor phase angle offsets
V1F1, V2F2 = stator, rotor frequency-to-voltage conversion factors
P1F1, P2F2 = stator, rotor frequency-to-phase angle conversion factors

The parameters (V01, V1F1, P01 and P1F1) are variable on-line by entering 'K' (the parameter command) while in SFM_AUTO mode. The mode display will change from SFM_AUTO to S_PAR_AUTO and prompts will appear on the screen for new parameter values (Fig. 6.6). Any parameter changes

are immediately reflected in the new value of F1A, V1A and P1A according to the set speed WS in effect (or according to the rotor mechanical speed WAM, for closed loop operation).

It is also possible to use MANUAL mode to control the speed of the single fed motor. In SFM_AUTO mode, if 'M' is entered in response to the rotor set speed prompt (W), the mode will change to W_MAN_AUTO. In this mode, the set speed can be ramped up and down continously from the keyboard according to the MANUAL mode command outlined in Section 6.3.3. The control algorithm is the same as for SFM_AUTO mode, except that now WAD comes manually from the keyboard instead of via the W set point.

Note that during SFM operation, the pseudo torque angle δ_v has no effect, since the rotor field is not externally supplied (it is induced via the air gap as a function of the slip), and there is no freedom in choosing F_1. This mode has been very useful for testing each cycloconverter individually.

Double fed operation provides the maximum number of degrees of freedom to control the motor, and the DFMDRV software is designed to take advantage of this. When bit 15 of MDESTS is set, the mode display will indicate DFM_AUTO and double fed operation is in effect.

The stator frequency is related to the rotor speed via the relationship $F_1 = W + F_2$ (where F_1, F_2 and W are all expressed in electrical hertz and electrical rps). The rotor voltage angle calculator (section 5.4.4) controls the phase of the rotor field such that F_2 will satisfy this relationship for all F_1 and W (within the 30 Hz frequency limit of the cycloconverters). Therefore, F_1, the stator frequency , can now be chosen independently of the rotor speed. F_1 can be chosen to

minimize either harmonics or torque pulsations, or can be chosen in conjunction with the stator voltage V_1 to control the stator cyclo-converter input power factor.

At present, two algorithms have been implemented to determine F_1. The choice of algorithm is specified by entering 'F' (for F_1 algorithm) and then entering a value for FMODE while in the MODE command. When FMODE = 1, the algorithm determined by the routine GETF1 is:

$$F1A = DFMF0 + DFMFW \times WAM \tag{6.2}$$

where

F1A = the actual stator frequency (in electrical hertz)
DFMF0 = an offset frequency F0 (for DFM operation)
DFMFW = a gain constant
WAM = the actual mechanical speed

The parameters DFMF0 and DFMFW are variable on-line by entering 'K' (the parameter command) while in DFM_AUTO mode. The mode display will change from DFM_AUTO to D_PAR_AUTO and prompts will appear on the screen for new parameter values. All parameter changes are immediately reflected in the new value of F1A according to the rotor mechanical speed WAM.

When FMODE = 2, GETF1 yields the algorithm F1A = F1S'. Where F1S' is the scaled and ramped set point value of the stator frequency. The stator set point frequency F_1 will therefore control the actual stator frequency directly (taking into account of course the effect of the present ramp value FR when F_1 is changed).

After F1A has been determined, the control algorithm uses the stored parameter values to determine V1A, P1A, V2A and P2A to control the flux in the machine. The equations have the same form as for the SFM

case, except now, an implied value for F_2 is also calculated, based on the stator frequency and the actual rotor speed. This value of F_2 is then used to determine the rotor voltage V_2 and phase angle P_2.

The corresponding control algorithm is:

```
WAD = WS'                          (with RAMP)      (6.3a)
F1A = F1W × WAD                                     (6.3b)

V1A = V01 + V1F1 × |F1A|                            (6.3c)
P1A = P01 + P1F1 × |F1A|                            (6.3d)
F2A = F1A - F1W  ×  WAM                             (6.3e)
V2A = V02 + V2F2 × |F2A|                            (6.3f)
P2A = P02 + P2F2 × |F2A|                            (6.3g)
```

These equations determine the flux in the machine, while the hardware implemented rotor voltage angle calculator ensures synchronized and stable operation. In addition, control of the speed requires dynamic determination of the speed error W_{err} and control of the torque to compensate.

Chapters 3 and 4 showed how the torque is dependent upon the pseudo torque angle δ_v, and can be calculated using estimates for δ_o and d_o. The initial torque control algorithm that was implemented though, used the simple relationship

```
DELA = DO + DW × WERR                               (6.4)
```

where

DELA = actual pseudo torque angle (δ_v)
DO = torque angle offset (δ_o)
DW = torque/speed gain
WERR = WAD - WAM = actual mechanical speed error

This assumed that the torque angle δ_o was constant, or at least was limited to a small range of values. As a result, the pseudo torque angle δ_v (DELA) was only valid for the particular basepoint which

corresponds to the value chosen for δ_o. Also, (6.4) does not account for the decrease in torque that occurs when $(\delta_v + \delta_o)$ becomes less than -90^o (4.20), and so does not give satisfactory performance. Despite this large control error, the motor remains synchronized, but there is loss of control over the torque, and subsequently of the rotor speed. A better algorithm, therefore, is required to determine δ_v on-line, while the other operating variables are continually varying.

With an estimate of δ_o and d_o, based on the rotor angle θ and the terminal voltages V_1 and V_2 (according to Section 4.2.3), the effect of changes in δ_v upon the torque Γ can be predicted.

A special case of automatic operation is where the MANUAL mode is used to control the pseudo torque angle δ_v directly. By intering 'M', in response to the delta ramp prompt (BR command), MANUAL mode provides direct ramping control of the torque control variable δ_v. The control algorithm is the same as for DFM_AUTO, but the DELA value now comes manually from the keyboard and the double fed motor can be operated without implementing the δ_v control scheme of Section 4.2.3.

6.4 Bank Enable and Disable Facilities

6.4.1 Manual Bank Enable/Disable

Proper testing of the cycloconverter banks requires that the operator be able to selectively enable and disable each converter bank. As mentioned in Chapter 5, there are DIP switches which allow each SCR

and/or each converter bank to be individually disabled, and these cannot be overriden by the software. It is very useful though, to be able to also set up a bit mask, corresponding to each of the stator and rotor converter banks, settable from the keyboard, which can enable or disable the converter banks (provided the appropriate DIP switches are all enabled). This is done using the B1 and B2 commands (Fig. 6.2), for the stator and rotor banks respectively.

In response to either of these commands, the user is prompted for a 6 digit string of ones and zeros which correspond to the 6 banks of each converter. The current Bank Enable status (bit mask) is displayed in the upper portion of the screen (Fig. 6.1). In addition, the Enable command 'E' allows the stator or rotor converters to be enabled (according to the bit mask), or disabled, without affecting the bit mask. This is indicated by an 'E' or 'D' to the left of the appropriate Bank Enable bit mask which is shown in the display.

If there is a short circuit detected by the hardware, and the short circuit protection logic is enabled, the converter bank with the short is immediatly disabled by the hardware. The screen display will be updated and the stator or rotor current status will indicate, by the presence of a 1, each bank where a short has occurred. If bit 10 of MDESTS is set, the software will also change the operating mode to STOP and display the error message BNK_SHRT. Otherwise, the system remains running on the remaining banks.

At this point, if 'H' is typed, the software issues a Hardware Bank Reset (HBR) and all the firing circuits are reset. If the fault doesn't reoccur, the Current Status display will be cleared and the

disabled bank will be reenabled. From the Mode command, typing 'B' will toggle the console bell on and off. When 'on', any change in the short circuit current status causes the bell to beep. This audible indicator is very useful when monitoring the oscilliscope screens during calibration and testing.

The short circuit detection logic for each converter bank can also be disabled, if necessary, by means of a DIP switch for each bank. This is very risky though, since the circuit breakers are unable to protect the SCR's from any transient overcurrent that might occur. This constitutes a Manual Bank Enable command (MBE), and the error message NO SC PRTN (No Short Circuit Protection) will be displayed. The letters MBE will also appear beside the appropriate stator or rotor Current Status display to indicate that one or more of the respective banks is manually enabled.

6.4.2 Automatic Bank Reset Feature

The features of Section 6.4.1 greatly facilitated testing and calibrating the individual converter banks on passive loads. However, the interaction between the converter banks, when they were operated simultaneously on the motor windings, made it extremely difficult to recalibrate the SC and off-detection circuits with the actual motor impedances. For this reason the Automatic Short Circuit Reset (ASCR) circuits of Section 5.6.4 were developed, along with the two interrupt service routines (ISR's), PSCISR and CLRISR.

PSCISR checks the current status of each converter phase (2 banks per phase). If there is a new Phase Short Circuit (PSC), then a counter for that phase is set to the value of DELAY. At each occurrence of the ReqA interrupt, PSCISR decrements any non-zero phase counters, and if one reaches zero, it issues a Software Bank Reset (SBR) for that phase and then updates the PSC count for that phase on the screen.

SCCMAX (Short Circuit Count Maximum) is an upper limit on the number of PSC's that can occur on any phase. If this count is reached, then no SBR command is issued for that phase. ReqB generates a low frequency interrupt to the second interrupt service routine CLRISR, to periodically clear all non-zero PSC counts. This prevents the counters from eventually reaching SCCMAX due to isolated non-repetitive shorts (or false SC signals). If there is a repetitive bank short though, due to a hardware failure, then SCCMAX is reached very quickly and the bank is disabled until ReqB occurs, or the 'R' (Reset) command is typed.

The system is currently set up to generate a ReqA interrupt approximately every 1 ms and a ReqB interrupt every 4 seconds. DELAY is set to 8 and SCCMAX is set to 3. Therefore, when ReqA and ReqB are enabled, any bank short is cleared (or reset) in a little over 8 ms, about one half of a cycle. If 3 shorts occur on the same phase within 4 seconds, that phase stays off for approximately 4 seconds. This provides a very robust, fault tolerant system that can be calibrated and run without prior knowledge of the motor impedances, or of the level of interference due to transient-induced noise pulses between the various converter output phases.

CHAPTER 7

DISCUSSION AND EXTENSIONS TO FURTHER WORK

7.1 DFMDRV Performance

The double fed motor hardware and software described in this thesis were developed and tested using a 2 KW wound rotor induction machine. Being a development system, the emphasis throughout has been to keep the system flexible, both in terms of the hardware configuration and the software programmability. This has worked well, and the present system is easily expandable for implementing further work. Some of these avenues will be outlined more fully in Sections 7.2 and 7.3, but first, a summary of the overall DFMDRV system performance is in order.

The modular design of the cycloconverters has been very convenient for testing, since faulty circuits could be isolated quickly. One of the most useful features here is that the interconnections between the input lines, the converter banks (4 half banks per phase), and the current detection circuits, are not hard-wired. Instead, binding posts and interchangeable flat (signal) cables are used for all interconnections. In this way, every possible combination of; gate pulse logic board, gate pulse isolation board, SCR bank (including individual SCR's), and off/SC detection board, can be tested by either switching

the wiring harnesses, using jumpers on the front panel, or swapping the circuit boards.

The software also makes it very easy to enable/disable individual banks of the cycloconverters. This facilitates testing individual banks by minimizing the changes in interconnections to disable unused banks. Given the complexity of isolating one or more damaged components, or of finding a wiring error in such a large system, this design methodology has proven to be indispensible.

The DFM drive system can be broken into two major sections: the control section and the power section. The control section was developed quite independently from the power section. It includes the user interface software, the control algorithms, the I/O hardware interface, and all the circuits associated with deriving and controlling the reference waves (including the rotor voltage angle calculator and speed measuring circuit).

The power section transforms the reference waves into suitable 3-phase AC voltages for supplying the stator and rotor currents. It includes the comparator and gate pulse circuits, the SCR banks with their associated drive circuits, the bank off-detection circuits and the short circuit detection circuits. The cosine wave method of control has been implemented with SCR's, in a naturally commutated system. However, different power section topologies and devices could also be used, quite independently of the source of the reference waves or DFM control algorithm.

Suitable control of the reference waves in frequency, amplitude and phase is the key to proper control of the cycloconverters and the

DFM drive. Most of the DFMDRV software was developed in conjunction with a 4 channel oscilloscope to monitor the reference waves (R_{1a-1c}, R_{2a-2c}) and the resulting gate pulses. During the initial development stages, a separate DC motor was used to rotate the DFM, simulating various operating conditions. This made it possible to verify the ability of the rotor voltage angle calculator to synchronize the stator and rotor voltage waves by directly observing the voltage, frequency and phase of the reference waves.

The MANUAL mode feature has been particularly useful, because it allows the output variables to be swept smoothly back and forth over their entire range (quickly or slowly), or to easily make small changes in the set point values. A situation where this is very important is the calibration of the off-detection and short circuit detection circuits. In this procedure, because the noise spikes vary in amplitude according to the firing angle, they change with every cycle in a non-periodic way. This makes it impossible to observe the effect of any small adjustment. Using MANUAL mode, F_1 can easily be set to 0 and V_1 (or V_2) can be varied from 0 to 120 V, as in a single phase controlled rectifier (See example on page 122). With F_1 = 0 though, the noise spikes become periodic and controllable, with an amplitude that is determined directly by the value of V_1 (or V_2). This greatly facilitates tuning the circuit, because the effect of any adjustment is now observable.

The ability to vary the parameters on-line makes it easy to adjust the drive performance. The motor can be run in MANUAL mode, to set up specific operating conditions, and then these values can be used to derive new parameter values. The phase angles P_1 and P_2 were

determined in this way for various frequencies, and then used to derive P01, P1F1, P02 and P2F2 (See equation (6.1).

The major effort in developing the power section was in determining accurately when to switch banks. This was dependent on a reliable bank current off-detection circuit. Hand in hand with this, is the need to protect the equipment from short circuits during the initial development stages and later in the event of a fault condition.

At first, 3 Ω resistors were connected between the positive and negative converter banks to limit short circuit currents to 40 A. This value is well within the 350 A single-cycle surge rating of the SCR's. Once the short circuit detection logic was working, these resistors were removed, and the equipment worked reliably without damage from shorts.

Both the off-detection and short circuit detection circuits use very simple sensors. In the first case, a pulse transformer in parallel with a series connected diode, and in the second case, 45 turns of wire on a small ferrite rod placed inside the di/dt limiting coil. Both circuits are fast and have a very wide range of sensitivity adjustment. The ability to control the minimum pulse amplitude cutoff threshold, and to set a minimum duration time on the width of a single pulse, made it possible to discriminate between switching transients and the desired signal. High amplitude noise spikes of short duration, and low amplitude transients of long duration, are effectively ignored with the result that the resulting off pulses (K_P and K_N) and short circuit pulses ($\overline{SC}_P$ and $\overline{SC}_N$) are reliable indicators of converter operation.

Even with the control flexibility offered by MANUAL mode, it was very difficult to simultaneously calibrate all the detectors when

the cycloconverters were connected to the mutually coupled windings of the motor. The Automatic Short Circuit Reset (ASCR) provision described in Section 5.6.4 overcomes this problem very nicely.

When incorrectly calibrated, the detector circuits can cause either of two types of errors. Either a short circuit occurs and it is ignored, or no short circuit occurs but one is 'detected'. The first case is minimized by starting with the SC detectors set too sensitive, and then slowly decreasing their sensitivity. The second case is more of a problem though because the hardware and software are generally set up to disable the bank(s) in the event of a short(s). False triggering of the SC detectors therefore disables the outputs, and calibration can't continue. If the SC logic is disabled in an attempt to calibrate the off-detectors, then when a short does occur, it is ignored and inevitably some thyristors are damaged and need to be replaced.

Without the ASCR circuit the motor could be run on two phases (in SFM mode) at low torque. When one attempts to enable the third bank, a $\overline{SC}$ signal occurs, disabling one of the other banks, and three phase operation can not be achieved. The ASCR circuit was very effective in eliminating this problem. Initially, the motor was started up on two phases, as before, but now when the third phase was enabled, causing a false $\overline{SC}$ pulse, the disabled bank was reenabled 8 ms later. On the next cycle, the transient was not present and the system kept running. Even with short circuits (real or false) occurring as much as five times per second, no damage is incurred and calibration of the off-detectors and current detectors can proceed. In terms of the overall DFM drive, the automatic SC reset facility has been the most instrumental feature in

achieving a practical working drive.

During single fed operation, the system was run open loop and the speed followed closely the ramped value of the rotor set speed. The cycloconverters perform well in regenerative mode and speed reversals from +900 to -900 rpm (the full range using $F_1 = \pm 30$ Hz) were achieved at a rate of 70 rpm/100 ms or (700 rpm/sec). This was without optimizing the control parameters.

For double fed operation, the field calculator for the rotor voltage angle worked very well and kept the stator and rotor voltage vectors synchronized in the air gap. Operation up to a rotor frequency of $W = \pm 60$ Hz was achieved.

The upper limit on the stator frequency is 30 Hz, due to the digital VCO used to generate α and the stator reference waves. The frequency of the rotor reference waves is determined by the rotor speed and stator frequency, according to $F_2 = F_1 - W$, and has no fixed limit. Operation of either Ref_1 or Ref_2 much beyond 30 Hz is limited though by the present data synchronization circuit (Fig. 5.9), which was only designed for an upper limit of 30 Hz. This can easily be increased.

The rotor speed is determined by the torque balance in the machine. Precise speed control therefore requires accurate control of the developed torque Γ, at all speeds. The present torque control scheme of equations (6.4) does not provide a good estimate for δ_v. As a result, when the value of δ_v is wrong, the developed torque does not balance the load torque and the rotor speed will change accordingly. As the speed and basepoint change, δ_o also changes. Therefore, if δ_v is held constant, the rotor speed will eventually reach a speed where Γ equals

the load torque and the speed will stabilize. The speed in this case is uncontrolled (or only very loosely controlled), but the DFM is still stable (Section 4.2.1). Thus, one of the major objectives of this research has been determined favorably; the inherent instability of the DFM can be overcome in a dual cycloconverter drive system by dynamically controlling the phase angle of the rotor voltage.

It was possible to control the speed of the double fed motor without implementing the pseudo torque angle control scheme of Section 4.2.3 by using MANUAL mode to control δ_v. The value of δ_v (DELA) had to be varied greatly, corresponding somewhat to the rotor speed, in order to maintain a sufficiently large motoring torque. This is consistent with the observed variation in δ_o for different values of slip in Figures 3.14, 3.15 and 3.16. Operation up to ± 1900 rpm (P=2) was thus obtained.

7.2 Hardware Refinements

The most difficult aspect of the hardware development was that of reliable bank switching. This problem was dealt with effectively by the current off-detection and short circuit detection circuits, and the ASCR software. A more direct solution would be to simply use suitable high power switching devices that are capable of forced turn-off.

Initially GTO's were not used in this work, because it was desirable to avoid the additional complexity of the necessary gate turn-off circuits. However, it is clear now that this is not as

cumbersome a problem as it used to be, especially since only a low power turn-off circuit is required.

Since the cycloconverters are operated in the natural commutation mode, the GTO's would normally be reverse biased at the time of turn-off, and will turn off naturally without reverse gate current. At the instant of load current reversal and bank switching, by definition, the load current and GTO currents are zero (or very close to zero). Thus, even when not reverse biased at turn-off, the gate circuit does not need to sink a large level of current. In this case, a rating of 10% of the normal GTO current would be a conservative estimate of the required gate drive capacity. Therefore a GTO implementation of the cycloconverter drive would make optimum use of the GTO's high power ratings, and also minimize the gate drive circuitry and provide very reliable bank switching.

The hardware implementation of the cosine wave method of control has proven to be very fast and reliable, and does not require any processing overhead by the control computer. Several refinements though would simplify the circuit and reduce the parts count substantially.

A reduction from 10-bit to 8-bit quantization of the timing and reference waves would still give very good accuracy, and yet reduce the required number of chips for each counter from 3 chips to 2, and for each look-up table from 4 EPROMS to 3. Equally helpful, in reducing the chip count would be the use of programmable gate arrays for much of the logic, especially because of the high level of symmetry and repetition of many of the circuits.

There are also many time delays implemented using monostable

chips, which all require external components (4 components per 4538 dual monostable). The use of a suitable multi-phase clock would allow these delays to be conveniently implemented with logic only, eliminating the need for the timing components. This would also eliminate the problem of component tolerance variations and the effects of temperature and aging.

Implementation of the Jitter control strategy could be affected quite simply by introducing a programmable time delay immediately after the comparators, and before the gate pulse logic of Figures 5.10 and 5.11. By introducing a uniform phase delay to all gate pulse lines, a phase advance can be obtained by reducing the standard delay, and a phase delay can be obtained by increasing the standard delay.

7.3 Software Refinements

The DFMDRV control software has worked very well for controlling the cycloconverters, in both single fed and double fed modes. The most obvious extension to the software is to implement the pseudo torque angle control algorithm of Section 4.2.3 for accurate speed control of the DFM (Figure 4.3).

One of the advantages of using the circle diagram to analyze the double fed motor, is that it transforms the standard matrix equations, with their time-varying coefficients, into a simple geometric relationship. The interrelationships between the control variables are then easily visualized with the help of the circle diagram plotting program (DFMPLT). Also, since the equations to be solved in finding δ_v

no longer require matrix algebra, their solution is very straight forward and can be done in real-time without requiring an extremely fast microprocessor.

The other major refinement to the software would be to implement the frequency hopping algorithm of Section 4.3.3. In this way, the fullest speed range of the DFM can be utilized by running the cycloconverters at very high output to input frequency ratios (ie. $1/3 \leq fo/fi \leq 2/3$). The most reasonable approach is to precalculate a trajectory similar to Figure 4.8, and include a small amount of hysterisis to provide a slightly different trajectory for increasing and decreasing speeds. This can then be incorporated into look-up tables based on F_1 and W to give the stator voltage V_1, the basepoint (x_o, y_o), and the rotor voltage magnitude $R_o = |I_{1r}|$. From these, the calculation of δ_o and d_o is simple.

When δ_v is adjusted to be near the angle for maximum torque (ie. $\delta_v = -90^o - \delta_o$, then the magnitude of V_2 (and hence R_o) has a direct effect on the developed torque (4.8) and (4.12). Therefore, an error in the basepoint when δ_v is in this region, can be compensated for by a quick change in V_2. On the other hand, when δ_v is adjusted to be near $\delta_v = -\delta_o$, then changing V_2 has no effect on the torque. In this case, δ_v itself can be used to compensate for errors in the basepoint.

In both of these cases, the sense of the change in V_2 or δ_v, to achieve the required torque change, is known and good speed control should be achieved. This means that the number of precomputed values for the basepoint does not have to be large. As few as 20 or 30 may be sufficient.

Converting the software to run on a different computer will make the system more convenient to use, and will not be difficult. The control requirements of the DFMDRV hardware are all handled by one 16-bit output data word, one 16-bit input data word, 2 interrupt requests and a control status register. This means that the software can be implemented on any standard PC without having to worry about hardware compatibility of timer interrupts and so forth.

7.4 Summary

The development of a double fed motor drive using dual cyclo-converters has been undertaken as a step towards providing a high power traction drive with smooth traction-limited torque at standstill, and wide-range speed control up to base speed. Several new control strategies have been proposed and developed to reduce the effect of the cycloconverter output harmonics, minimize the production of harmonic torques, and increase the usable speed range.

The Jitter control method has been shown to be a viable way of spreading the harmonic energy of the cycloconverter output over a wider band of frequencies. This has little effect on the desired output voltage but reduces the filtering requirements of the cycloconverter.

At higher output frequencies, the lower side-band harmonics of the cycloconverter output lead to parasitic torques, and these normally limit the usuable output frequency range of the cycloconverter to approximately 1/3 of the input frequency. The use of two independently-

controlled variable frequency power sources introduces great flexibility into the control of the double fed motor. For example, saturation problems are eliminated at low speed because both stator and rotor frequencies can be kept relatively high, with the rotor speed being proportional to the difference between F_1 and F_2. The output voltages can therefore also be kept high according to some volts/Hz criterion. If the power sources are cycloconverters, which they are in this case, then this higher output voltage has the additional benefit of reducing the cycloconverter output harmonics and improving the input power factor.

Another feature of the double fed drive is that it now becomes possible to avoid operating either cycloconverter at the specific frequencies which generate the most undesirable harmonic torques. A frequency hopping strategy has been proposed which makes use of this principle and allows operation up to, and even above, the supply frequency. That is, $W_{max} = F_1 - F_2 = 60$ Hz, and for a 2 pole motor, this corresponds to a rotor speed of $n = 1800$ rpm.

A simulation program has been written to plot the circle diagram for the double fed machine and analyze the relationship between the terminal variables and developed torque. From this analysis, a control algorithm was developed using the pseudo torque angle δ_v (the angle between the stator and rotor voltage phasors) to control the torque of the double fed motor over its entire speed range.

Two naturally-commutated cycloconverters were built using a hybrid digital-analogue implementation of the cosine wave method of control. Reliable bank switching was achieved by sensing the reverse

bias voltage across a diode connected in series with each converter bank. Detection circuits with an adjustable energy threshold provided good bank switching in the presence of large switching transients.

Short circuit protection was also implemented using similar detection circuits. This worked very well to prevent damage to the SCR's in the event of a short circuit, by immediately disabling the gate pulses to the affected bank. In the event of spurious non-repetitive shorts, an automatic short circuit reset circuit (ASCR) was developed to reset the banks automatically after the short occurred. This feature proved to be invaluable in calibrating the off-detection circuits, which in turn control the bank switching function.

Control software was developed to monitor and display the status of the complete double fed motor drive system. The system parameters are variable on-line and several modes of manual and automatic operation are possible. MANUAL mode was particularly useful for testing the system during double fed operation because it provides direct control over δ_V.

The double fed motor was stabilized by ensuring that the stator and rotor mmf vectors rotated synchronously with each other at all times. This was done by implementing $\beta = \alpha - \theta - \delta_V$ with two binary adders, at the hardware level. Thus, the rotor voltage angle β was precisely determined by the rotor shaft angle θ, the stator voltage angle α, and the pseudo torque angle δ_V. The system was shown to be stable and remained synchronized at all times.

This work has shown the flexibility of a double fed motor drive system fed by two cycloconverters. This combination overcomes the frequency limitations of the cycloconverters and is very amenable to

field oriented control. It was shown that stable operation over a wide speed range is possible, and that it should be possible to operate the system with a high shaft torque and minimal harmonic torques, from standstill right up to base speed.

REFERENCES

[1] Stemmler, H., Meyer, A., "Variable-Speed Converter-Fed Three-Phase Drives", Brown Bavari Rev. 69,4/5 1982, pp. 114-121.

[2] Bourbeau, F. J., "Synchronous Motor Railcar Propulsion", IEEE/IAS, 1974-Part 1, pp. 533-540.

[3] G.M.Brown, "Hybrid Control Of A Cycloconverter For Double Fed Motors In Traction Drives", M.Eng. Thesis, McMaster University, Hamilton, Ontario, 1984.

[4] Oguchi, K., Sugawara, K., Kakizume, Y., "A Stabilized Doubly Fed Motor with a Separately Controlled Current Source Converter", IEEE Trans., IECI-28, Nov. 1981, pp. 336-341.

[5] M.Riaz, "Energy-Conversion Properties of Induction Machines in Variable-Speed Constant-Frequency Generating Systems", AIEE Trans., Vol. 78, Part II, 1959, pp. 25-30.

[6] N.L.Schmitz, V.D.Albertson, "The Stabilized Doubly Fed Synchronous-Induction Machine: Test Results and Computer Solutions", Conf. Rec. IEEE Winter Power Conf., 1964, pp. 858-864.

[7] P.Franz, H.W.Lorenzen, R.Nuscheler,G.Wang, "Transient Behavior and Eigenvalues of the Doubly Fed Induction Machine", Int'l. Conf. on Elec. Machines, Lausanne, Switzerland, 1984, pp. 1037-1041.

[8] M.Ohi, J.G.Kassakian, "Dynamic Characteristics and Speed Feedback Stabilization of the Doubly-Fed Machine", Conf. Rec. IEEE PES Summer Meeting, July 1976, pp. 1-8.

[9] A.J.Said, "Survey of Controlled Induction Motor-Thyristor Cascades", Int'l. Conf. on Elec. Machines, Lausanne, Switzerland, 1984, pp. 1060-1063.

[10] M.A.Saleh, A.M.Issawi, M.N.Iskander, "Double Excited Induction Generators Operating with WECS", (WECS stands for Wind Energy Conversion System), Int'l. Conf. on Elec. Machines, Lausanne, Switzerland, 1984, pp. 1064-1067.

[11] W.F.Long, N.L.Schmitz, "Cycloconverter Control of the Doubly Fed Induction Motor", IEEE Trans. on Ind. and Gen. Appl. IGA-7, Jan./Feb. 1971, pp. 95-100.

[12] J.M.Pacas, "The Field Oriented Control of the Series Connected Doubly Fed Induction Machine", Int'l. Conf. on Elec. Machines, Lausanne, Switzerland, 1984, pp. 1054-1059.

[13] G.M.Brown "Technical Manual for DFMDRV: A Dual Cycloconverter Double Fed Motor Drive System", Power Research Laboratory, McMaster University, Hamilton, Ontario, 1989.

[14] M.A.Boost, P.D.Ziogas, "State-of-the-Art Carrier PWM Techniques: A Critical Evaluation", IEEE Trans. On Ind. Appl. IA-24, March/April 1988, pp. 271-281.

[15] G.M.Brown, L.Magnard, B.Szabados, "Improving the Harmonic Performance of a Cycloconverter by Novel Jitter Control Method", Presented at the 3rd Conf. on Harmonics in Power Systems, Lafayette, Ill., 1988.

[16] L.Gyugyi, B.R. Pelly, Static Power Frequency Changers, New York: Wiley Interscience, 1976.

[17] B.R.Pelly, Thyristor Phase-Controlled Converters and Cyclo-converters, New York: Wiley, 1971.

[18] The 3-D plotting program and the program to calculate the cyclo-converter output harmonics were done by S.J.Spencer and L.Magnard respectively.

[19] A.Robson, An Introduction to Analytical Geometry, Cambridge University Press, London, 1940.

[20] M.Liwschitz-Garik, Electric Machinery, D. Van Nostrand Co., New York, 1946.

[21] D.W.Novotony, T.A.Lipo, "Principles of Vector Control and Field Orientation', presented in IEEE Trans. on Ind. Appl. Tutorial Course Introduction to Field Orientation and High Performance AC Drives, IEEE IAS Annual Meeting, Toronto, Ontario, Oct. 1985, pp. 2-1 to 2-65.

[22] T.Nakano, H.Ohsawa, K.Endoh, "A High Performance Cycloconverter-Fed Synchronous Machine Drive System", IEEE Trans. On Ind. Appl., IA-20, Sept. 10th. 1984, pp. 1278-1284.

[23] S.Nishikata, T.Kataoka, "Dynamic Control of a Self-Controlled Synchronous Motor Drive System, "IEEE Trans. on Ind. Appl. IA-20, May/June 1984, pp. 598-604.

[24] T.H.Barton, "The Generalized Theory of Electric Machines", presented in IEEE Trans. on Ind. Appl. Tutorial Course Introduction to Field Orientation and High Performance AC Drives, IEEE IAS Annual Meeting, Toronto, Ontario, Oct. 1985, pp. 1-1 to 1-46.

[25] B.K.Bose, Power Electronics and AC Drives, Prentice-Hall, New Jersey, 1986.

[26] T.Kume, T.Iwakane, "High Performance Vector Controlled AC Motor Drives-Applications and New Technologies-, IAS Annual Meeting, Toronto, Oct. 1985, pp. 690-697.

[27] L.A.Finzi, L.C.Wellard, "The Geometric Loci of the Synchronous Tie", AlEE Trans., Vol. 68, pt. I, 1949, pp. 168-171.

[28] R.Ueda, T.Sonoda, T.Machizuki, S.Takata, "Stabilization of Bank Selection in No-Circulating Current Cycloconverter by Means of Reliable Current-Zero and Current-Polarity Detection", IEEE Trans. on Ind. Appl. IA-20 July/Aug. 1984, pp. 827-833.

BIBLIOGRAPHY

1. H.Hosoda, S.Tafara, R.Kurosawa, H.Hakata, K.Doi, "A High-Performance Cross-Current Type Cycloconverter-Fed Induction Motor Drive System", IEEE Trans. on Ind. Appl. IA-24, May/June 1988, pp. 479-486.

2. D.A.Jarc, D.W.Novotny, "A Graphical Approach to AC Drive Classification", IEEE Trans. on Ind Appl., IA-23, Nov/Dec 1987, pp. 1029-1035.

3. T.H.Barton, "Variable Speed Electric Drives", Presented at the 1st Annual Symposium on Electric Variable-Speed Drives, Sponsored by Ontario Hydro and the Ontario Ministry of Energy, Toronto, Ontario, April 28, 1987.

4. N.U.Rao, "The General Motors GF6C Electric Locomotive", IEEE Trans. on Ind. Appl. IA-22, May/June 1986, pp. 502-511.

5. M.J.Hapeman, J.Long, D.L.Plette, "Diesel Electric Locomotive Propulsion Systems -- A Look Into the Future", IEEE Trans. on Ind. Appl. IA-22, May /June 1986, pp. 495-501.

6. H.Akagi, A.Nabae, "High-Performance Control Strategy of Cycloconverter-Fed Induction Motor Drive System Based on Digital Control Theory", IEEE Trans. on Ind. Elec., IE-33, May 1986, pp. 126-131.

7. S.Sathjakumar, S.K.Biswas, J.Vithayathil, "Microprocessor-Based Field-Oriented Control of A CSI-Fed Induction Motor Drive, IEEE Trans. on Ind. Elec., IE-33, Feb. 1986, pp. 39-43.

8. G.A.Smith, D.Donegani, "Performance Comparison of Single and Dual Speed Range Slip Recovery Devices", 2nd Int'l. Conf. on Power Electronics and Variable Speed Drives, 1986, pp. 98-105.

9. J.S.Heard, W.Crookes, D.Robinson, D.Brooks, "Novel GTO Inverter for High Performance Locomotive Main Drive", 2nd Int'l. Conf. on Power Electronics and Variable Speed Drives, 1986 pp. 204-207.

10. H.Zelaya de la Parra, P.S.Excell, "Microprocessor Control of a Doubly-Fed Induction Machine with a Cycloconverter in the Rotor Circuit", 2nd Int'l. Conf. on Power Electronics and Variable Speed Drives, 1986, pp. 221-225.

11. S.K.Tso, K.H.Tang, "Closed-Loop Operation of a Microprocessor-Controlled Cycloconverter", 2nd Int'l. Conf. on Power Electronics and Variable Speed Drives, 1986 pp. 226-229.

12. H.Ichida, A.Miyazaki, K.Ishii, "Microprocessor-Based Digital Control Cycloconverter (DCC) Application to Induction Motor Speed Control", IEEE Trans. on. Ind. Elec., IE-32, Nov. 1985, pp. 414-422.

13. B.K.Bose, "Motion Control Technology -- Present and Future", IEEE Trans. on Ind. Appl. IA-21, Nov./Dec. 1985, pp. 1337-1342.

14. R.E.Betz, R.J.Evans, "Microprocessor Control of a Cycloconverter", IEEE Trans. on Ind. Elec., IE-32, May 1985, pp. 120-129.

15. J.R.P.Gupta, B.Singh, B.P.Singh, "A Closed-Loop Rotor Resistance Control Method for Improved DC Dynamic Braking of Wound Rotor Induction Motor", IEEE Trans. on Ind. Appl. Jan./Feb. 1985, pp. 235-240.

16. K.Ohnishi, H.Suzuki, K.Miyachi, M.Terashima, "Decoupling Control of Secondary Flux and Secondary Current in Induction Motor Drive with Controlled Voltage Source and Its Comparison with Volts/Hertz Control", IEEE Trans. on Ind. Appl. IA-21, Jan/Feb 1985, for Induction Motor Electric Drive", Int'l. Conf. on Elec. Machines pp. 241-247.

17. Motorola Thyristor Device Data, Motorola Semiconductor Products Inc., Phoenix, Arizona, 1985.

18. C.R.Waslco, "AC Drives In Traction Applications", IAS Annual Meeting, Toronto, 1985.

19. K.W.J.Bishop, "Practical Assessment of GTO Thyristors for AC Motor Speed Control", IAS Annual Meeting, Toronto, 1985.

20. F.F.Nouvion, "Three-Phase Motors in Electric Rail Traction", IEEE Trans. on Ind. Appl. TA-20 Sept/Oct 1984, pp. 1152-1170.

21. H.Akagi, A.Nabae, "A New Control Scheme for Compensating the Torque Transfer Function of a Self-Controlled Synchronous Motor", IEEE Trans. on Ind. Appl. IA-20, July/Aug. 1984, pp. 795-802.

22. R.L.Smith Jr., R.P.Stratford, "Power System Harmonics Effects from Adjustable-Speed Drives," IEEE Trans. on Ind. Appl. IA-20, July/Aug. 1984, pp. 973-977.

23. W.Becker, R.Janssen, A.Mueller-Hellmann, H.Skudelny, "Analysis of Power Converters for AC Fed Traction Drives and Microcomputer-Aided On-Line Optimization of Their Line Response", IEEE Trans. on Ind. Appl. IA-20, May/June 1984, pp. 605-614.

24. E.L.Owen, M.M.Morack, C.C.Herskind, R.S.Grimes,"AC Adjustable-Speed Drives with Electronic Power Converters -- The Early Days", IEEE Trans. on Ind. Appl. IA-20 Mar/Apr 1984, pp. 298-308.

25. F.J.Brady, "A Mathematical Model for the Doubly-Fed Wound Rotor Generator", IEEE Trans., PAS-103, No. 4, Apr. 1984, pp. 798-802.

26. D.P.Connors, D.A.Jarc, R.H.Daugherty, "Considerations in Applying Induction Motors with Solid-State Adjustable Frequency Controllers", IEEE Trans. on Ind. Appl. IA-20 Jan/Feb 1984, pp. 113-121.

27. B.K.Bose, "Scalar Decoupled Control of Induction Motor", IEEE Trans. on Ind. Appl. Jan/Feb 1984, pp. 216-225.

28. H.Skudelny, M.Weinhardt, "An Investigation of the Dynamic Response of Two Induction Motors in a Locomotive Truck Fed by a Common Inverter", IEEE Trans. on Ind. Appl. Jan/Feb 1984, pp. 173-179.

29. M.G.Ioannidou, J.A.Tegopoulos, "Controlled Mechanical Output Power for Induction Motor Electric Drive", Int'l. Conf. on Elec. Machines, Lausanne, Switzerland, 1984, pp. 1050-1053.

30. S.B.Dewan, G.R.Slemon, A.Straughen, Power Semiconductor Drives, Wiley-Interscience, New York, 1984.

31. H.Shakarian, V.Chitechian, A.Safarian, "Double-Fed Machines in Autonomous Power Systems", Int'l. Conf. on Elec. Machines, Lausanne, Switzerland, 1984, pp. 1068-1071.

32. F.P.Emad, I.D.Mayergoyz, F.M.Abdel-Kader, "The Performance of Variable Speed Constant Frequency (VSCF) Machines", Int'l. Conf. on Elec. Machines, Lausanne, Switzerland, 1984, pp. 1033-1036.

33. W.Timpe, "Cycloconverter Drives for Rolling Mills", IEEE Trans., IA-18, July/August 1982, pp. 400-404.

34. L.Terens, J.Bommeli, K.Peters, "The Cycloconverter-Fed Synchronous Motor", Brown Bovari Rev. 69, 4/5 1982, pp. 122-132.

35. Linear Databook, National Semiconductor Corp., Santa Clara, Calif., 1982.

36. Thyristors-Rectifiers, General Electric Co., Auburn, New York, 1982.

37. L.J.Jacovides, M.F.Matouka, D.W.Shimer, "A Cycloconverter-Synchronous Motor Drive for Traction Applications", Trans., IA-17, July/August 1981, pp. 407-418.

38. G.A.Smith "A Current-Source Inverter in the Secondary Circuit of a Wound Rotor Induction Motor Provides Sub- and Supersynchronous Operation", IEEE Trans., IA-17, July/August 1981, pp. 399-406.

39. Motorola CMOS Integrated Circuits, Motorola Semiconductor Products Inc., Austin, Texas, Series C, 1978.

40. K.P.Basu, A.Anwar, B.Singh, "Very Low Speed Drive with Doubly Fed Induction Motor", IEEE Trans. on Ind'l. Elec. and Control Inst., IECI-24, May 1977, pp. 220-222.

41. B.Szabados, A.Banihaschemi, "Circle Diagram of Induction Machines From Practical Test Results", Can. Elec. Eng. J. Vol 1, No 3, 1976, pp. 27-32.

42. C.V.Jones, The Unified Theory of Electrical Machines, Butterworths, London, 1967.

43. B.M.Bird, R.F.Burbidge, "Analysis of Doubly Fed Slip-Ring Machines", Proc. Iee, Vol 113, No.6, June 1966, pp. 1016-1020.

44. J.C.Prescott, B.P.Raju, "The Inherent Instability of Induction Motors Under Conditions of Double Supply", Proc. IEE, 105 C, 1958, pp. 319-329.

45. R.E Bedford, "The Synchronous Double-Fed Induction Machine", AIEE Trans., PAS-75, part III, Feb. 1957, pp. 1486-1491.

46. C.Concordia, S.B.Crary, G.Kron, "The Doubly Fed Machine", AIEE Trans., vol 61, May 1942, pp. 290-296.